

# ガンマ線・宇宙線物理

副題:Tibet AS $\gamma$  実験により  
宇宙線の起源・加速機構・伝播  
の解明に挑む

瀧田正人, ICRR, U. of Tokyo

Spring School, @ICRR U. of Tokyo,  
11/Mar/2016

# CONTENTS

0. Introduction
1. Tibet AS $\gamma$  Experiment
2.  $\gamma$ -ray Physics
3. Knee Physics
4. Anisotropy
5. The Sun's Shadow
6. Future Prospects

# 0. Introduction

# 宇宙線観測の歴史

1912年 オーストリア人のヘスによって発見される

上空に行くほど放射線の強度が強くなることを見出した

1936年 ノーベル物理学賞を受賞

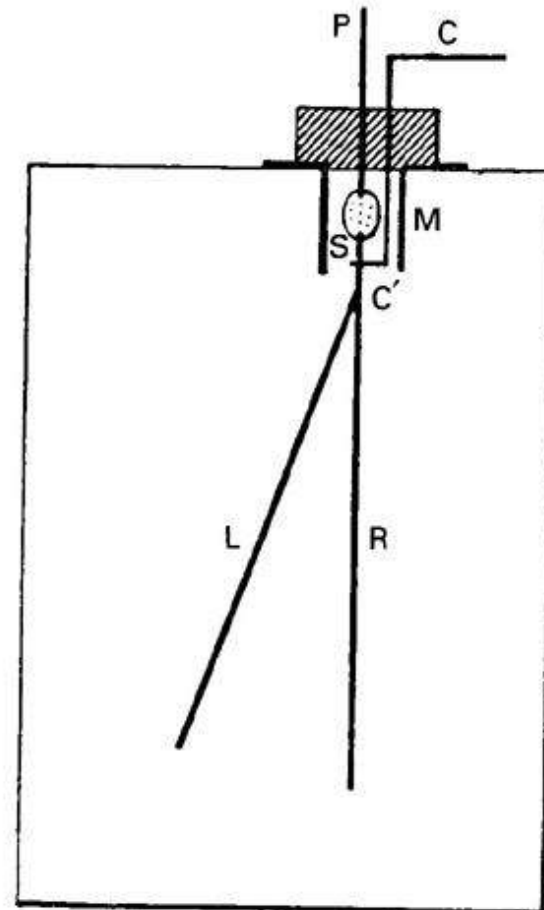
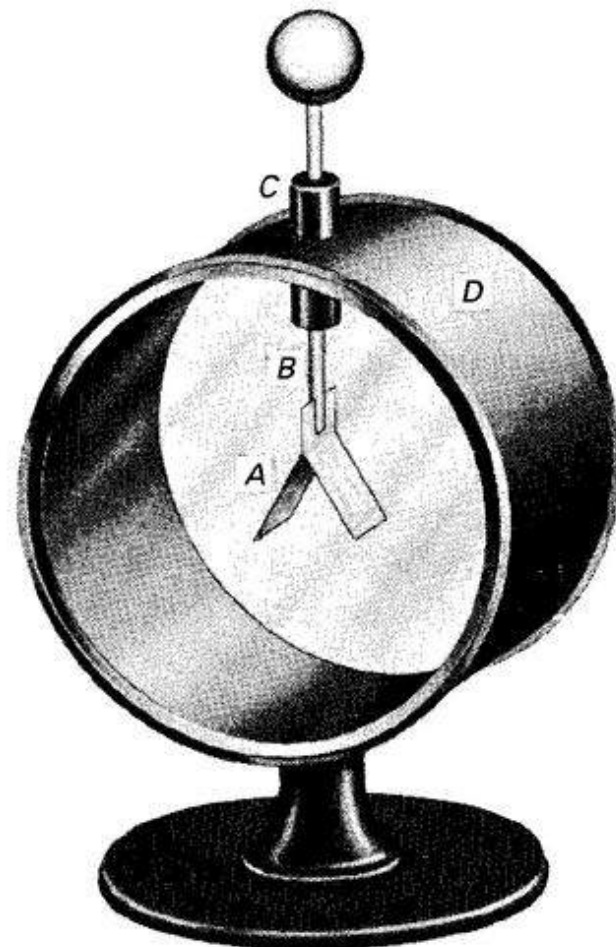
1950年 乗鞍岳に朝日の小屋が建つ(東京大学宇宙線観測所の前身)  
日本での宇宙線研究の幕開け

1950年代から1970年代  
原子核物理学としての側面が強い

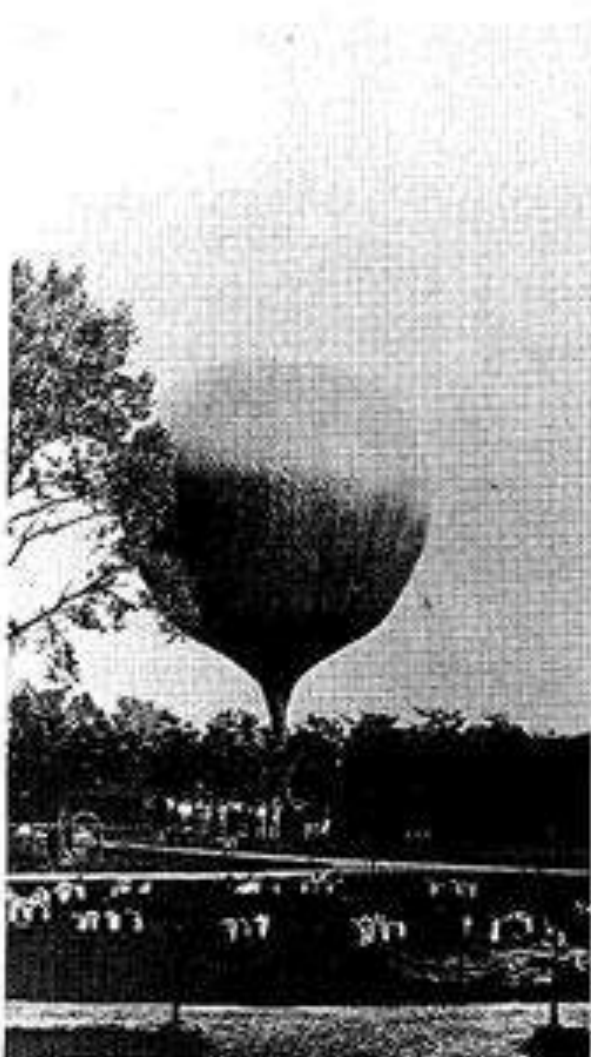
1989年 かに星雲からTeVガンマ線が観測される

1990年代以降  
天文学としての側面が強くなる

# 宇宙線発見のきっかけとなった 箔検電器



# 熱気球に乗り込むヘス



(a)

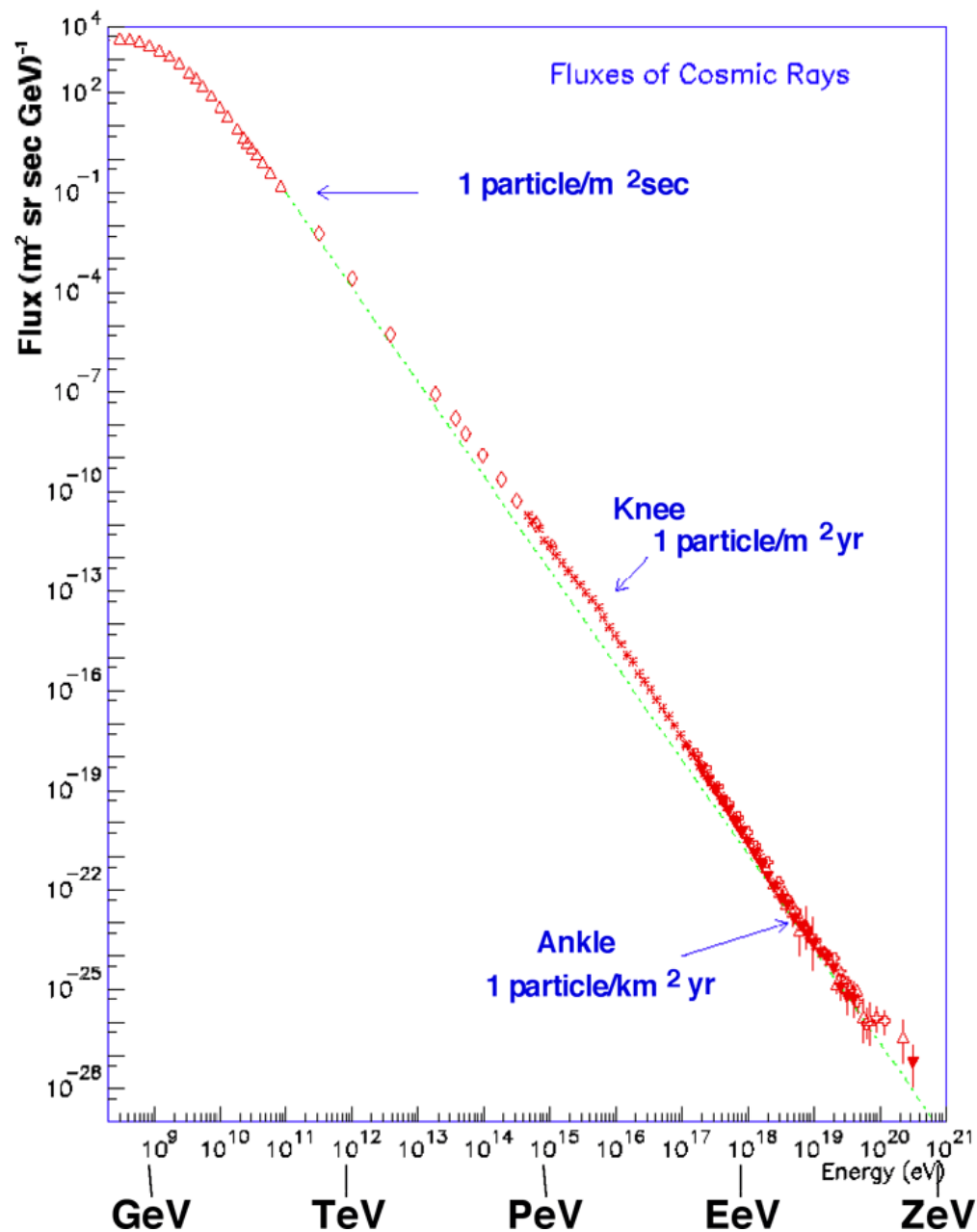


(b)

# 原子核宇宙線のエネルギースペクトル

ニー (Knee, およそ  $10^{15}$  eV) 以下のエネルギーの宇宙線は銀河系内で、それ以上のエネルギーの宇宙線は銀河系外からやってきていると考えられている。

エネルギーの高い宇宙線は極端に頻度が低くなるので、巨大な有効面積を持つ観測装置が必要になる。

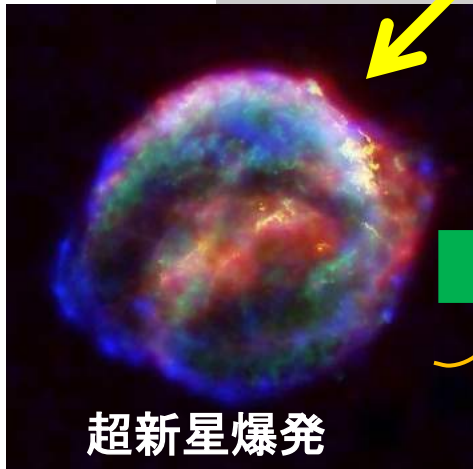
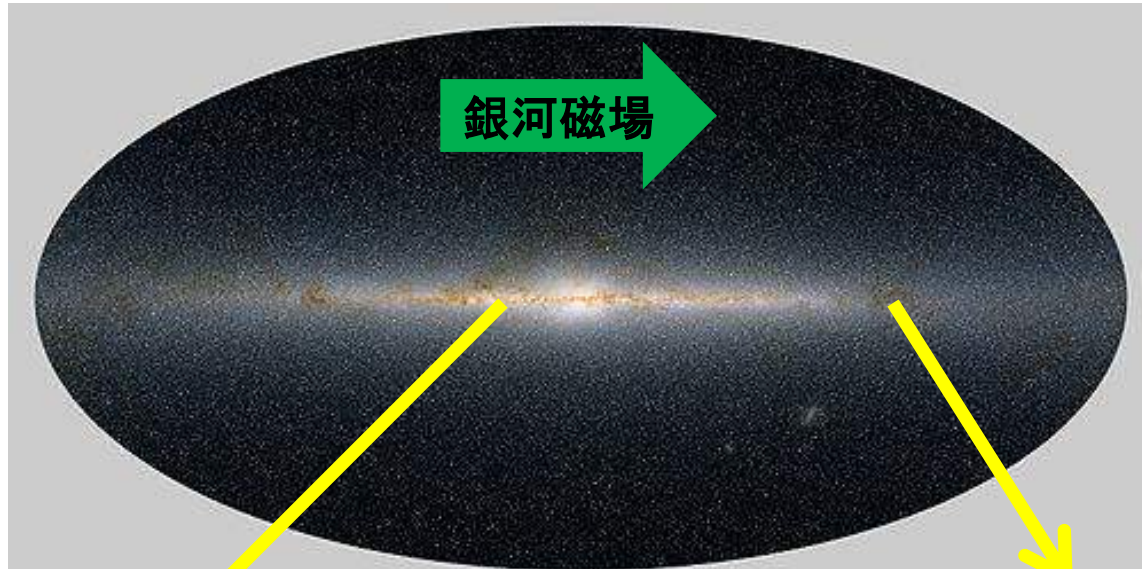


# 銀河系

約10万光年

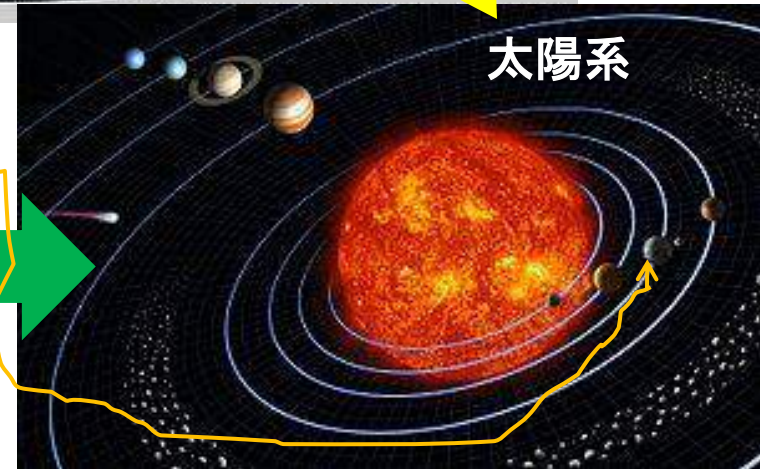


銀河磁場



銀河磁場

宇宙線  
螺旋軌道  
半径約  
0.001光年



約0.001光年



# 宇宙線の源を捜すには…

原子核宇宙線は宇宙空間の磁場に曲げられて、  
地球に到達したときには元の方向の情報を失って、  
全天ほぼ一様にやってくる。

原子核宇宙線の到来方向を観測しても、源はわからない。

原子核宇宙線は源の近くでガンマ線を生成することがある。

非常にエネルギーの高いガンマ線が特定の方向から来ていると、  
その方向に原子核宇宙線の起源がある可能性が高い。

# 宇宙線の観測

衛星・気球

原子核宇宙線・電子線

$10^9 \text{ eV} \sim 10^{14} \text{ eV}$

チェレンコフ望遠鏡

ガンマ線

$10^{11} \text{ eV} \sim 10^{14} \text{ eV}$

空気シャワーアレイ

原子核宇宙線・ガンマ線

$10^{12} \text{ eV} \sim 10^{20} \text{ eV}$

大気蛍光法

原子核宇宙線

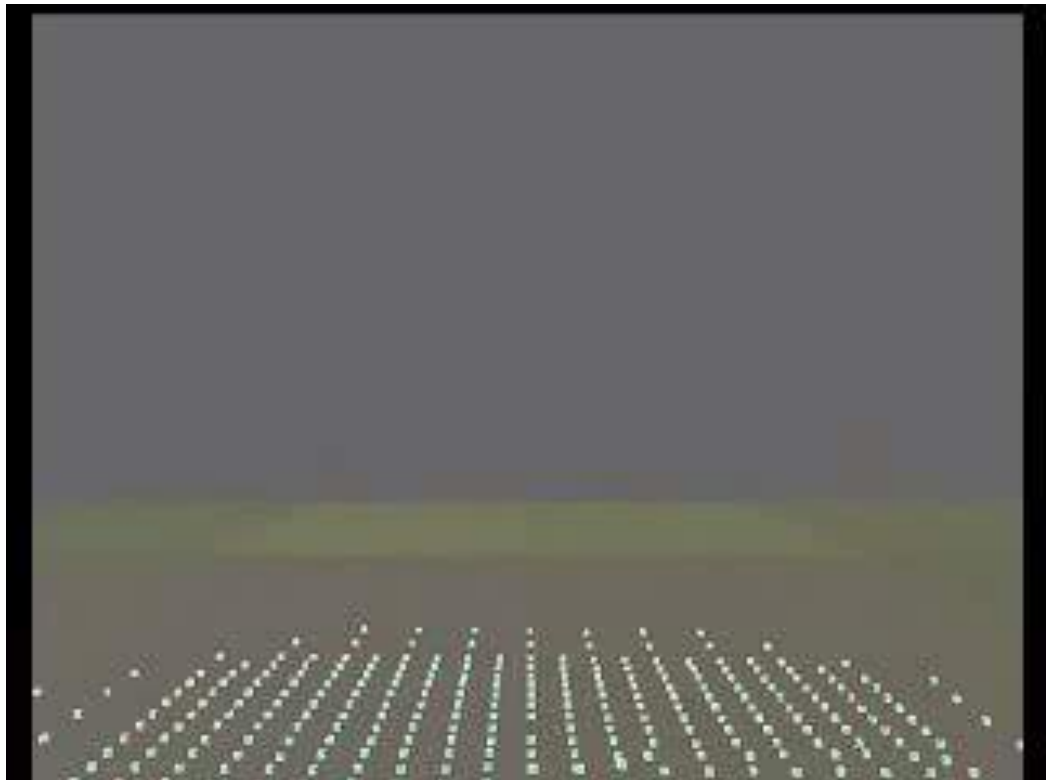
$10^{18} \text{ eV} \sim 10^{20} \text{ eV}$

# 空気シャワー

空気シャワーを起こす前の宇宙線を一次宇宙線、  
空気シャワーの粒子を二次粒子と呼ぶ

地表に到達するのは  
ほとんどが二次粒子で  
ミューオンが多い

手のひら程度の面積で  
1秒間に1個



宇宙線の大気圏突入 (空気シャワー)

# 1. Tibet AS $\gamma$ Experiment

= Tibet A(ir)S(hower) gamma Experiment  
の略称



# The Tibet ASy Collaboration



M. Amenomori<sup>1</sup>, X. J. Bi<sup>2</sup>, D. Chen<sup>3</sup>, T. L. Chen<sup>4</sup>, W. Y. Chen<sup>2</sup>, S. W. Cui<sup>5</sup>, Danzengluobu<sup>4</sup>, L. K. Ding<sup>2</sup>, C. F. Feng<sup>6</sup>, Zhaoyang Feng<sup>2</sup>, Z. Y. Feng<sup>7</sup>, Q. B. Gou<sup>2</sup>, Y. Q. Guo<sup>2</sup>, H. H. He<sup>2</sup>, Z. T. He<sup>5</sup>, K. Hibino<sup>8</sup>, N. Hotta<sup>9</sup>, Haibing Hu<sup>4</sup>, H. B. Hu<sup>2</sup>, J. Huang<sup>2</sup>, H. Y. Jia<sup>7</sup>, L. Jiang<sup>2</sup>, F. Kajino<sup>10</sup>, K. Kasahara<sup>11</sup>, Y. Katayose<sup>12</sup>, C. Kato<sup>13</sup>, K. Kawata<sup>14</sup>, M. Kozai<sup>13</sup>, Labaciren<sup>4</sup>, G. M. Le<sup>2</sup>, A. F. Li<sup>15,6,2</sup>, H. J. Li<sup>4</sup>, W. J. Li<sup>2,7</sup>, C. Liu<sup>2</sup>, J. S. Liu<sup>2</sup>, M. Y. Liu<sup>4</sup>, H. Lu<sup>2</sup>, X. R. Meng<sup>4</sup>, T. Miyazaki<sup>13</sup>, K. Mizutani<sup>11,16</sup>, K. Munakata<sup>13</sup>, T. Nakajima<sup>13</sup>, Y. Nakamura<sup>13</sup>, H. Nanjo<sup>1</sup>, M. Nishizawa<sup>17</sup>, T. Niwa<sup>13</sup>, M. Ohnishi<sup>14</sup>, I. Ohta<sup>18</sup>, S. Ozawa<sup>11</sup>, X. L. Qian<sup>6,2</sup>, X. B. Qu<sup>19,2</sup>, T. Saito<sup>20</sup>, T. Y. Saito<sup>21</sup>, M. Sakata<sup>10</sup>, T. K. Sako<sup>14</sup>, J. Shao<sup>2,6</sup>, M. Shibata<sup>12</sup>, A. Shiomi<sup>22</sup>, T. Shirai<sup>8</sup>, H. Sugimoto<sup>23</sup>, M. Takita<sup>14</sup>, Y. H. Tan<sup>2</sup>, N. Tateyama<sup>8</sup>, S. Torii<sup>11</sup>, H. Tsuchiya<sup>24</sup>, S. Udo<sup>8</sup>, H. Wang<sup>2</sup>, H. R. Wu<sup>2</sup>, L. Xue<sup>6</sup>, Y. Yamamoto<sup>10</sup>, K. Yamauchi<sup>12</sup>, Z. Yang<sup>2</sup>, S. Yasue<sup>25</sup>, A. F. Yuan<sup>4</sup>, T. Yuda<sup>14</sup>, L. M. Zhai<sup>2</sup>, H. M. Zhang<sup>2</sup>, J. L. Zhang<sup>2</sup>, X. Y. Zhang<sup>6</sup>, Y. Zhang<sup>2</sup>, Yi Zhang<sup>2</sup>, Ying Zhang<sup>2</sup>, Zhaxisangzhu<sup>4</sup>, X. X. Zhou<sup>7</sup>

<sup>1</sup>Department of Physics, Hirosaki University, Japan

<sup>2</sup>Key Laboratory of Particle Astrophysics, Institute of High Energy Physics, Chinese Academy of Sciences, China

<sup>3</sup>National Astronomical Observatories, Chinese Academy of Sciences, China

<sup>4</sup>Department of Mathematics and Physics, Tibet University, China

<sup>5</sup>Department of Physics, Hebei Normal University, China <sup>6</sup>Department of Physics, Shandong University, China

<sup>7</sup>Institute of Modern Physics, SouthWest Jiaotong University, China

<sup>8</sup>Faculty of Engineering, Kanagawa University, Japan <sup>9</sup>Faculty of Education, Utsunomiya University, Japan <sup>10</sup>Department of Physics, Konan University, Japan

<sup>11</sup>Research Institute for Science and Engineering, Waseda University, Japan

<sup>12</sup>Faculty of Engineering, Yokohama National University, Japan

<sup>13</sup>Department of Physics, Shinshu University, Japan

<sup>14</sup>Institute for Cosmic Ray Research, University of Tokyo, Japan

<sup>15</sup>School of Information Science and Engineering, Shandong Agriculture University, China

<sup>16</sup>Saitama University, Japan

<sup>17</sup>National Institute of Informatics, Japan

<sup>18</sup>Sakushin Gakuin University, Japan

<sup>19</sup>College of Science, China University of Petroleum, China

<sup>20</sup>Tokyo Metropolitan College of Industrial Technology, Japan

<sup>21</sup>Max-Planck-Institut fuer Physik, Deutschland

<sup>22</sup>College of Industrial Technology, Nihon University, Japan

<sup>23</sup>Shonan Institute of Technology, Japan

<sup>24</sup>Japan Atomic Energy Agency, Japan

<sup>25</sup>School of General Education, Shinshu University, Japan

# Yangbajing Cosmic Ray Observatory



$90^{\circ} 522\text{E}$ ,  $30^{\circ} 102\text{N}$ , 4,300 m a.s.l. ( $606\text{g/cm}^2$ )



Yangbajing,  
Tibet, China  
4300 m a.s.l. = 606 g/cm<sup>2</sup>

その他... 地図 航空写真 地形

# Tibet Air Shower Array

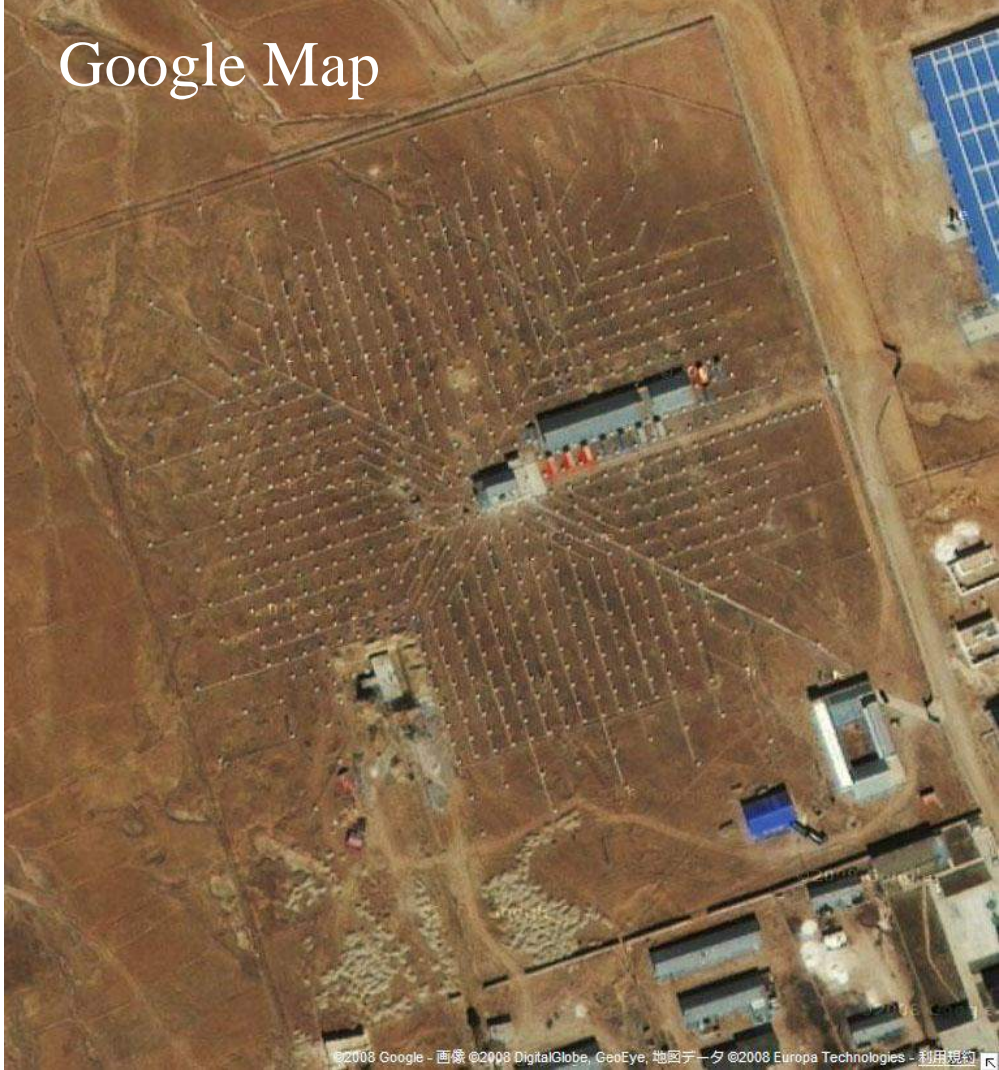
## Tibet III (37000 m<sup>2</sup>)

Total 789 detectors

Mode Energy  
~3 TeV

Angular Resolution  
~0.9 deg @ 3 TeV

Trigger Rate  
~1700 Hz



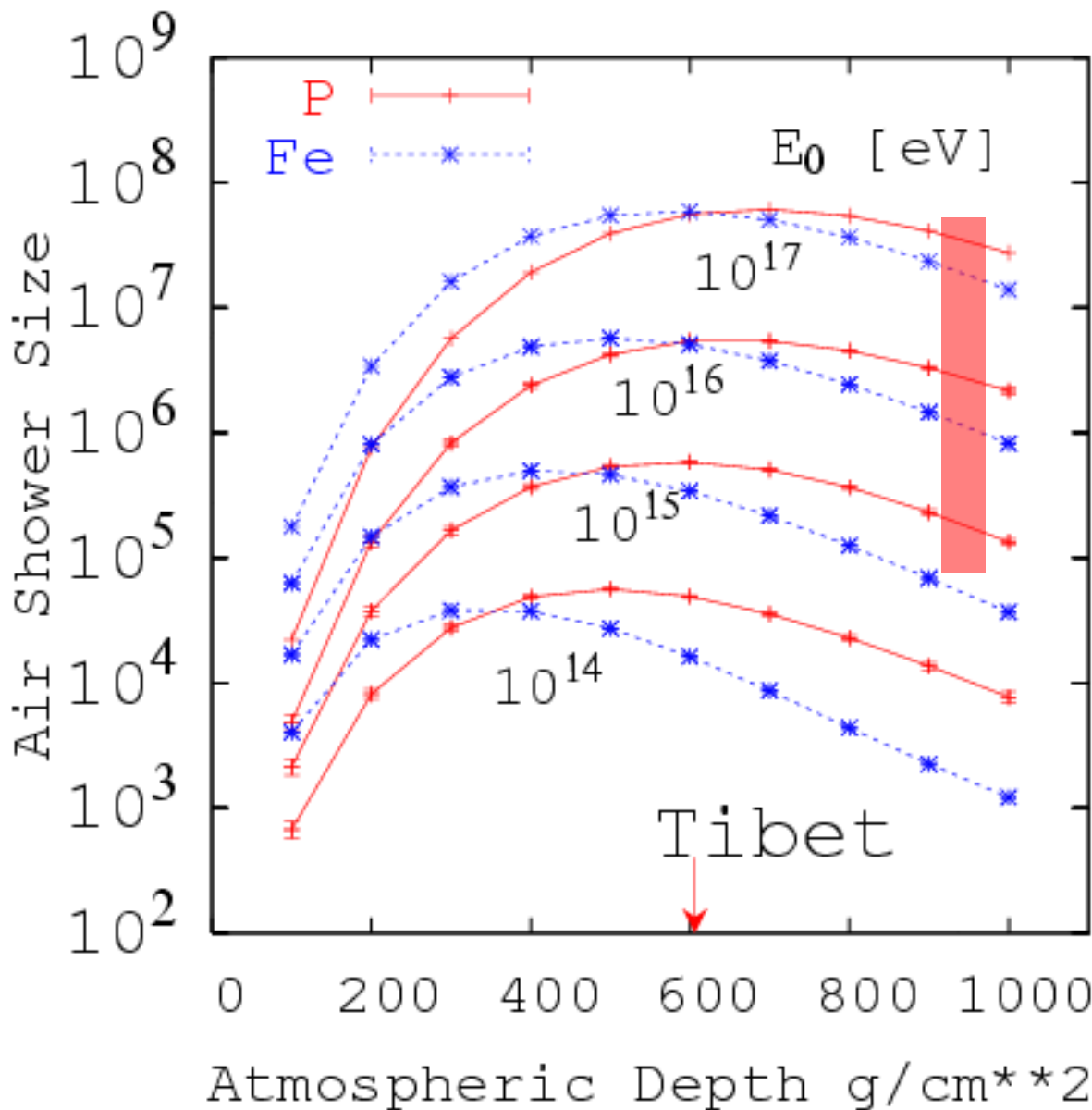
Google Map

# Research Purpose

**Complementary to Air Cherenkov Telescopes  
Wide-field-of-view (~2sr) high-duty cycle CR telescope**

1. **3TeV~100TeV cosmic  $\gamma$  rays**
  2. **3TeV ~100 PeV primary cosmic rays**
- > **Origin, acceleration, propagation mechanism of cosmic rays**
3. **The Sun's shadow in cosmic rays  
(Shielding effect on cosmic rays by the Sun)**
- > **Global structure of solar and interplanetary magnetic fields**

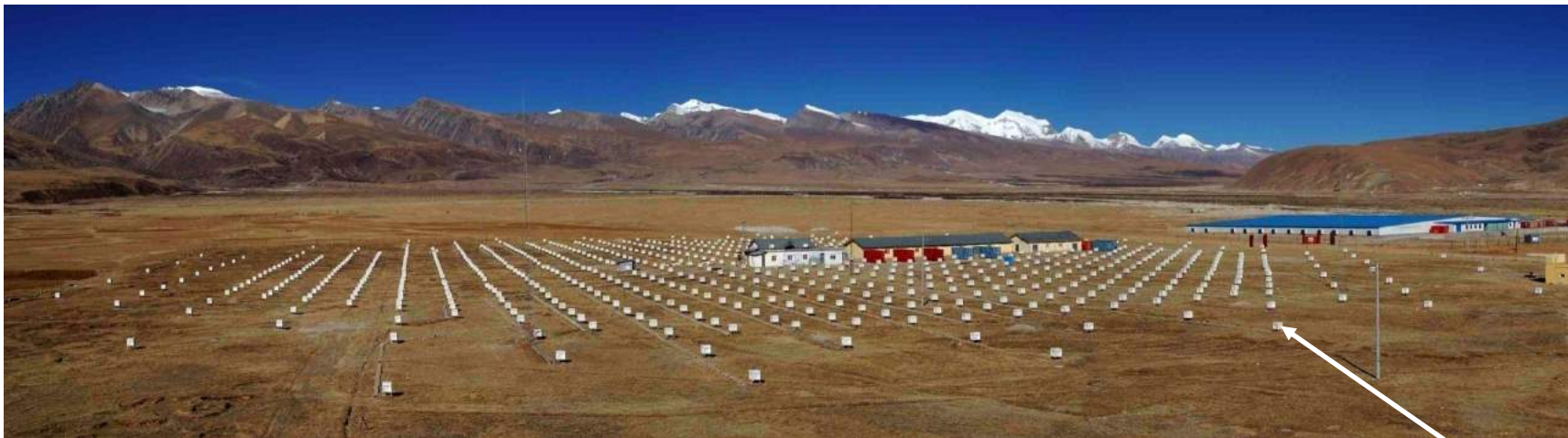
# Longitudinal development of AS



Why Tibet?

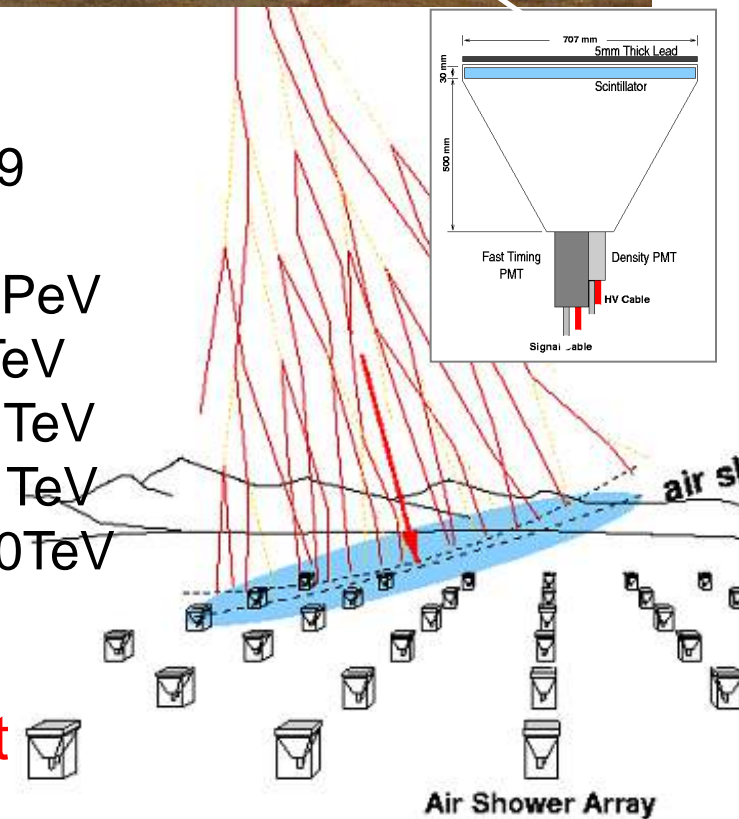
1. TeV CR/ $\gamma$   
Attenuation  
@ sea level
2. Good Energy  
determination  
in Knee  
 $(10^{15}-10^{16}\text{eV})$   
(p or Fe)

# Tibet-III Air Shower (AS) Array



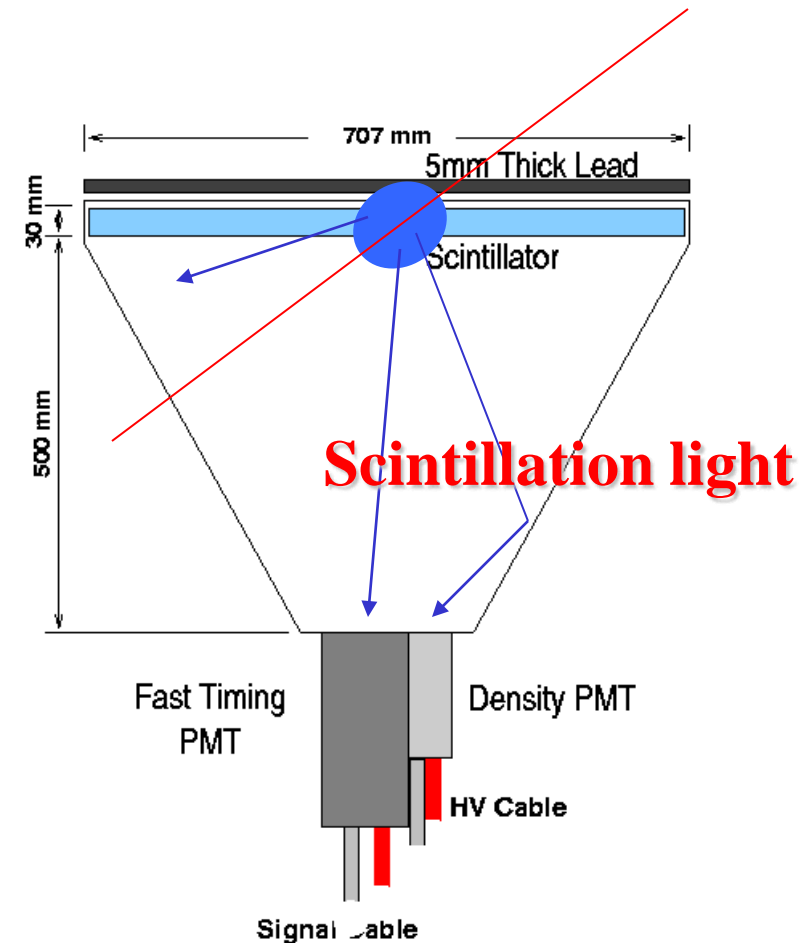
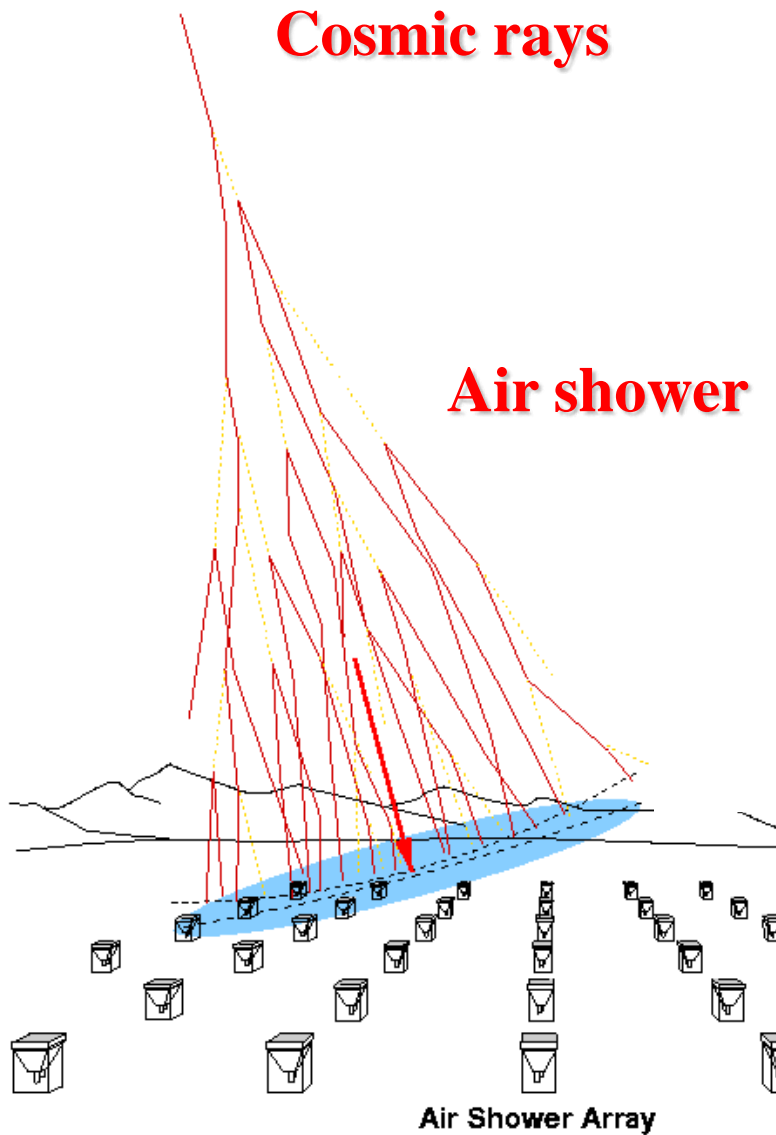
- Number of Scinti. Det.
- Effective Area for AS
- Energy region
- Angular Resolution  
(Gamma rays)
- Energy Resolution  
(Gamma rays)
- F.O.V.

0.5 m<sup>2</sup> x 789  
~37,000 m<sup>2</sup>  
~TeV - 100 PeV  
~0.4 @ 10 TeV  
~0.2 @ 100 TeV  
~70% @ 10 TeV  
~40% @ 100 TeV  
~2 sr



2<sup>nd</sup> particles Timing & Energy deposit

# Detection Principle

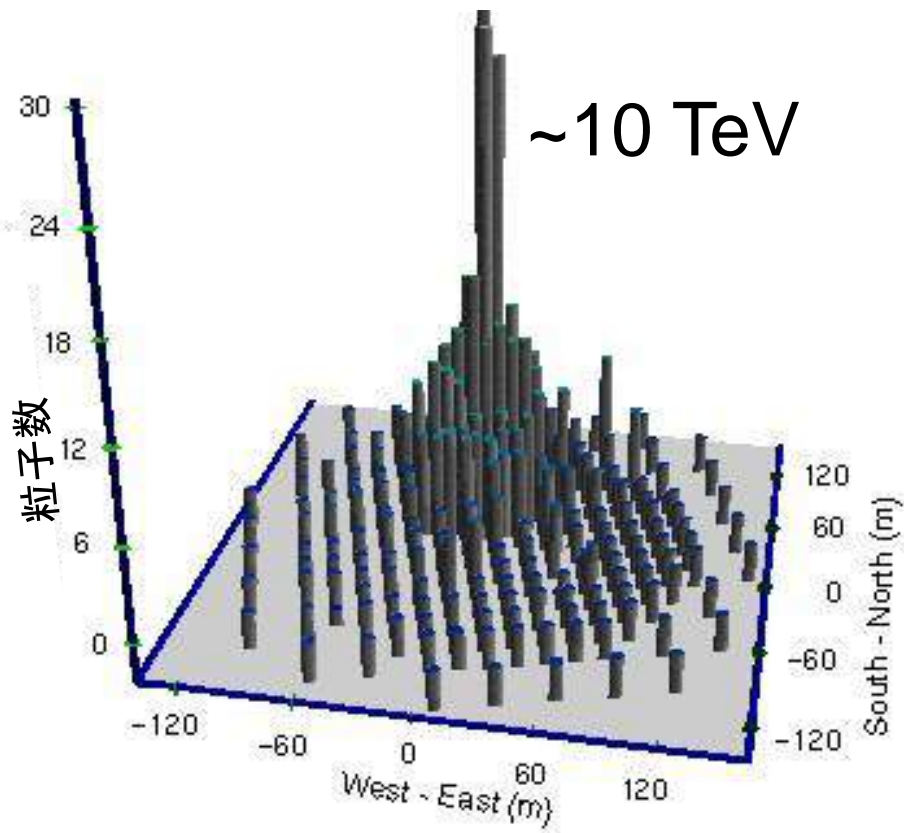


# Air Shower Detection

2<sup>nd</sup> particle density



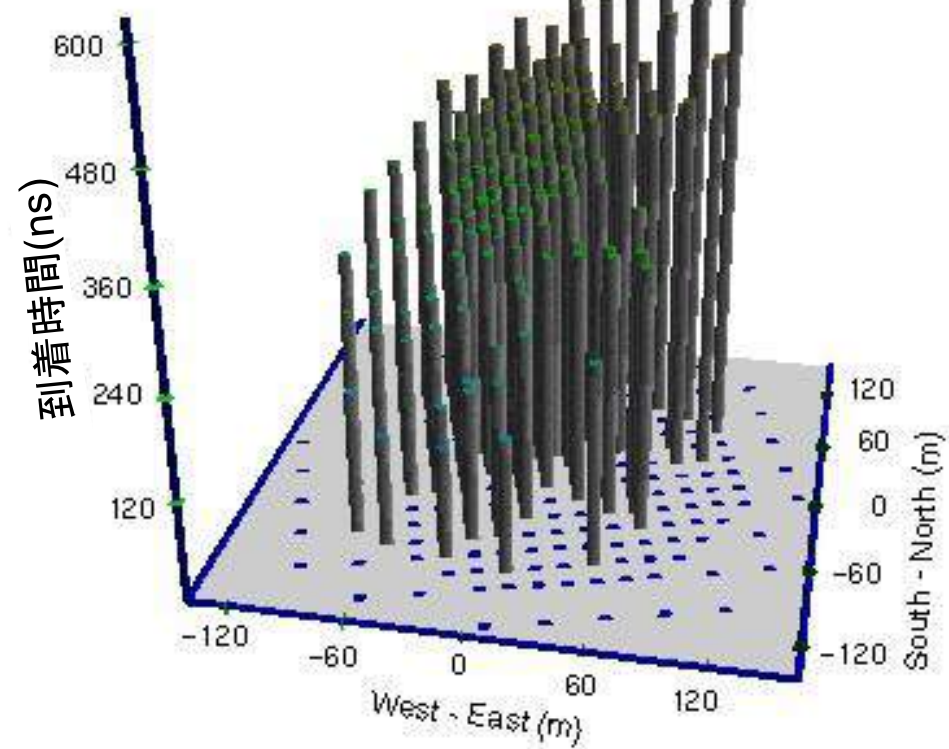
Cosmic ray energy



2<sup>nd</sup> particle timing



Cosmic ray direction

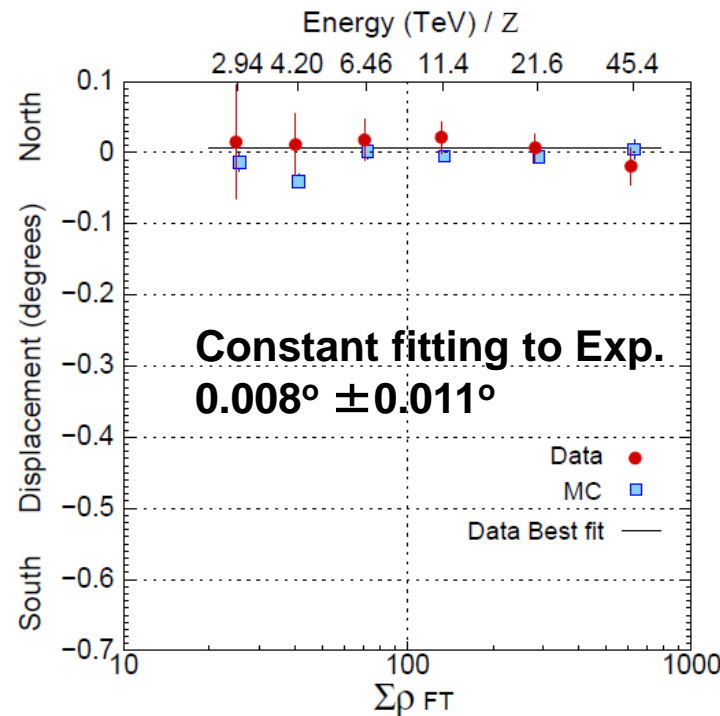


Air shower rate triggered by Tibet III ~1700Hz

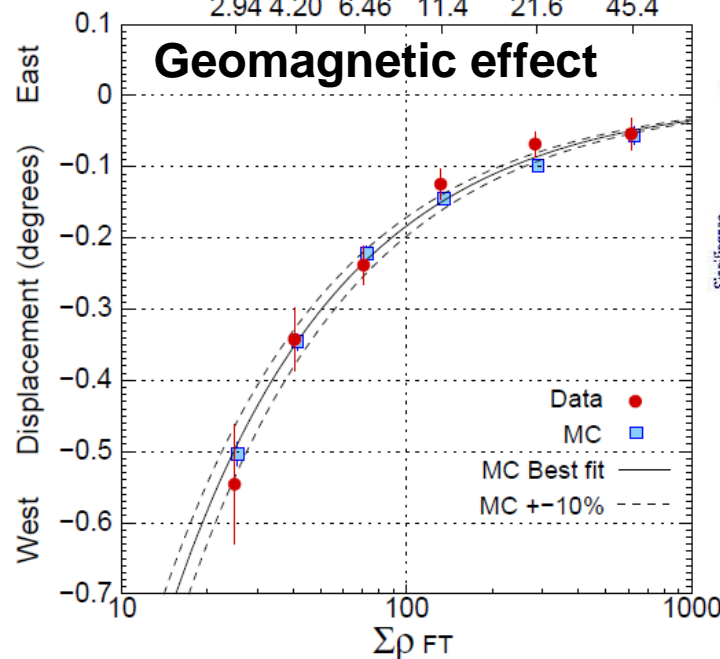
# Performance by Moon's Shadow

The Astrophysical Journal,  
692, 61–72(2009)

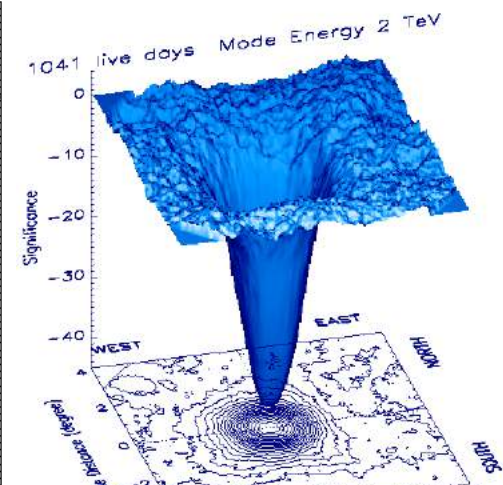
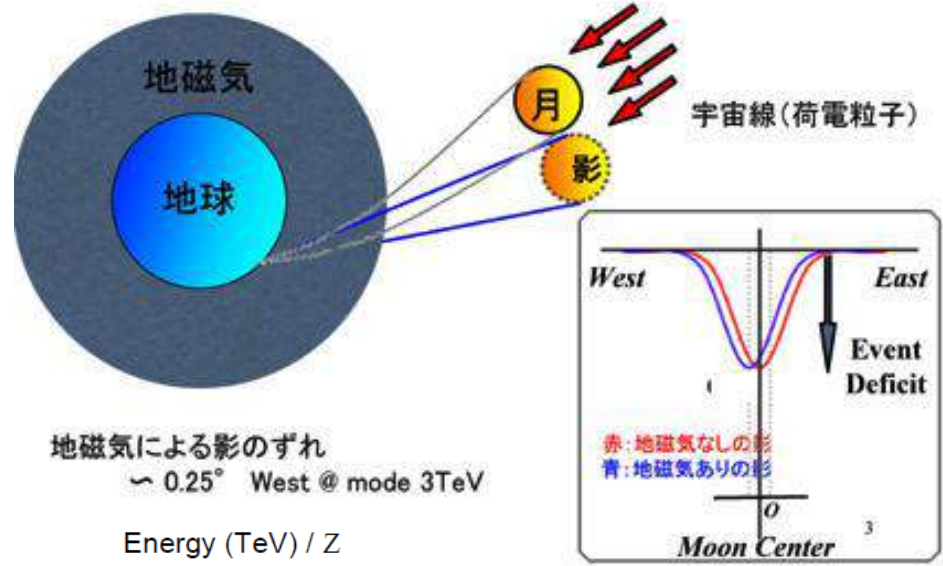
- Absolute Energy Scale
- Angular Resolution
- Pointing Accuracy



Pointing Error  
 $< 0.011^\circ$

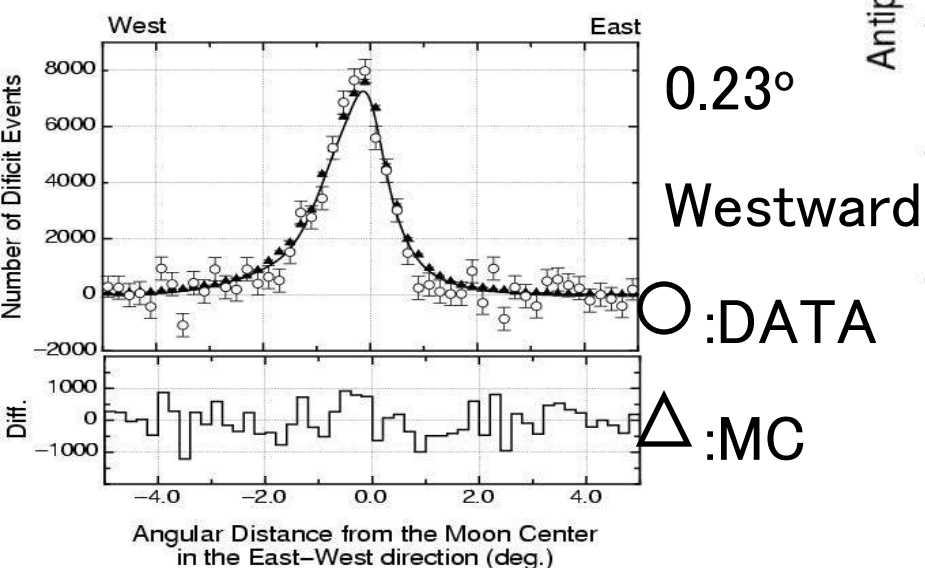
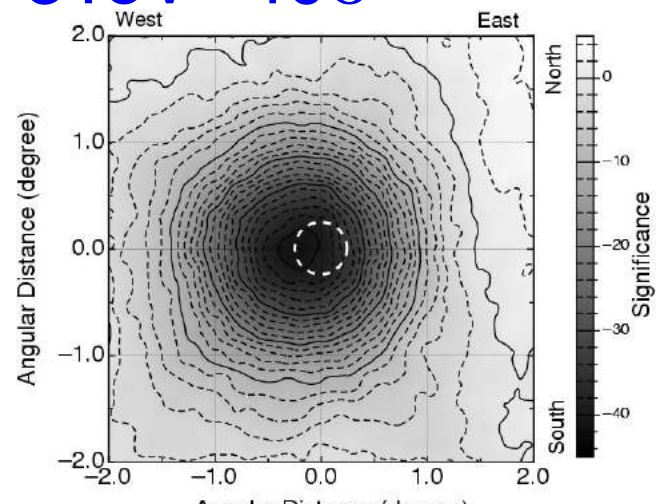


Absolute Energy Scale Error  $< 12\%$   
 $+4.5\% (\pm 8.6\text{stat.} \pm 6.7\text{syst.})\%$

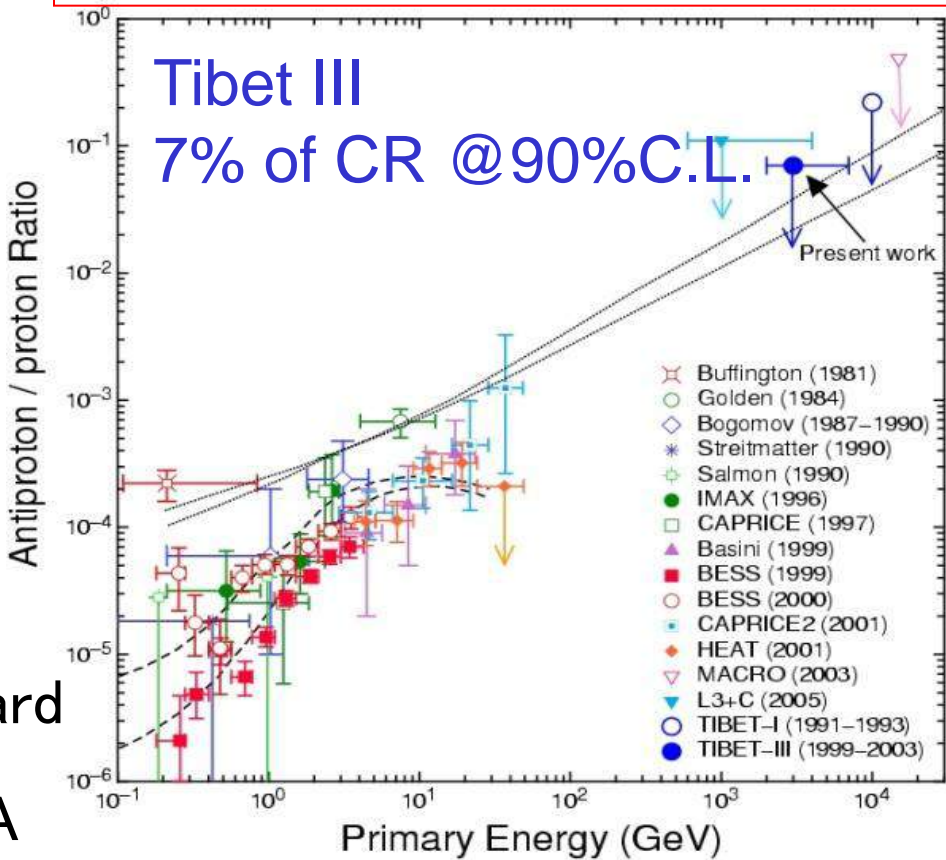


# Search for TeV anti-protons by the Moon's shadow

3TeV 40 $\sigma$



Amenomori et al.  
Astroparticle Physics, 28, (2007) 137-142



M.Simon et al. ApJ 499 (1998)250.

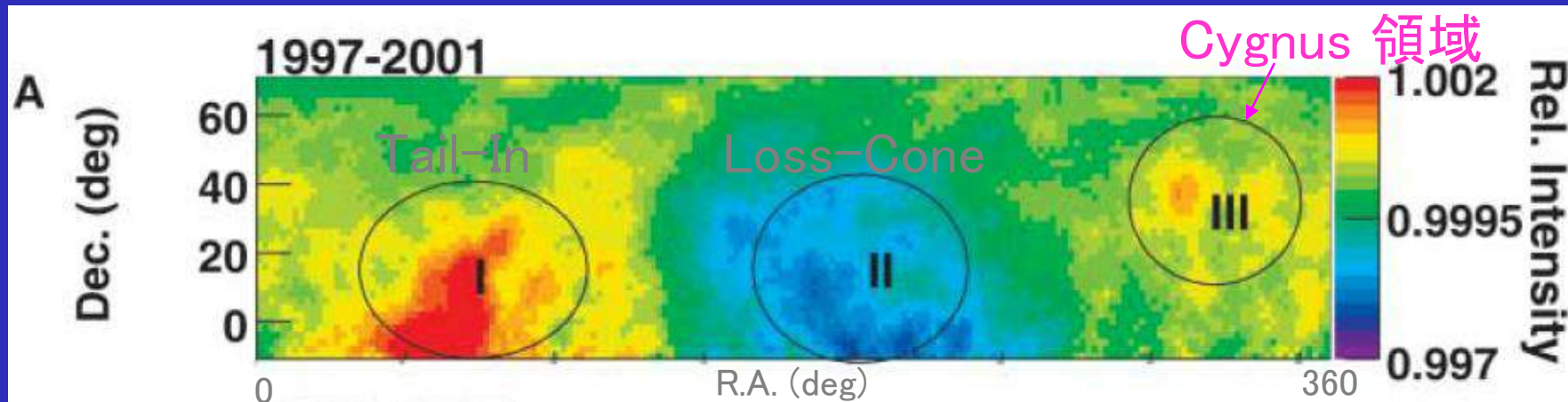
Dotted line: extragalactic anti-matter model

S.A. Stephan et al. Space Sci. Rev. 46 (1987) 31.

## 2. $\gamma$ -ray physics

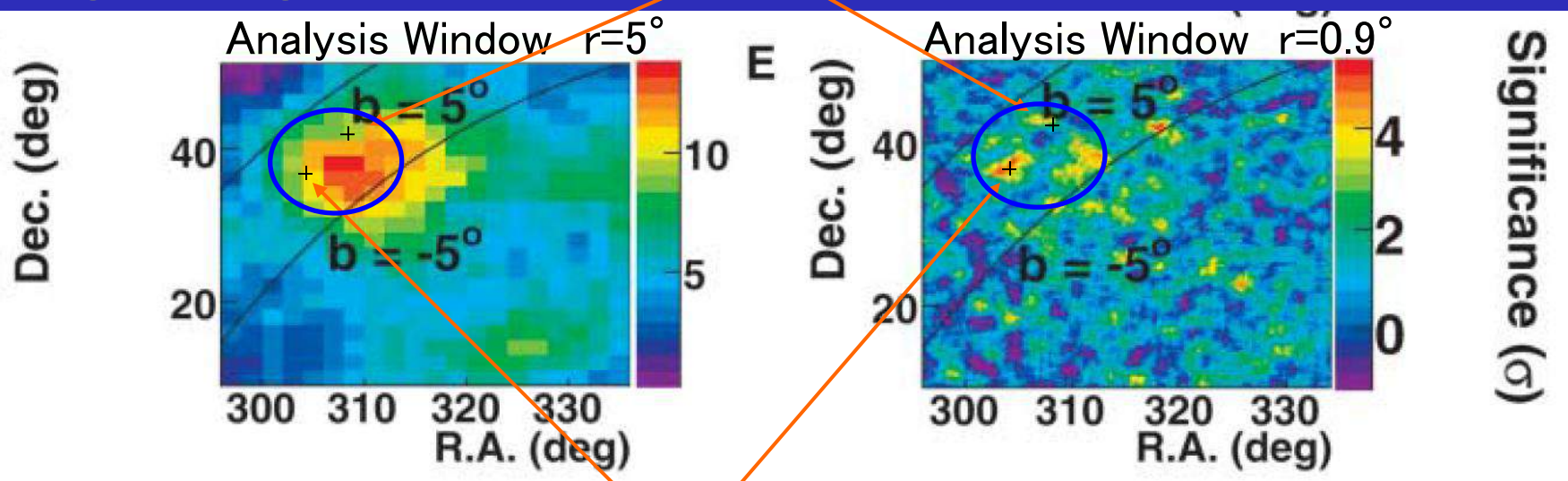
# Cosmic Ray Anisotropy at sidereal time frame (Tibet AS $\gamma$ )

## Anisotropy Map Amenomori et al, Science, 314, 439 (2006)



## Cygnus Region

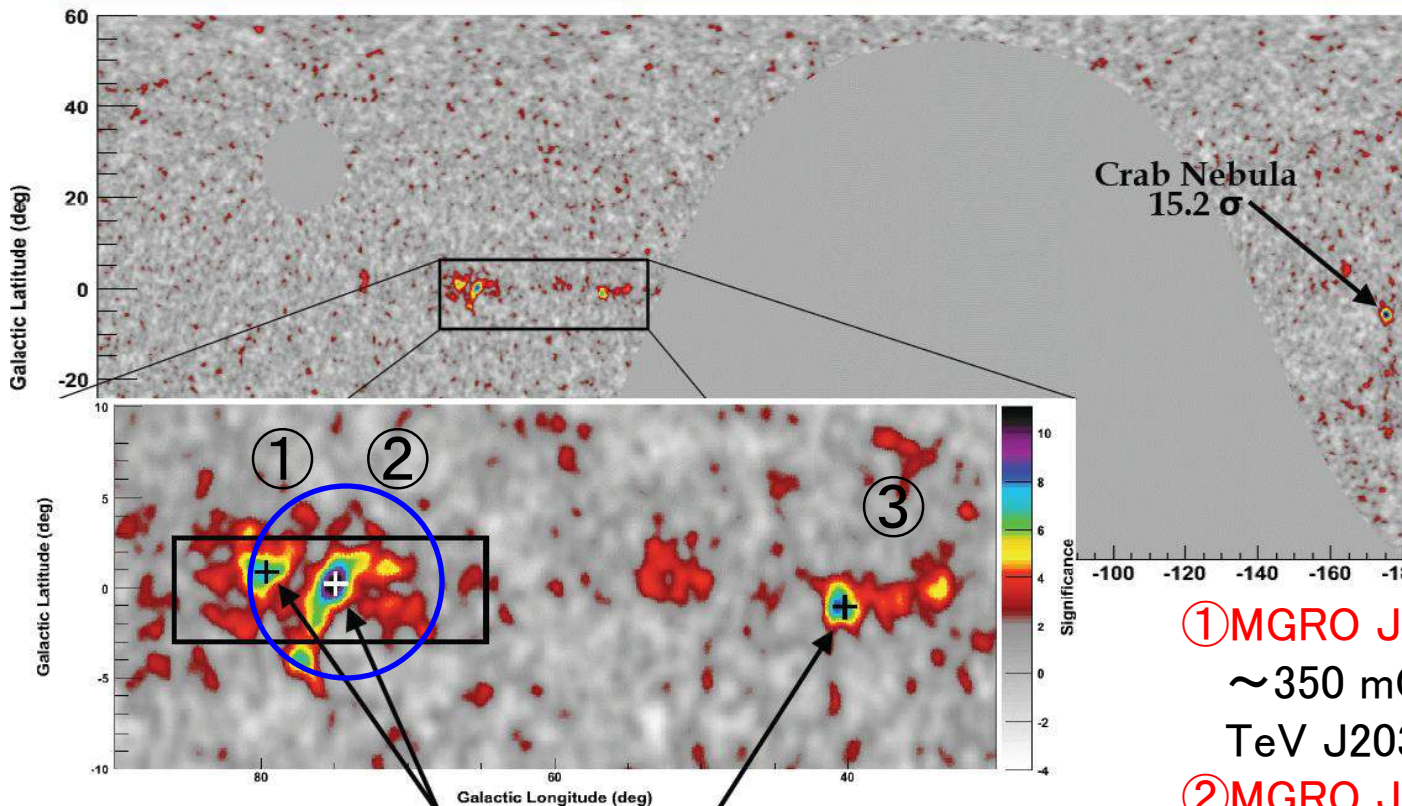
① MGRO J2033+42



# Cygnus領域 Milagro 全天サーベイ(2007年)

## A Closer Look at the Galactic Plane

12TeV



- Cygnus region shows two new TeV gamma-ray sources
- Diffuse emission from Cygnus region
- A new TeV source at low declinations

*First GLAST Symposium,*

*A. Abdo, "Discovery of TeV Gamma Ray Emission from the Cygnus Region with Milagro Using a New Background Rejection Technique"*

[http://glast.gsfc.nasa.gov/science/symposium/2007/thursday/7.3\\_Abdo.pdf](http://glast.gsfc.nasa.gov/science/symposium/2007/thursday/7.3_Abdo.pdf)

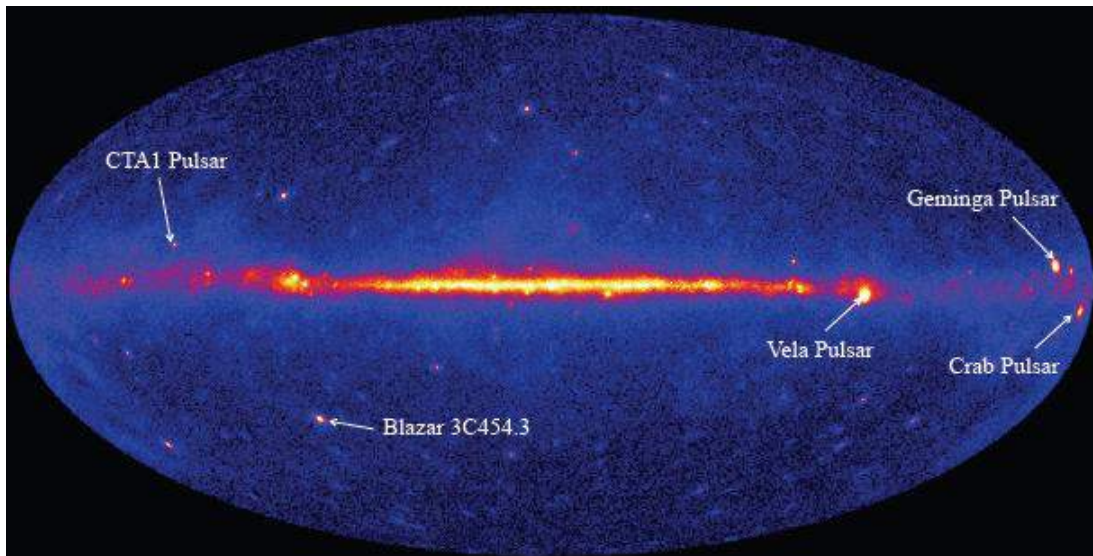
Observation of TeV Gamma Rays  
from the Fermi Bright Galactic Sources  
with the Tibet Air Shower Array  
(Amenomori et. al.)

ApJ 709(2010)L6-L10  
**(arXiv:0912.0386)**

# Introduction

Large Area Telescope(LAT)  
on the Fermi Gamma-Ray  
Space Telescope

Lunched in June 2008



*FERMI/LARGE AREA TELESCOPE BRIGHT GAMMA-RAY SOURCE LIST*  
*Abdo, A. A. et al. 2009, ApJS, 183, 46 (July 2009, astrar-ph submitted in Feb. 2009)*

Fermi LAT 3 month observation  
>100MeV,  
>10 $\sigma$



205 most significant sources (<math>>20</math> extragalactic sources)  
A typical 95% uncertainty radius of source position:  $10' \sim 20'$

# Milagro Observation of TeV Emission from Galactic Sources In the Fermi Bright Source List (*Abdo, A. A. et al 2009, ApJ, 700, L127*)

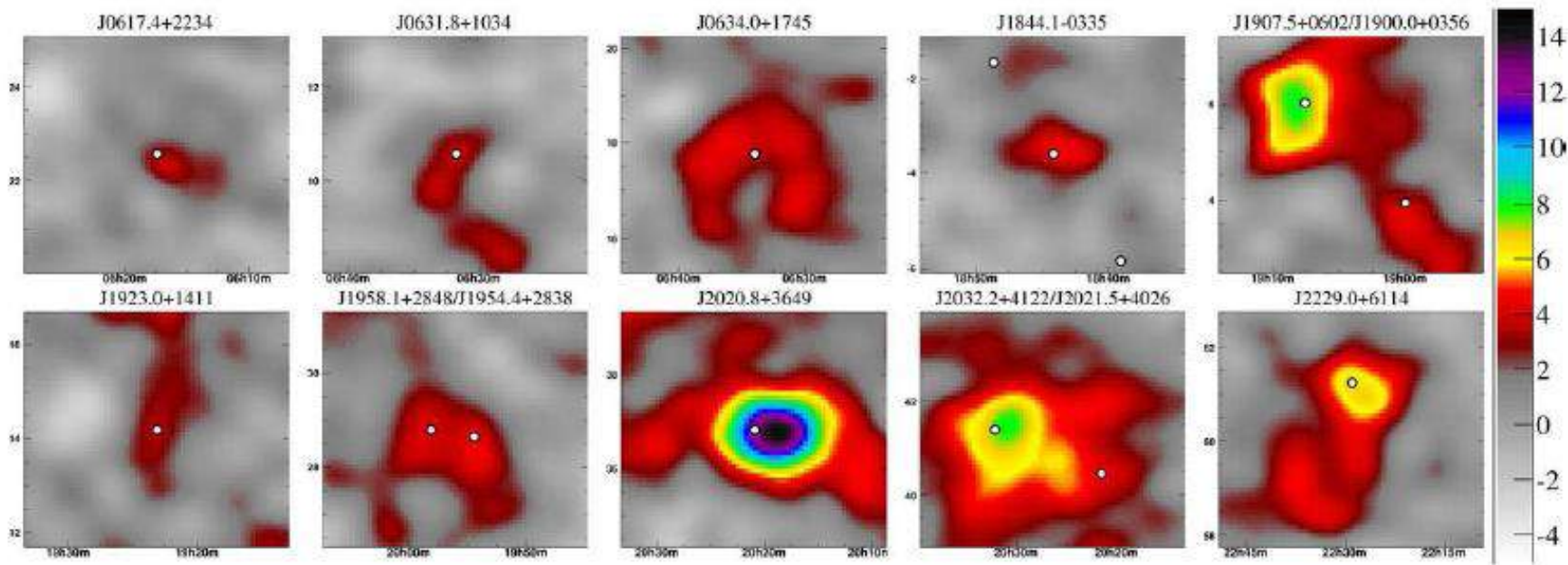


Fig. 1.— The  $3\sigma$  sources from Table 1, omitting the Crab. Each frame shows a  $5^\circ \times 5^\circ$  region with the LAT sources indicated by white dots. The data has been smoothed by a Gaussian of width varying between  $0.4^\circ$  and  $1.0^\circ$ , depending on the expected angular resolution of events. Horizontal axes show Right-Ascension and vertical axes show Declination. The colors indicate the statistical significance in standard deviations.

34 sources selected from 205 Fermi sources  
(Not extragalactic & Dec. $>-5.0^\circ$ )

$E\gamma \sim 35 \text{ TeV}$

PSR	16
HXB	1
SRN	5
UNID	12

# Milagro Results

Name (0FGL)	type	RA (deg)	DEC (deg)	<i>l</i> (deg)	<i>b</i> (deg)	Flux $(\times 10^{-17} \text{ TeV}^{-1}$ $\text{sec}^{-1} \text{ cm}^{-2})$	Signif. ( $\sigma$ 's)	TeV assoc.
J0007.4+7303	PSR	1.85	73.06	119.69	10.47	< 90.4	2.6	
J0030.3+0450	PSR	7.60	4.85	113.11	-57.62	< 20.9	-1.7	
J0240.3+6113	HXB	40.09	61.23	135.66	1.07	< 26.2	0.7	LSI +61 303
J0357.5+3205	PSR	59.39	32.08	162.71	-16.06	< 16.5	-0.1	
J0534.6+2201	PSR	83.65	22.02	184.56	-5.76	$162.6 \pm 9.4$	17.2	Crab
J0613.9-0202	PSR	93.48	-2.05	210.47	-9.27	< 60.0	-0.0	
J0617.4+2234	SNR <sup>a</sup>	94.36	22.57	189.08	3.07	$28.8 \pm 9.5$	3.0	IC443
J0631.8+1034	PSR	97.95	10.57	201.30	0.51	$47.2 \pm 12.9$	3.7	
J0633.5+0634	PSR	98.39	6.58	205.04	-0.96	< 50.2	1.4	
J0634.0+1745	PSR	98.50	17.76	195.16	4.29	$37.7 \pm 10.7$	3.5	MGRO C3 Geminga
J0643.2+0858		100.82	8.98	204.01	2.29	< 30.5	0.3	
J1653.4-0200		253.35	-2.01	16.55	24.96	< 51.0	-0.5	
J1830.3+0617		277.58	6.29	36.16	7.54	< 32.8	0.2	
J1836.2+5924	PSR	279.06	59.41	88.86	25.00	< 14.6	-0.9	
J1844.1-0335		281.04	-3.59	28.91	-0.02	$148.4 \pm 34.2$	4.3	
J1848.6-0138		282.16	-1.64	31.15	-0.12	< 91.7	1.7	
J1855.9+0126	SNR <sup>a</sup>	283.99	1.44	34.72	-0.35	< 89.5	2.2	
J1900.0+0356		285.01	3.95	37.42	-0.11	$70.7 \pm 19.5$	3.6	
J1907.5+0602	PSR	286.89	6.03	40.14	-0.82	$116.7 \pm 15.8$	7.4	MGRO J1908+06 HESS J1908+063

14 sources were detected with  $>3\sigma$

J1911.0+0905	SNR <sup>a</sup>	287.76	9.09	43.25	-0.18	< 41.7	1.5	
J1923.0+1411	SNR <sup>a</sup>	290.77	14.19	49.13	-0.40	$39.4 \pm 11.5$	3.4	HESS J1923+141
J1953.2+3249	PSR	298.32	32.82	68.75	2.73	< 17.0	0.0	
J1954.4+2838	SNR <sup>a</sup>	298.61	28.65	65.30	0.38	$37.1 \pm 8.6$	4.3	
J1958.1+2848	PSR	299.53	28.80	65.85	-0.23	$34.7 \pm 8.6$	4.0	
J2001.0+4352		300.27	43.87	79.05	7.12	< 12.1	-0.9	
J2020.8+3649	PSR	305.22	36.83	75.18	0.13	$108.3 \pm 8.7$	12.4	MGRO J2019+37
J2021.5+4026	PSR	305.40	40.44	78.23	2.07	$35.8 \pm 8.5$	4.2	
J2027.5+3334		306.88	33.57	73.30	-2.85	< 16.0	-0.2	
J2032.2+4122	PSR	308.06	41.38	80.16	0.98	$63.3 \pm 8.3$	7.6	TEV 2032+41
								MGRO J2031+41
J2055.5+2540		313.89	25.67	70.66	-12.47	< 17.6	-0.0	
J2110.8+4608		317.70	46.14	88.26	-1.35	< 24.1	1.1	
J2214.8+3002		333.70	30.05	86.91	-21.66	< 20.7	0.6	
J2229.0+6114	PSR	337.26	61.24	106.64	2.96	$70.9 \pm 10.8$	6.6	MGRO C4
J2302.9+4443		345.75	44.72	103.44	-14.00	< 13.2	-0.6	

# Tibet-III Data Analysis

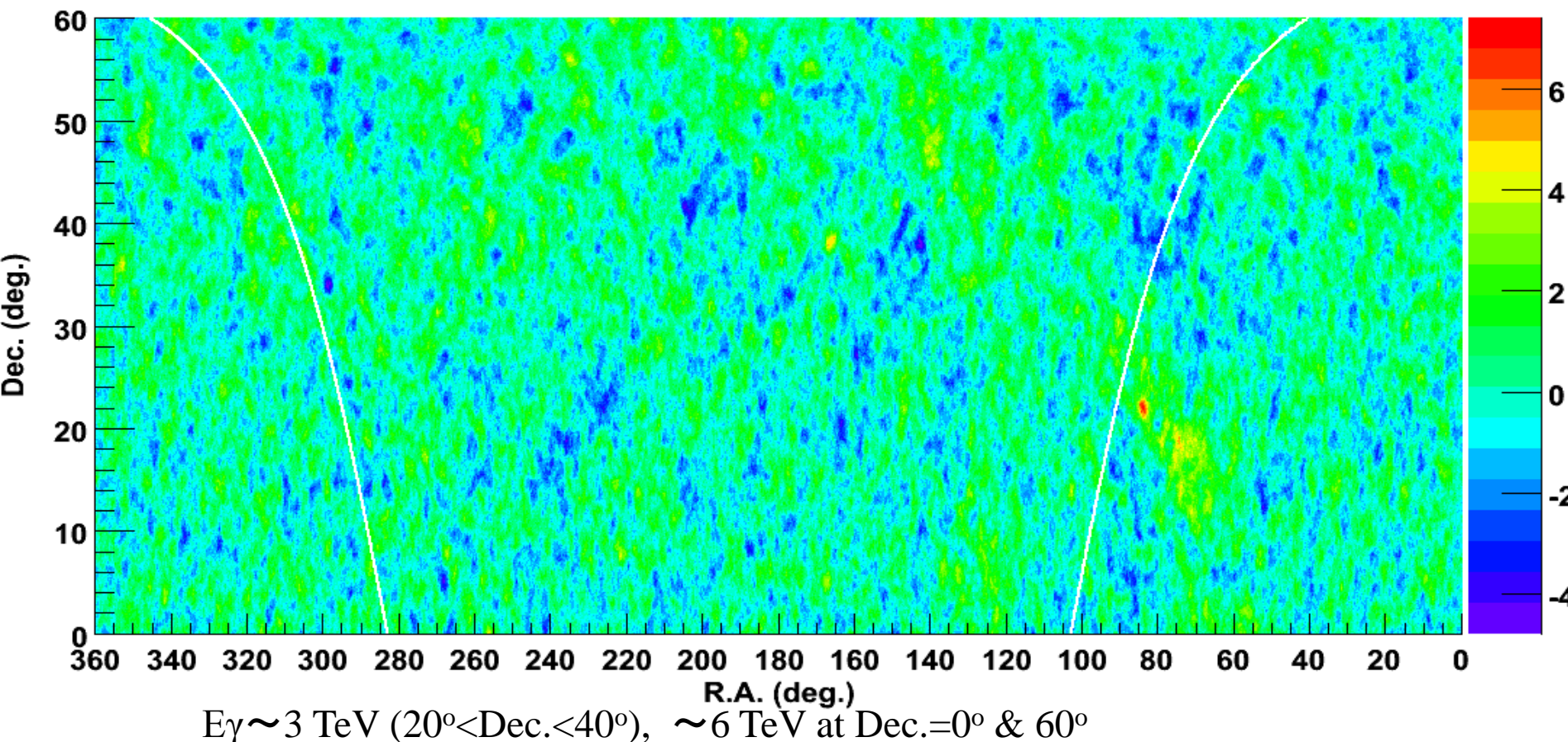
All-sky Data by the Tibet-III Array (Phase 1-9 Ver.B4)

$\Sigma\rho_{FT} > 10^{1.25}$  && zenith  $< 40^\circ$

Inout && 1.25p Any4 && Residual Error  $< 1.0\text{m}$

Search Window Size:  $R_s(\Sigma\rho_{FT}) = 6.9 / \sqrt{\Sigma\rho_{FT}}$  (Variable)

1999 Nov – 2008 Dec  
1915.5 live days



# Target sources in the Fermi Bright Source List

The Fermi Bright Source List: 205 sources

Not identified as extragalactic: 85 sources

$0^\circ < \text{Declination} < 60^\circ$  27 sources

Pulsar (PSR) 13

Supernova remnant (SNR) 5

Unidentified 9

**Table I**  
**Summary of the Tibet-III Array Observations of the *Fermi* Sources**

<i>Fermi</i> LAT Source (0FGL)	Class	R.A. (deg)	Decl. (deg)	Tibet-III Signi. ( $\sigma$ )	Milagro <sup>a</sup> Signi. ( $\sigma$ )	Source Associations
J0030.3+0450	PSR	7.600	4.848	1.7	-1.7	
J0357.5+3205	PSR <sup>b</sup>	59.388	32.084	-1.7	-0.1	
J0534.6+2201	PSR	83.653	22.022	6.9	17.2	Crab
J0617.4+2234	SNR	94.356	22.568	0.2	3.0	IC 443
J0631.8+1034	PSR	97.955	10.570	0.3	3.7	
J0633.5+0634	PSR <sup>b</sup>	98.387	6.578	2.4	1.4	
J0634.0+1745	PSR	98.503	17.760	2.2	3.5	Geminga
J0643.2+0858		100.823	8.983	-1.2	0.3	
J1830.3+0617		277.583	6.287	-0.2	0.2	
J1836.2+5924	PSR <sup>b</sup>	279.056	59.406	-0.3	-0.9	
J1855.9+0126	SNR	283.985	1.435	0.7	2.2	W44
J1900.0+0356		285.009	3.946	1.0	3.6	
J1907.5+0602	PSR <sup>b</sup>	286.894	6.034	2.4	7.4	MGRO J1908+06 HESS J1908+063
J1911.0+0905	SNR	287.761	9.087	1.7	1.5	G43.3 – 0.2
J1923.0+1411	SNR	290.768	14.191	-0.3	3.4	W51 HESS J1923+141

Tibet-III  $2\sigma$   
 $\sim 0.3$  Crabs

**Geminga**

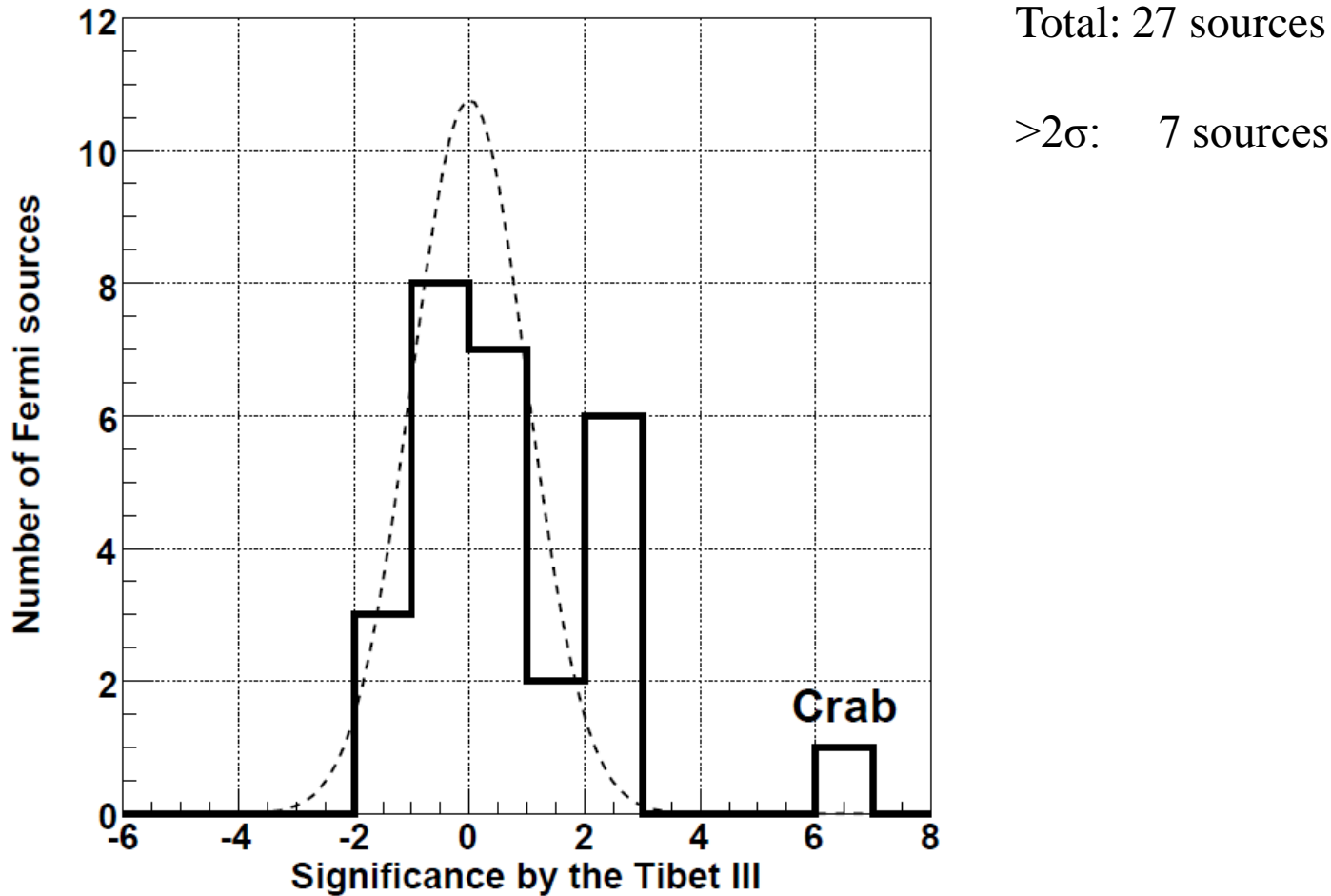
**Table 1**  
**Summary of the Tibet-III Array Observations of the *Fermi* Sources**  
**Tibet-III  $2\sigma \sim 0.3$  Crabs**

<i>Fermi</i> LAT Source (0FGL)	Class	R.A. (deg)	Decl. (deg)	Tibet-III Signi. ( $\sigma$ )	Milagro <sup>a</sup> Signi. ( $\sigma$ )	Source Associations
J1953.2+3249	PSR	298.325	32.818	-0.0	0.0	
J1954.4+2838	SNR	298.614	28.649	0.6	4.3	G65.1+0.6
J1958.1+2848	PSR <sup>b</sup>	299.531	28.803	0.1	4.0	
J2001.0+4352		300.272	43.871	-0.5	-0.9	
J2020.8+3649	PSR	305.223	36.830	2.2	12.4	MGRO J2019+37
J2021.5+4026	PSR <sup>b</sup>	305.398	40.439	2.2	4.2	
J2027.5+3334		306.882	33.574	-0.3	-0.2	
J2032.2+4122	PSR <sup>b</sup>	308.058	41.376	2.4	7.6	TeV J2032+4130 MGRO J2031+41
J2055.5+2540		313.895	25.673	-0.0	-0.0	
J2110.8+4608		317.702	46.137	0.3	1.1	
J2214.8+3002		333.705	30.049	-1.0	0.6	
J2302.9+4443		345.746	44.723	-0.0	-0.6	
LAT PSR J2238+59 <sup>c</sup>	PSR <sup>b</sup>	339.561	59.080	2.5	4.7	

All 7 sources  $>2\sigma$  are associated with pulsars. → PWNs?  
Six of them are coincident with Milagro sources.  
Remaining one has still positive significance  $1.4\sigma$  by Milagro.

**New**  
**Fermi-LAT**  
**Pulsar,**  
**Not included in**  
**analysis**

# Statistics



Total: 27 sources

$>2\sigma$ : 7 sources

Fig. 1.— Histograms show significance distribution of the *Fermi* bright sources observed by the Tibet-III array. The dashed curve indicates the expected normal Gaussian distribution.

# Chance Probability

Expected number of sources  $>2\sigma$   
 $27 \times 0.02275$  ( $2\sigma$  Upper prob.) = 0.61

Upper probability for 7 events against  $\lambda=0.61$   
assuming Poisson statistics

$$p(A=7) = 1 - \sum_{k=0}^{A-1} \frac{e^{-\lambda} \lambda^k}{k!}$$
$$= 3.8 \times 10^{-6} \sim 4.5\sigma$$

Without Crab

$\lambda = 26 \times 0.02275$  ( $2\sigma$  Upper prob.) = 0.59  
 $P(A=6) = 3.6 \times 10^{-5} \sim 4\sigma$

# Flux consistency between the Tibet-III and the Milagro

	Tibet $\sigma$	Milagro $\sigma$	Expected $\sigma$ from Milagro
J0534.6+2201	6.9	17.2	-
J0633.5+0634	2.4	1.4	0.56
J0634.0+1745	2.2	3.5	1.40
J1907.5+0602	2.4	7.4	2.97
<b>J2020.8+3649</b>	<b>2.2</b>	<b>12.4</b>	<b>4.97</b>
J2021.5+4026	2.2	4.2	1.68
J2032.2+4122	2.4	7.6	3.05

Underestimated?

J2020.8+3649 flux:

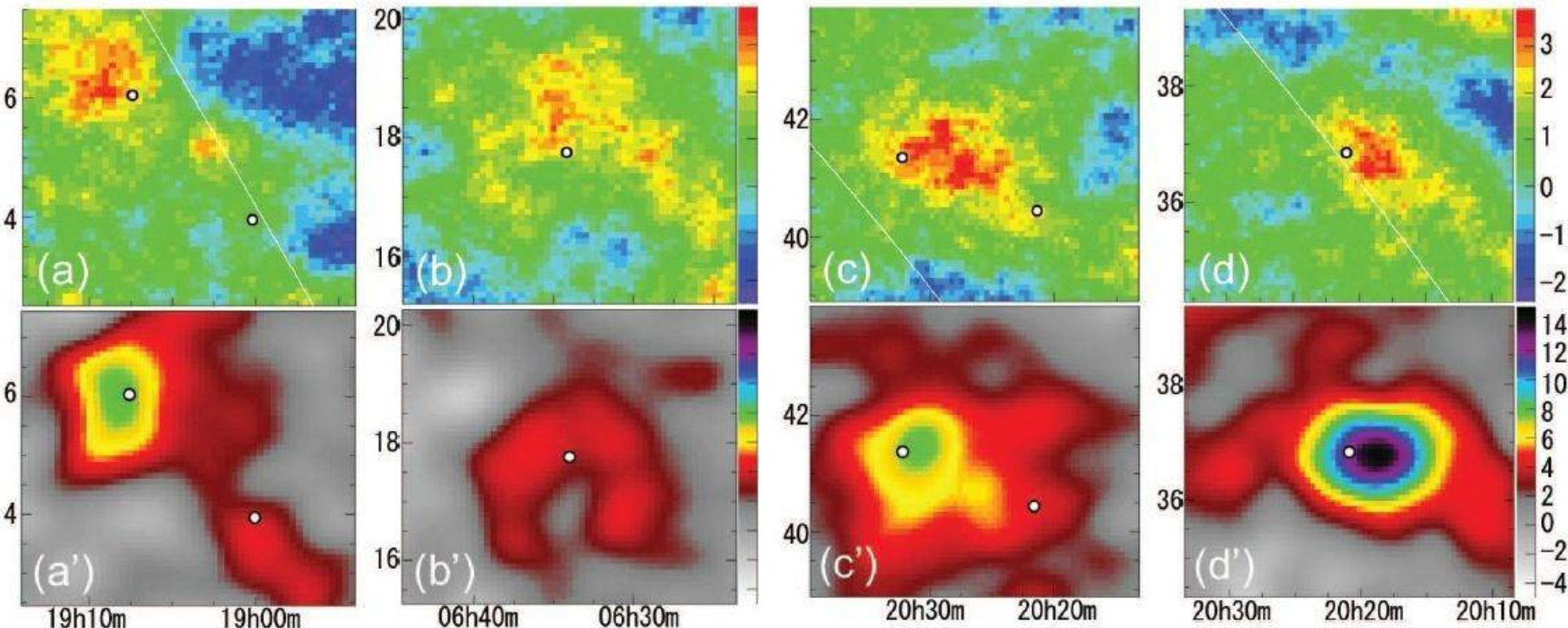
Tibet-III ( $30 \pm 14$ )% of the Crab flux above 3 TeV

Milagro ( $67 \pm 7$ )% of the Crab flux above 35 TeV

}  $\Delta = 2.3\sigma$

difference between them is calculated to be  $2.3\sigma$ . It can be interpreted by either statistical fluctuation, harder energy spectrum than the Crab, or an extended source instead of the assumed point-like source in this analysis.

# Tibet-III

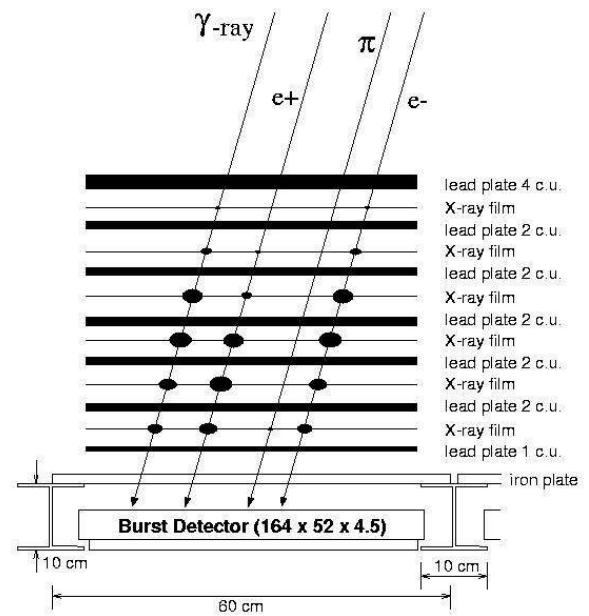


# Milagro

Fig. 2.— Comparisons of significance maps around the *Fermi* sources between the Tibet-III array (a)–(d) and the Milagro experiment (a')–(d') taken from Abdo et al. (2009c). Selected are *Fermi* sources with  $\geq 2\sigma$  significance by the Tibet-III array and  $\geq 3\sigma$  by the Milagro experiment except for the Crab. White points in each image show the *Fermi* source positions: (a)(a') J1907.5+0602/J1900.0+0356; (b)(b') J0634.0+1745 (Geminga); (c)(c') J2021.5+4026/J2032.2+4122; (d)(d') J2020.8+3649. The horizontal axis, vertical axis, and color contours indicate the right ascension, declination, and significance, respectively.

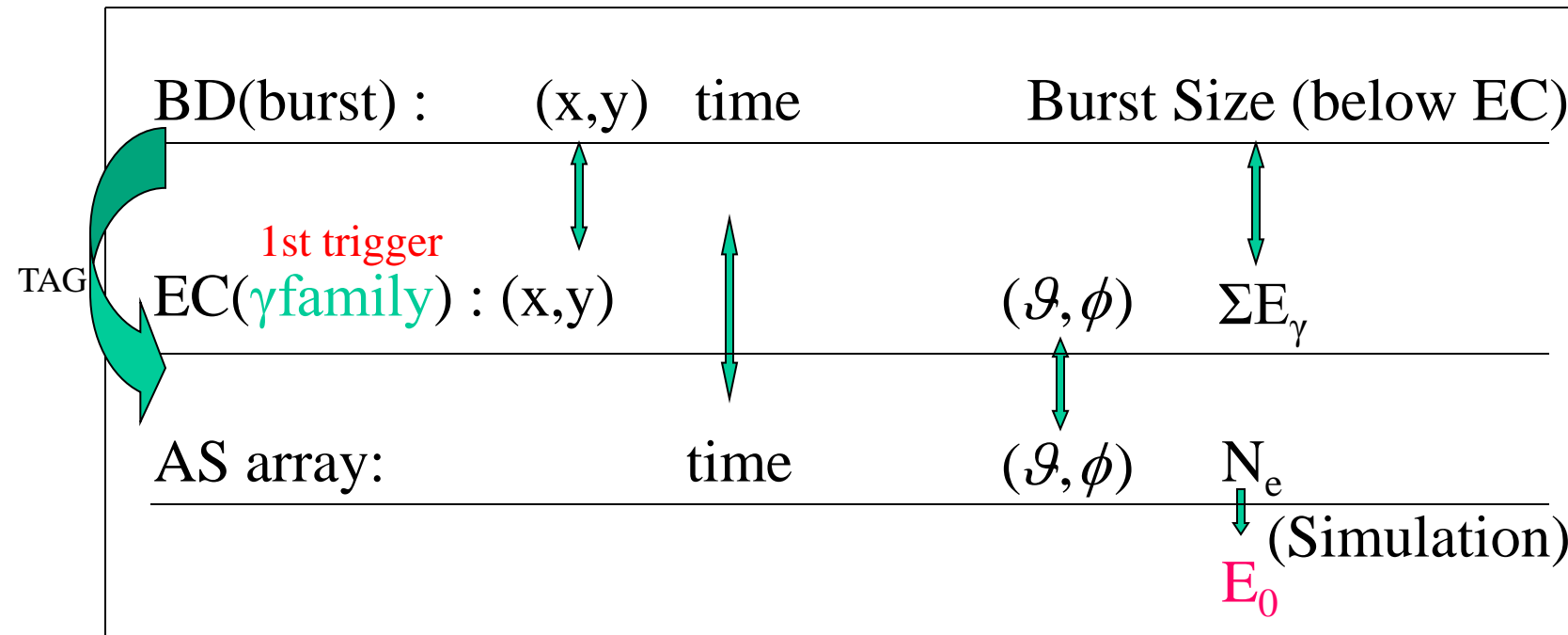
# 3. Knee Physics

# TIBET Hybrid Experiment



# How to obtain proton spectrum?

## Hybrid system



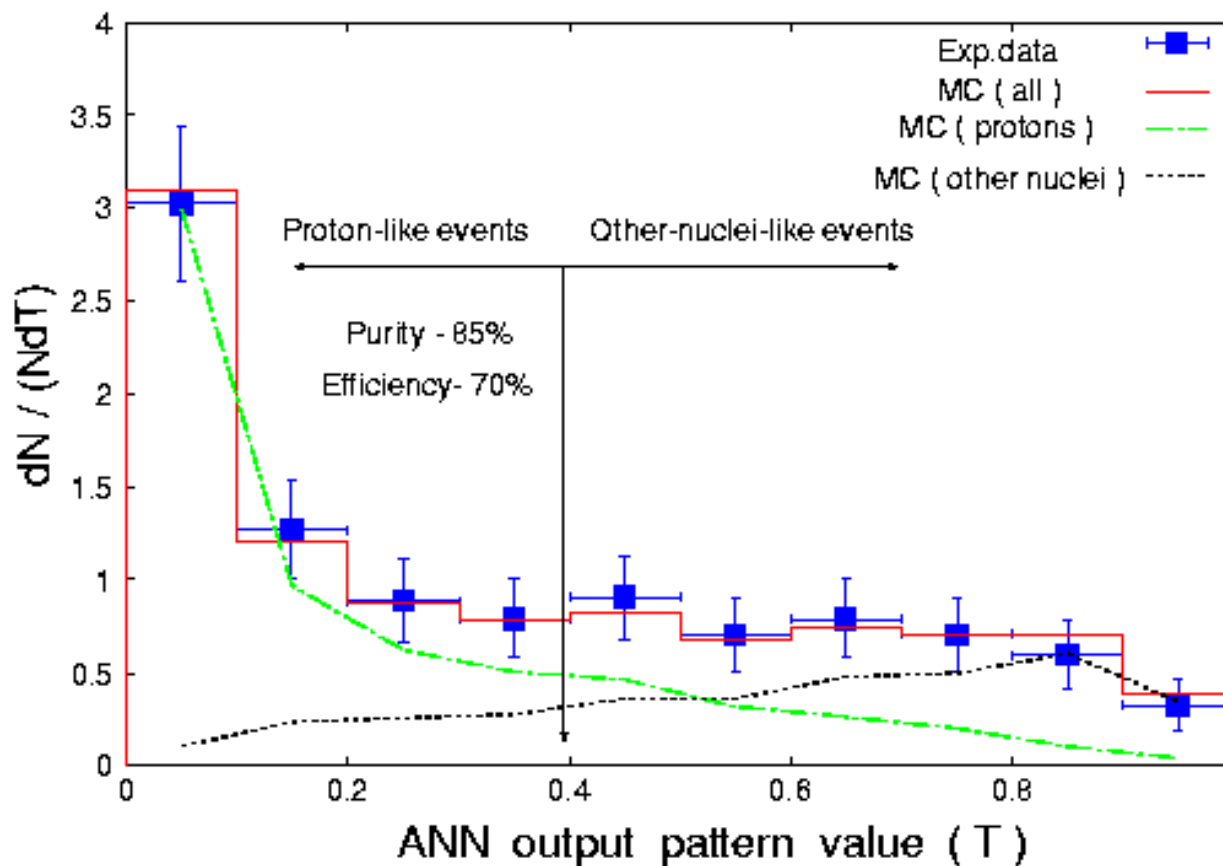
EC-Xray film image  $\rightarrow$  Scanner<sup>(GUI Software)</sup>  $\rightarrow$  family detection

AS+family matching event  $\rightarrow$  ANN  $\rightarrow$  Proton  
Identification  
 $\sim 100 \text{ eV}/699 \text{ days}$   
(Correlations)

# Artificial Neural Network

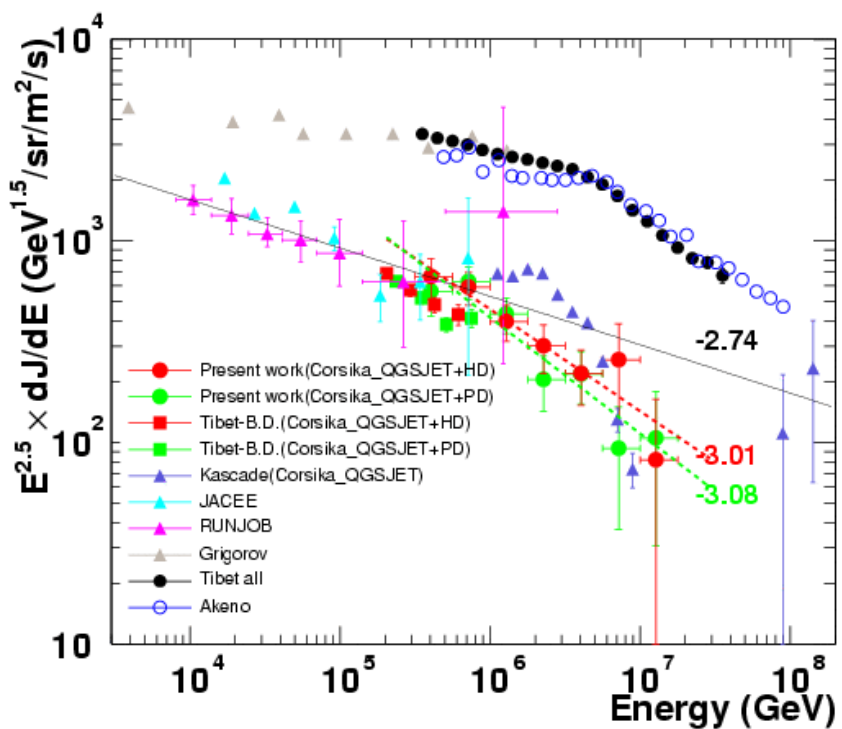
JETNET 3.5

Parameters for training:  $N_\gamma$ ,  $\Sigma E_\gamma$ ,  $\langle R_\gamma \rangle$ ,  $\langle ER_\gamma \rangle$ ,  $N_e$ ,  $\theta$

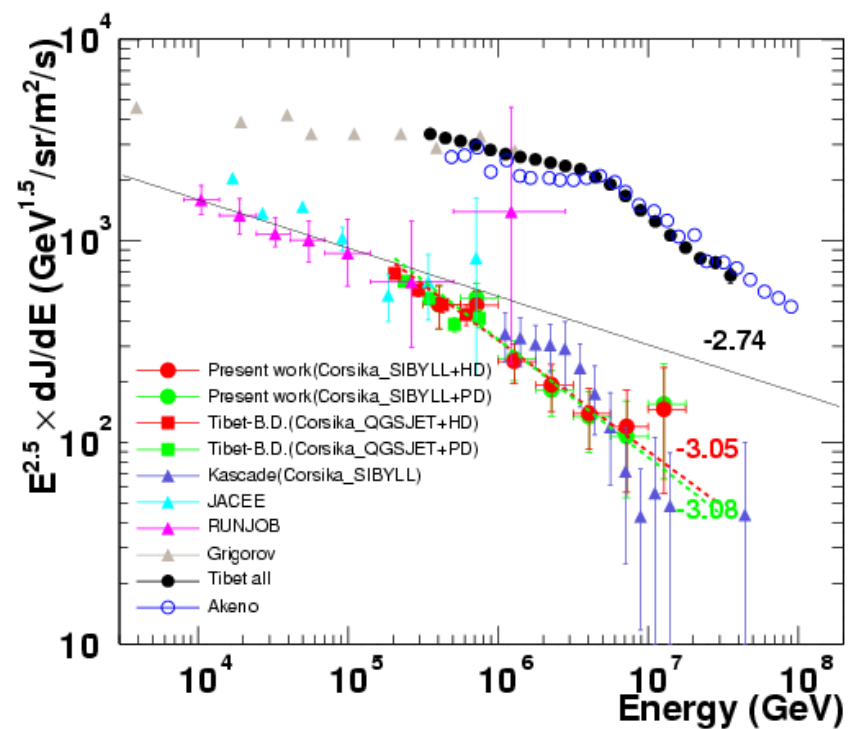


# Primary proton spectrum

(a) ( by QGSJET model )

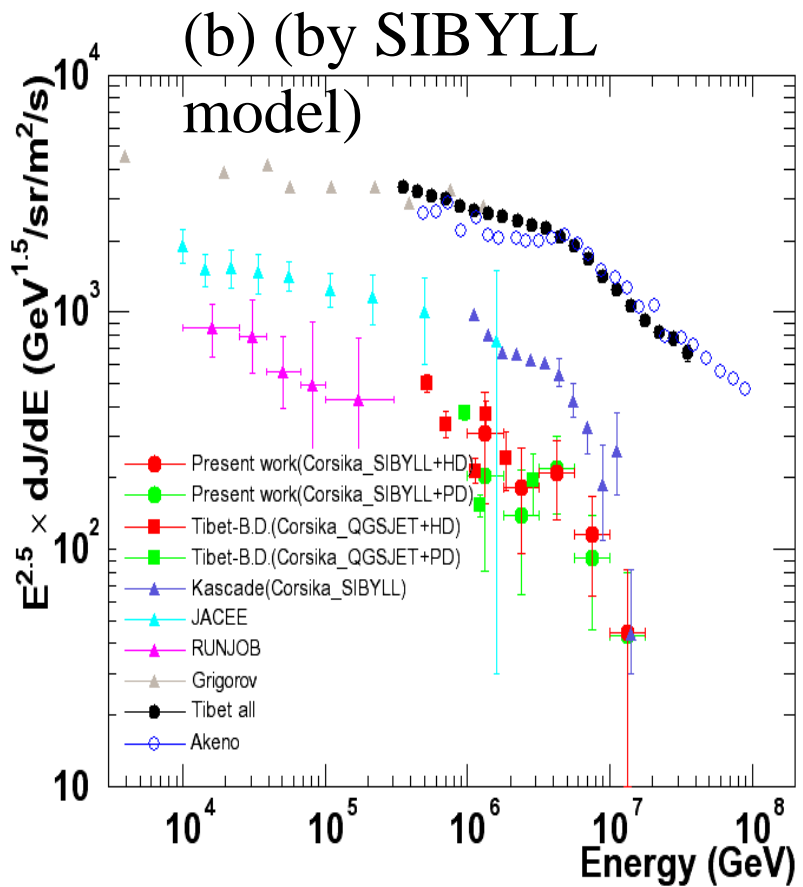
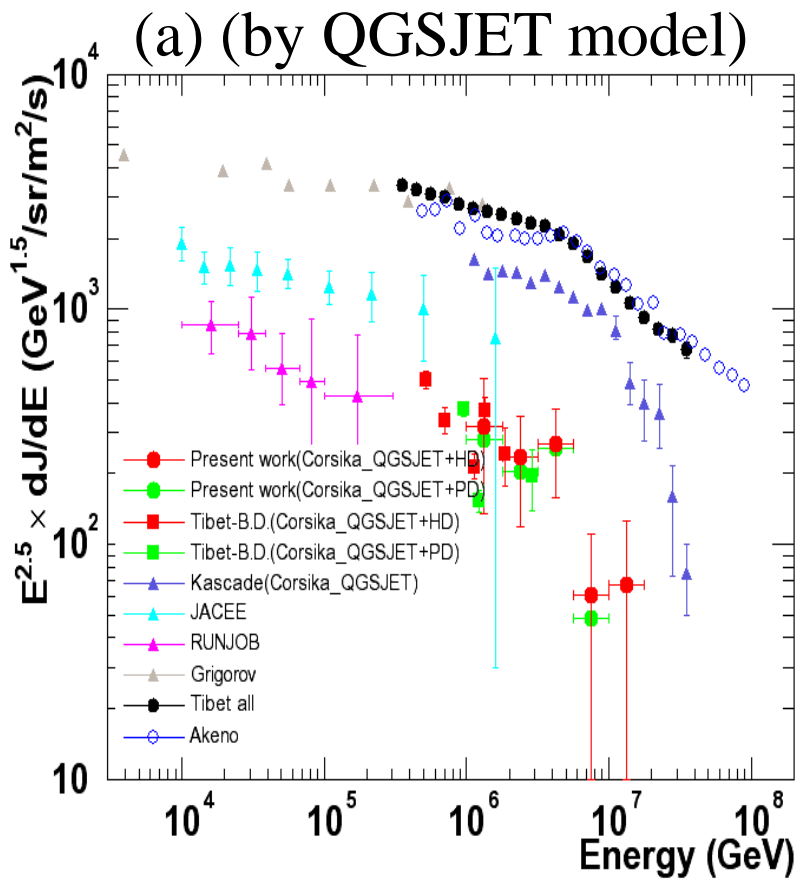


(b) ( by SIBYLL model )



(KASCADE data: astro-ph/0312295)

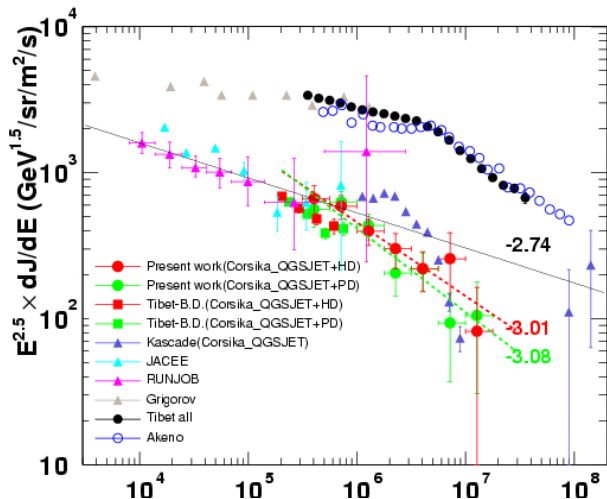
# Primary helium spectrum



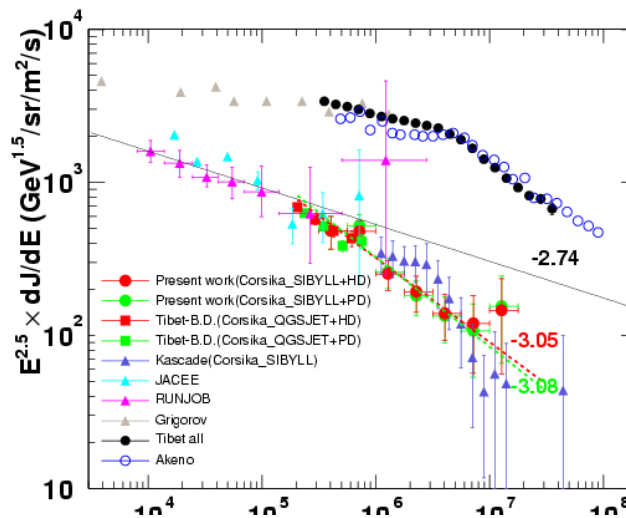
p+helium selection: purity=93%, efficiency=70%

# Primary Cosmic Ray Energy Spectrum

CORSIKA\_QGSJET

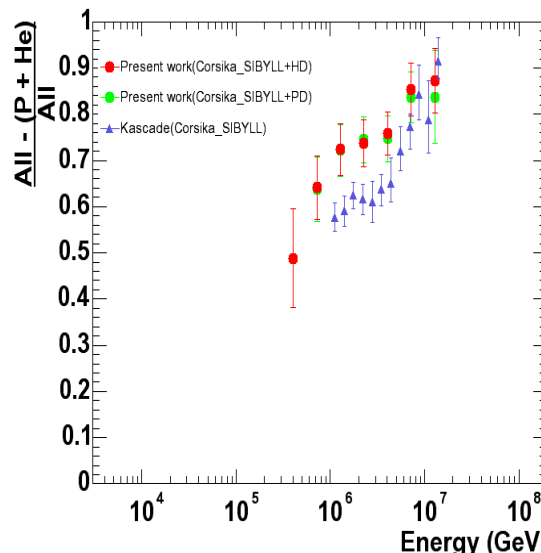
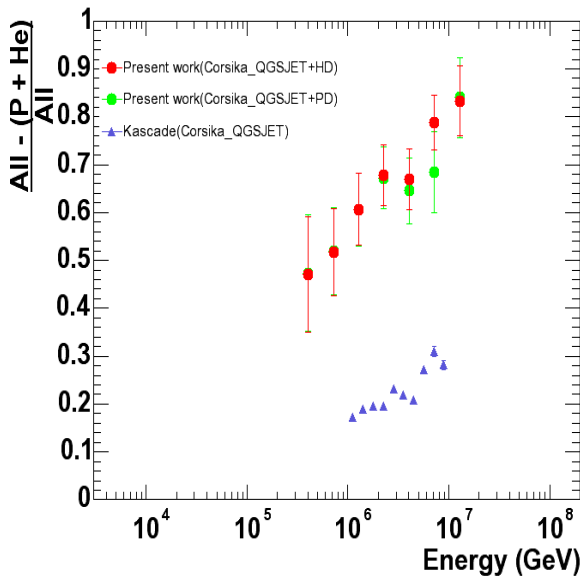


CORSIKA\_SIBYLL



Proton

Small model  
dependence  
(30 %)



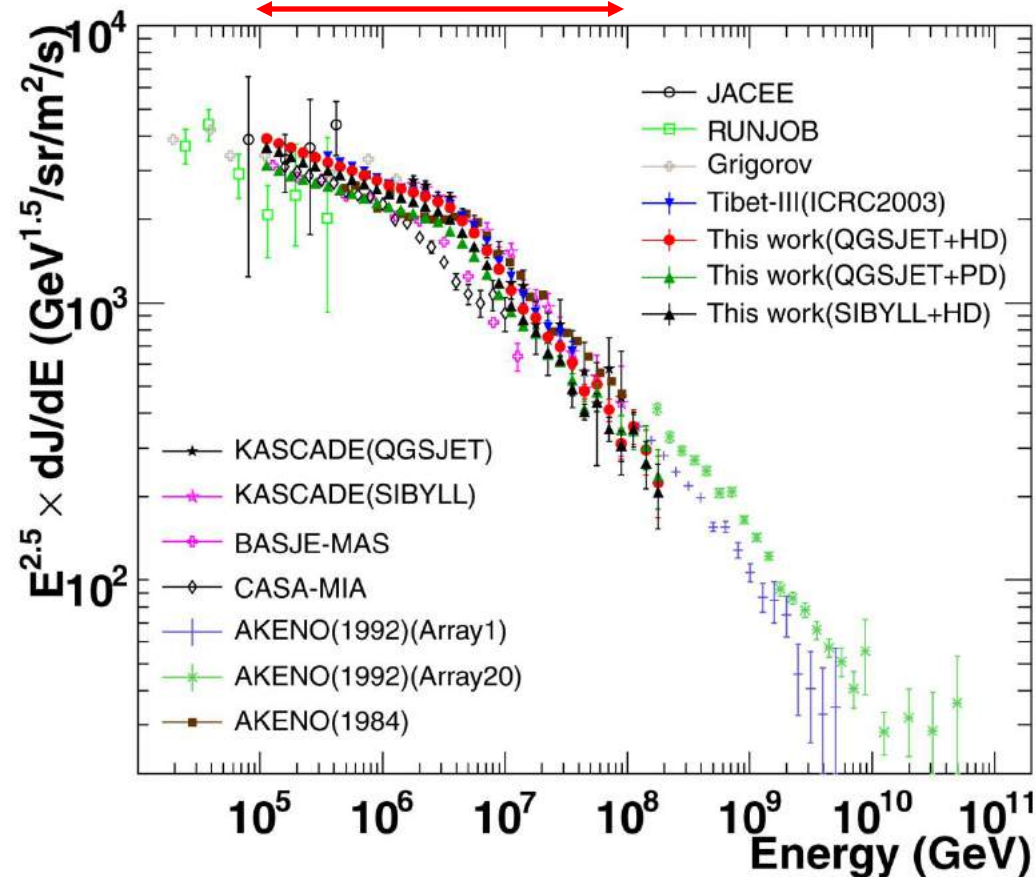
All - (p+He)

All

PL B632 (2006)  
58-64

# All Particle Energy Spectrum in the Knee region

$10^{14}\text{eV} \sim 10^{17}\text{eV}$  (3 orders)



Amenomori *et al.*,  
ApJ, 678, 1165 (2008)

Model	Index of spectrum	Energy range (eV)
QGSJET +HD	$-2.67 \pm 0.01$	$< 10^{15} \text{ eV}$
	$-3.10 \pm 0.01$	$> 4 \times 10^{15} \text{ eV}$
QGSJET +PD	$-2.65 \pm 0.01$	$< 10^{15} \text{ eV}$
	$-3.08 \pm 0.01$	$> 4 \times 10^{15} \text{ eV}$
SIBYLL +HD	$-2.67 \pm 0.01$	$< 10^{15} \text{ eV}$
	$-3.12 \pm 0.01$	$> 4 \times 10^{15} \text{ eV}$

# Multiple source model

Cutoff spectrum is written as

(Slide from M.Shibata, Y.N.U.)

$$\frac{dj(E, \varepsilon)}{dE} = j_0 E^{-\gamma} \exp(-\frac{E}{\varepsilon}).$$

Distribution of sources with acceleration limit  $\varepsilon$  is assumed as,

$$S(x) = \frac{1}{\Gamma(\Delta\gamma)} \frac{1}{x^{1+\Delta\gamma}} \exp(-\frac{1}{x})$$

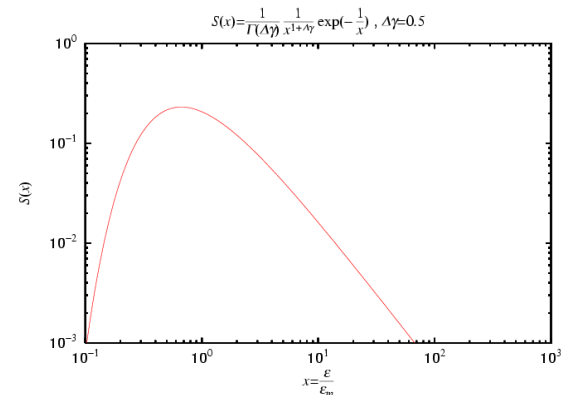
where  $x = \varepsilon/\varepsilon_m$ ,  $\varepsilon_m$  is the minimum value of the acceleration limit.  $S(x)$  is normalized as

$$\int_0^\infty S(x)dx = 1.$$

Then, superposition of the multiple sources gives following formula for cosmic-ray energy spectrum.

$$\frac{dJ}{dE} = \int_0^\infty \frac{dj(E, \varepsilon)}{dE} S\left(\frac{\varepsilon}{\varepsilon_m}\right) \frac{d\varepsilon}{\varepsilon_m} = \frac{j_0 E^{-\gamma}}{(1 + E/\varepsilon_m)^{\Delta\gamma}}$$

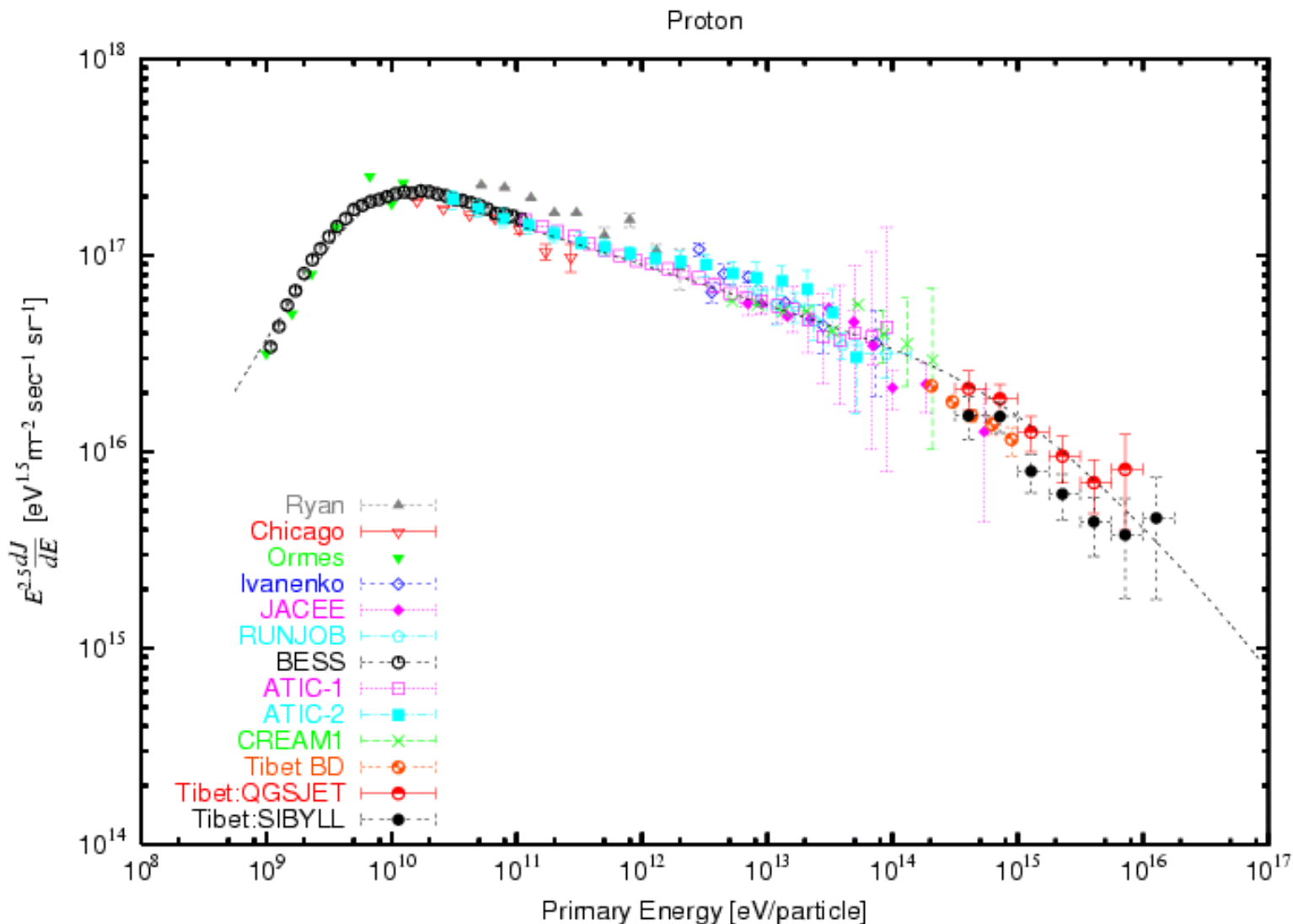
$$\varepsilon_m \equiv \varepsilon_b$$



Distribution of  
acceleration power  
of cosmic rays

# Proton Spectrum

## Direct measurement and Tibet combined



# Broken power law formula to describe proton spectrum

$$\frac{dj}{dE} = j_0 E^{-\gamma} \left[1 + \frac{E}{\varepsilon_b}\right]^{-\Delta\gamma}$$

$\varepsilon_b$  : break point ( $7 \times 10^{14}$  eV for proton)

$\Delta\gamma$ : difference of power index before and after the break  
point

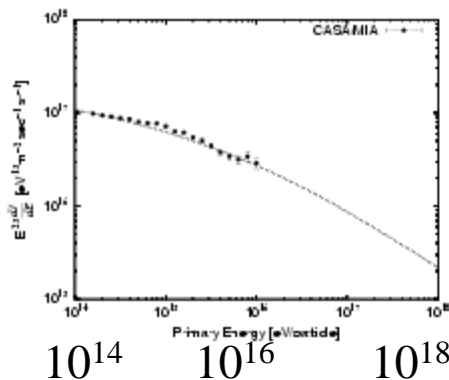
( $\Delta\gamma = 0.4$ )

(Slide from M.Shibata, Y.N.U.)

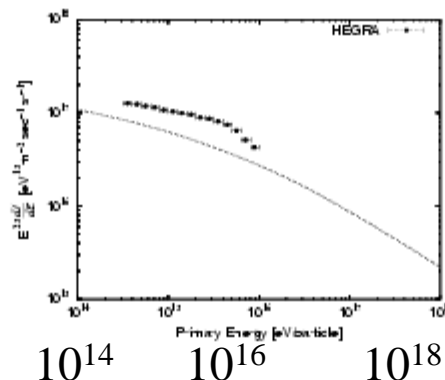
# All particle spectrum around the knee

(Slide from M.Shibata, Y.N.U.)

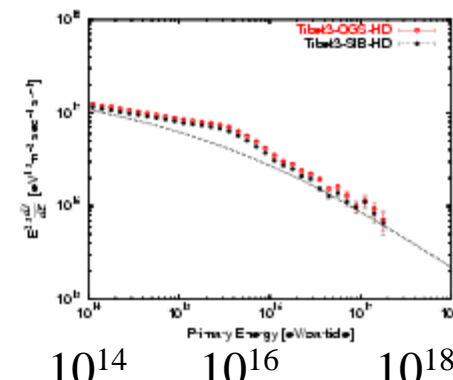
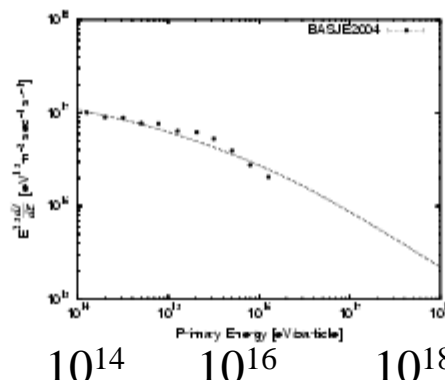
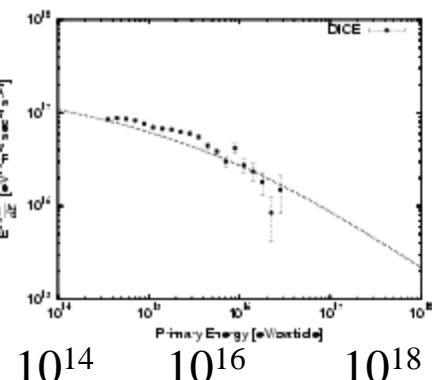
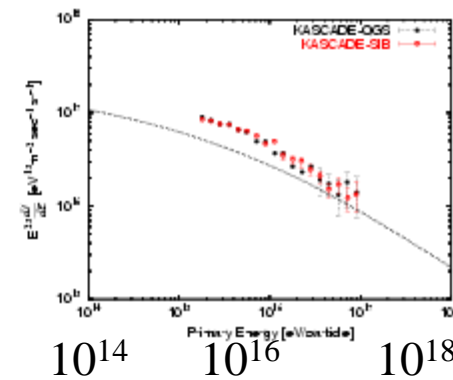
CASA/MIA



HEGRA



KASCADE



DICE

BASJE

TIBET

# Extra component

All data agree if we apply energy scale correction within 20% by normalizing to direct observations.

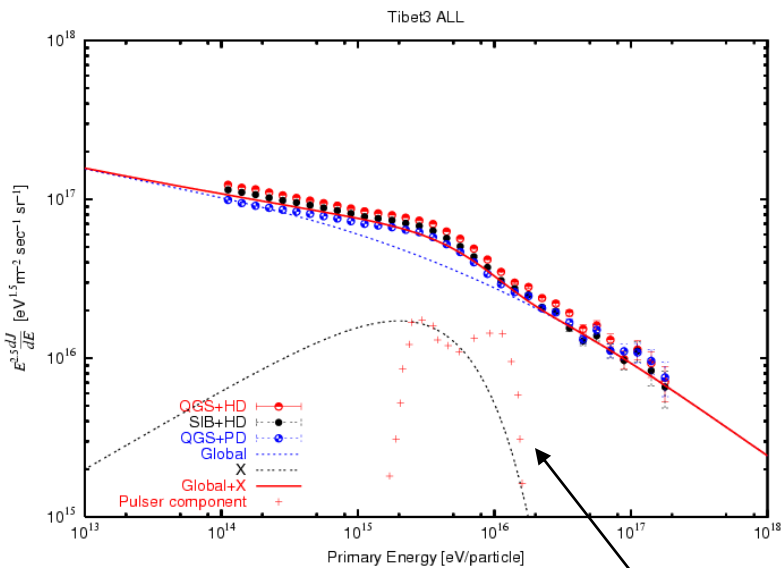
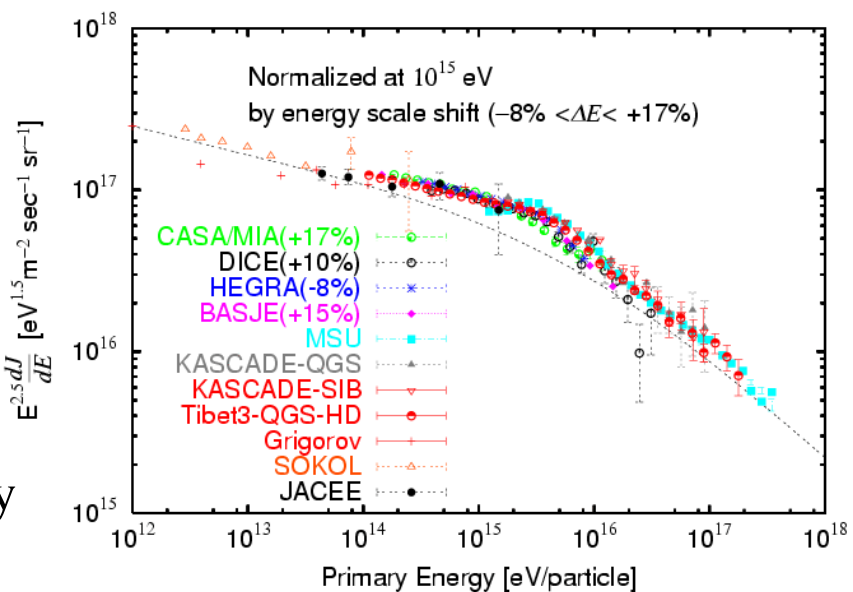
Extra component can be approximated by

$$E^{-2} \exp\left[-\frac{E}{4\text{PeV}}\right],$$

suggesting **nearby source(s)**.

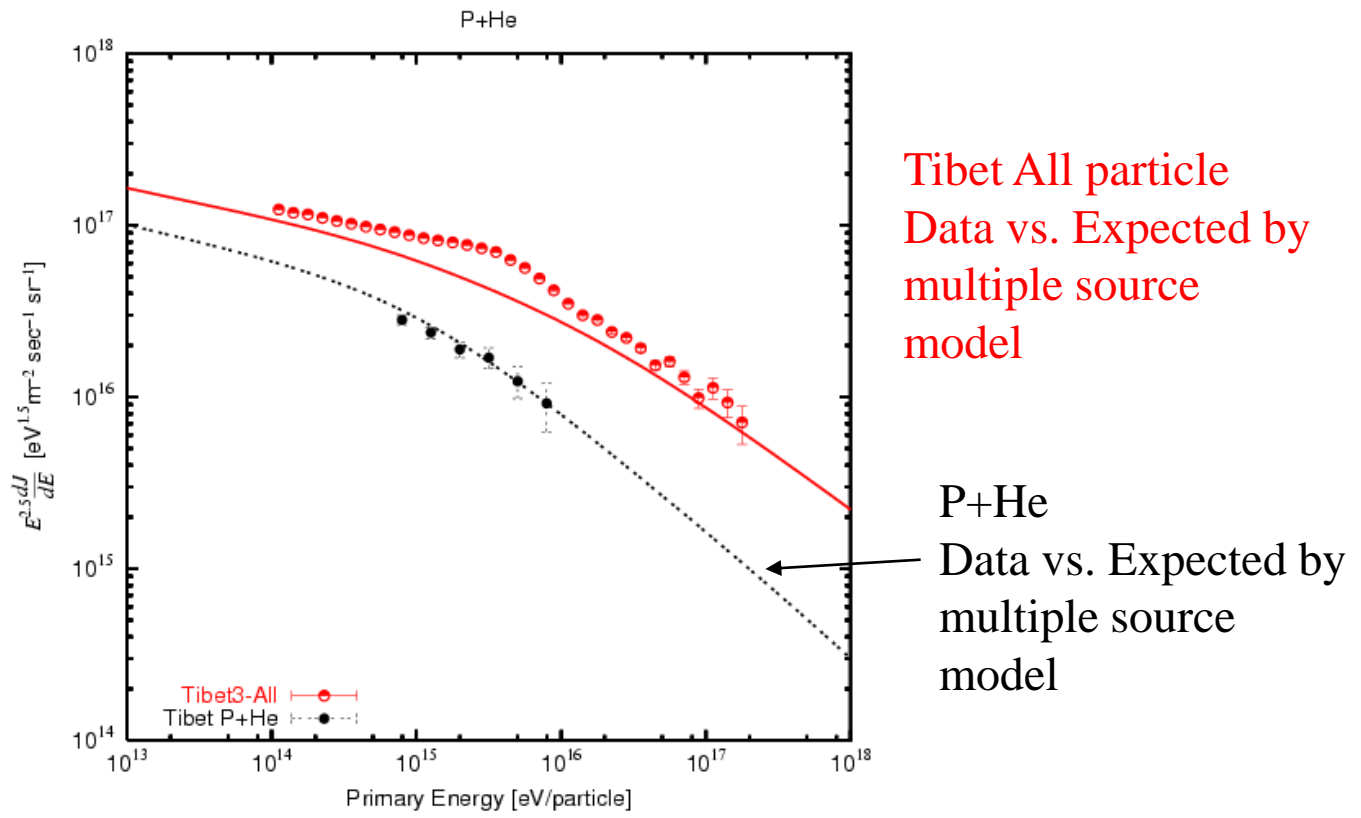
Since P and He component do not show the excess at the knee, the extra component should be attributed to heavy element such as Fe.

(Slide from M.Shibata, Y.N.U.)

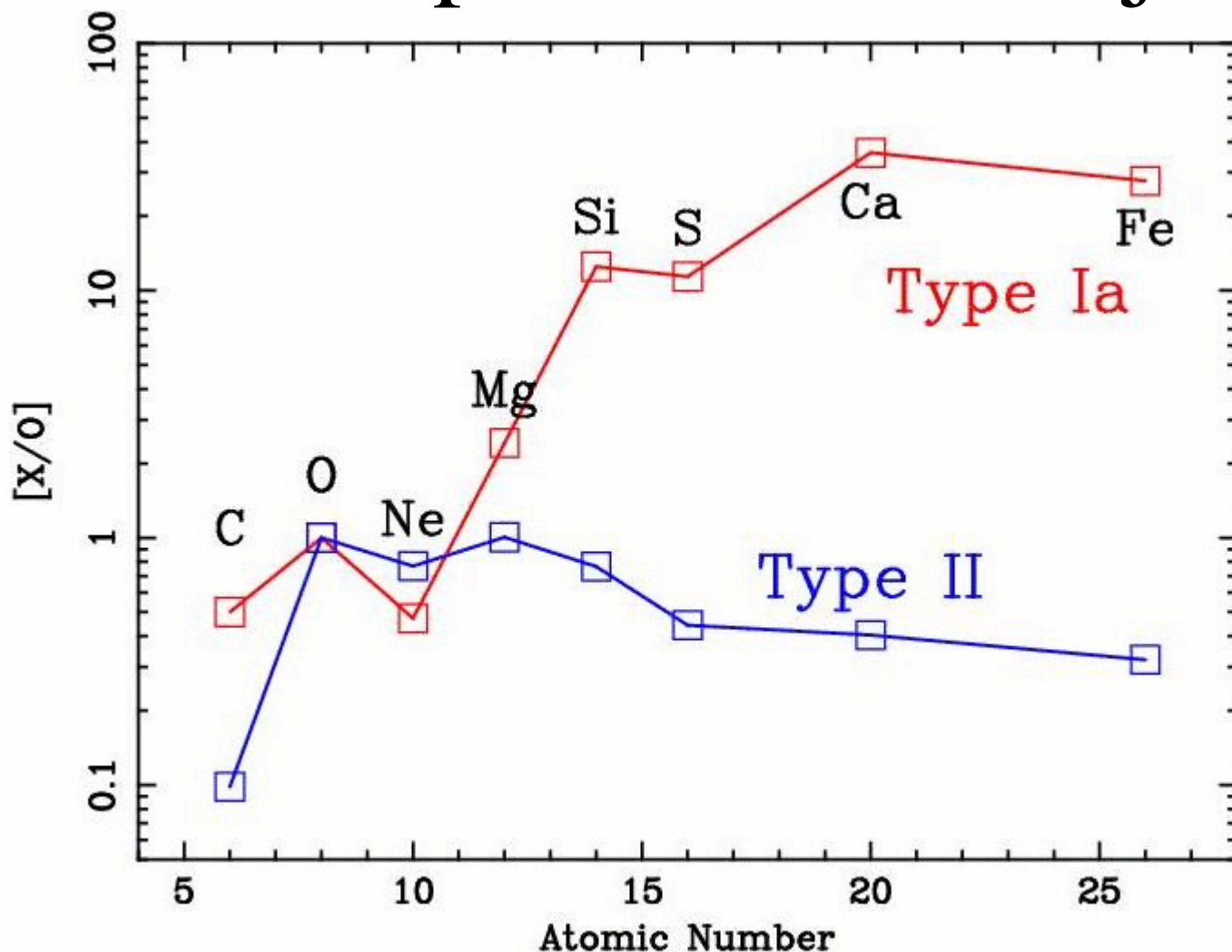


(W.Bednarek and R.J.Protheroe ,2002,APh)

# Tibet P +He spectrum does not show excess at the knee



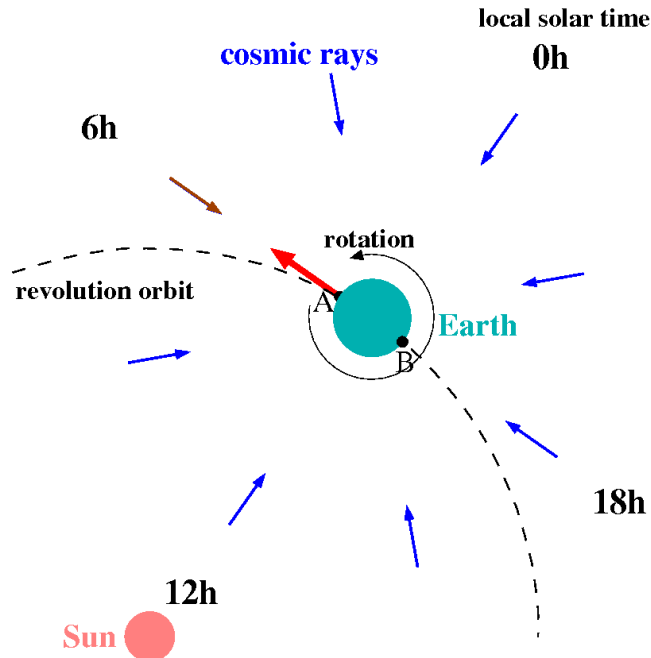
# Chemical composition of SN ejecta



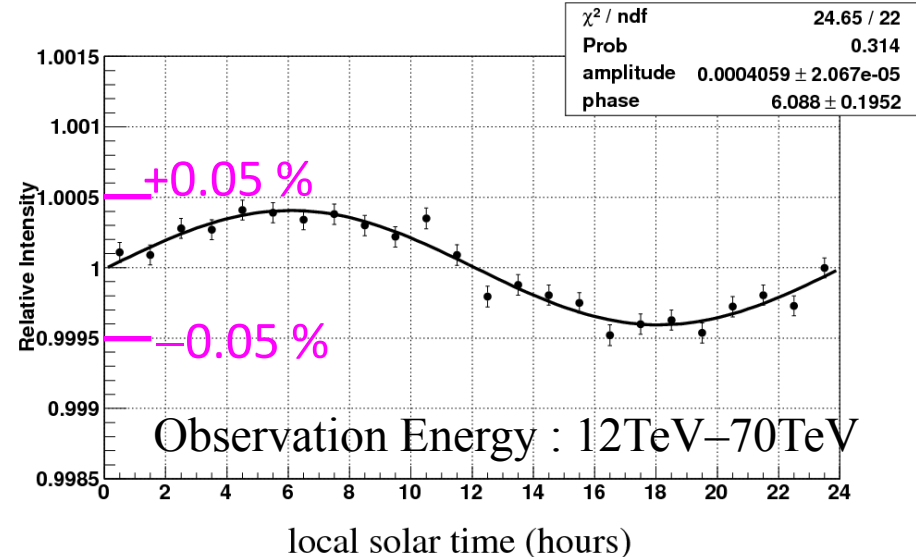
(Nomoto,K et al. Nucl. Phys. A, 621, 467, 1997)

# 4. Anisotropy

# Compton-Getting Anisotropy at Solar Time Frame



Amenomori et al., ApJL, 672 (2008) L53



**Expected** Amplitude  $3.86 \times 10^{-2} \%$

Phase 6 [hr]

**Data** Amplitude  $(4.06 \pm 0.21) \times 10^{-2} \%$

Phase  $6.1 \pm 0.2$  [hr]

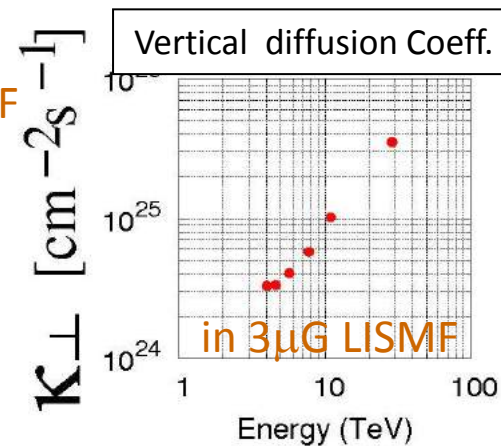
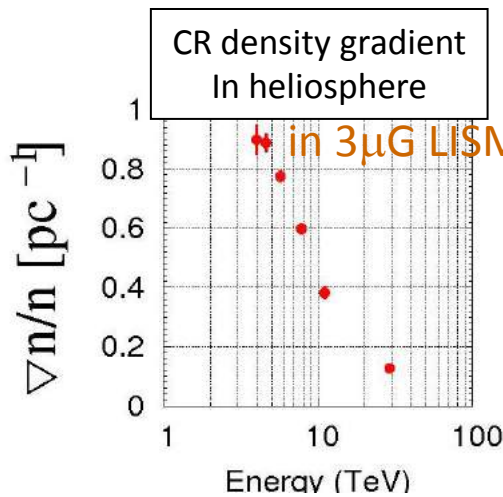
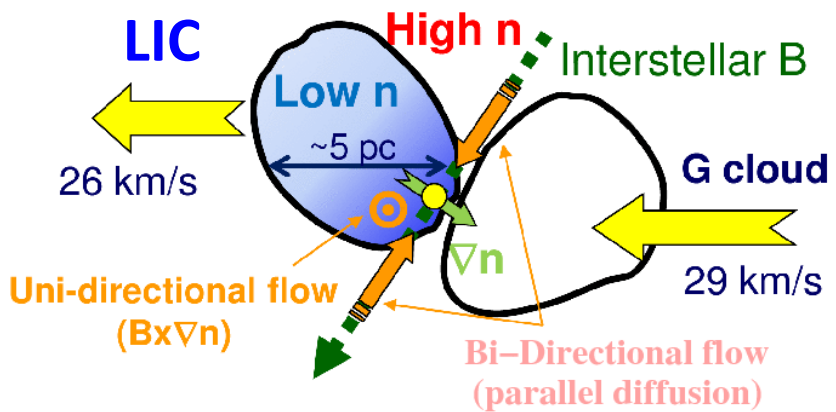
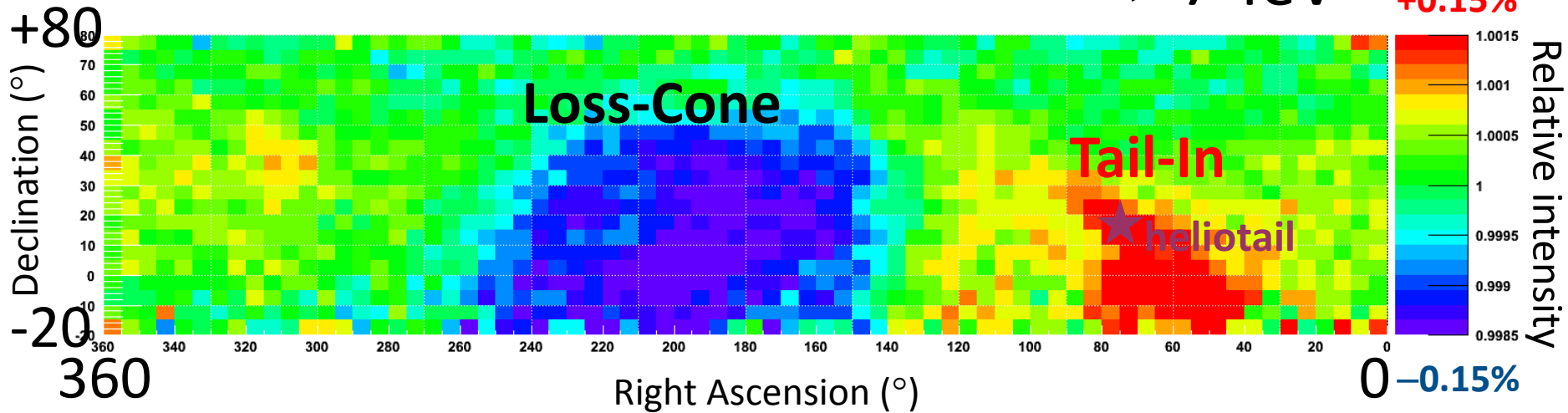
→ CG detected at  $19.6\sigma$  consistent with expected

- Reliability and calibration for sidereal anisotropy ( $\sim 0.01\%$ )
- Only Tibet AS $\gamma$  experiment showing a clear sinusoidal curve

# Modeling Sidereal Anisotropy : Origin of anisotropy

> 7 TeV

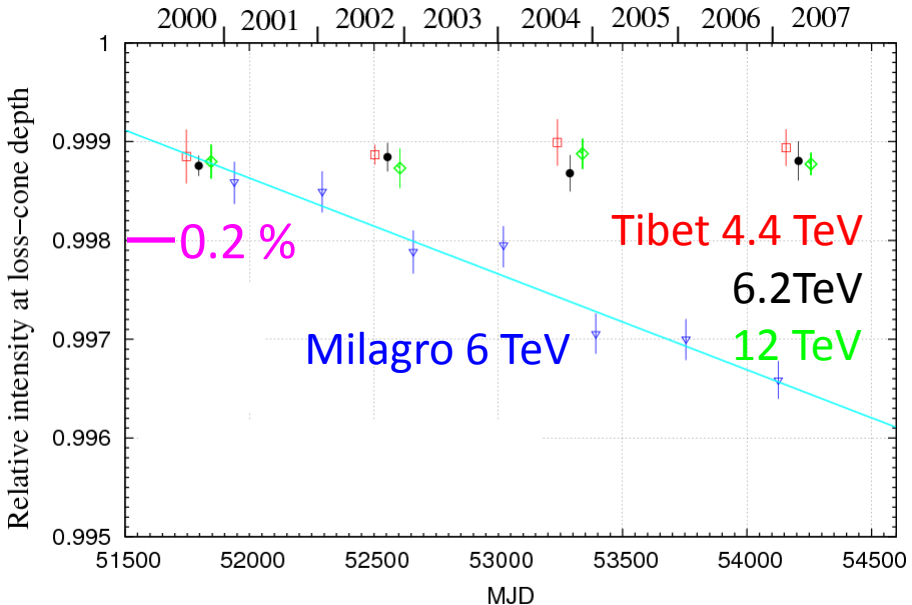
+0.15%



Stimulus to CR transport theory and future space-ship experiment like Voyagers

# Sidereal Anisotropy : Yearly Variation of Loss-Cone Amplitude?

Amenomori et al., App, 36 (2012) 237



Fitting by  $\alpha$  (MJD–53000) +  $\beta$

Milagro 6 TeV

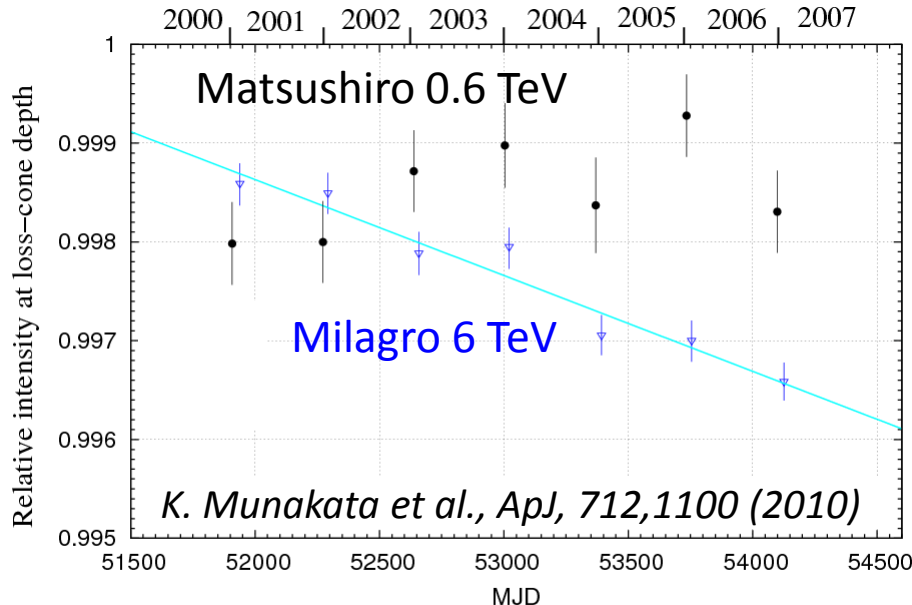
$$\alpha = (0.97 \pm 0.11) \times 10^{-4} \% \text{ [/day]}$$

Milagro 6 TeV

Tibet 4.4 TeV

6.2TeV

12 TeV



Tibet 4.4 TeV

$$\alpha = (0.05 \pm 0.13) \times 10^{-4} \% \text{ [/day]}$$

inconsistent with Milagro ( $6.1\sigma$ )

6.2 TeV

$$\alpha = (0.004 \pm 0.099) \times 10^{-4} \% \text{ [/day]}$$

inconsistent with Milagro ( $6.6\sigma$ )

11 TeV

$$\alpha = (-0.002 \pm 0.095) \times 10^{-4} \% \text{ [/day]}$$

inconsistent with Milagro ( $6.7\sigma$ )

Matsushiro 0.6 TeV

$$p_0 = (0.32 \pm 0.22) \times 10^{-4} \% \text{ [/day]}$$

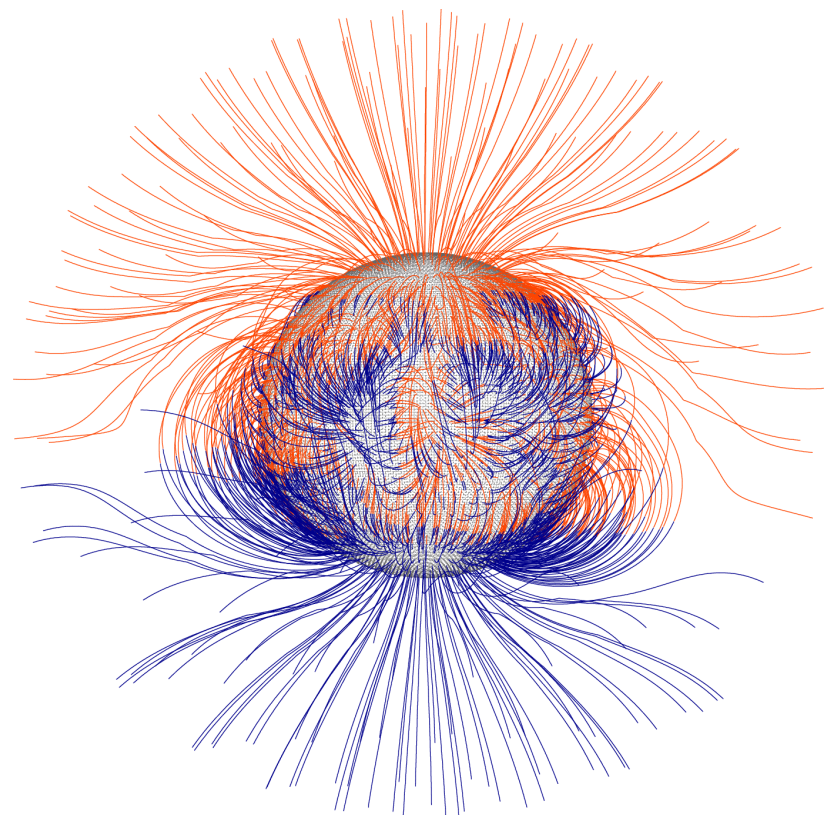
inconsistent with Milagro ( $5.3\sigma$ )



Milagro's yearly variation of Loss-Cone amplitude ruled out at multi-TeV & sub-TeV

# 5. The Sun's Shadow

# Probe of the Solar Magnetic Field with the “Cosmic-Ray Shadow” of the Sun



# Tibet-III Air Shower Array (>1999)

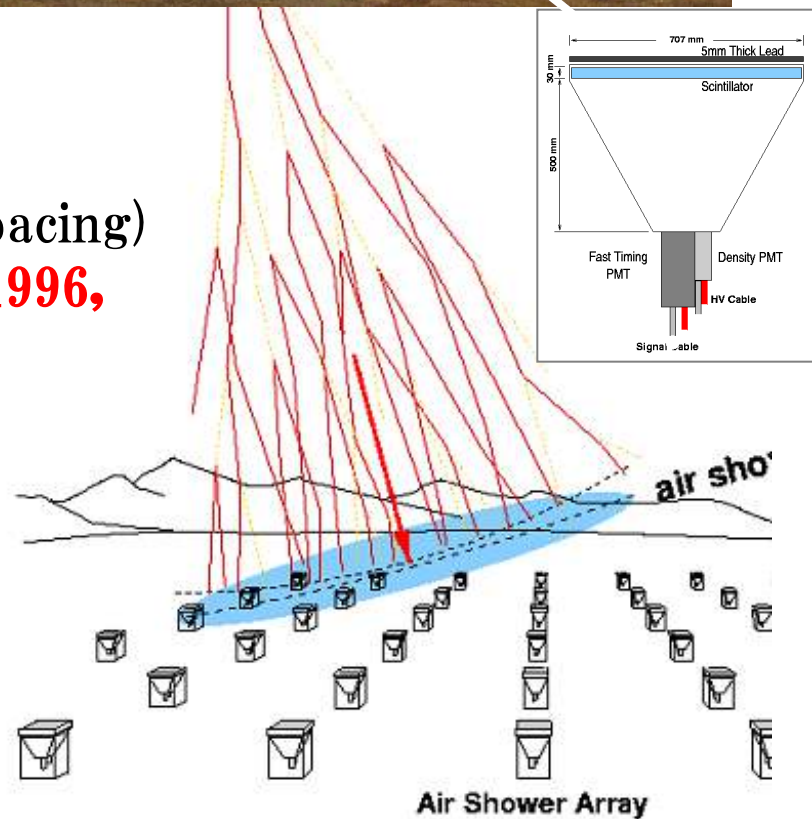


□ Tibet ( $90.522^{\circ}\text{E}$ ,  $30.102^{\circ}\text{N}$ ) 4300m a.s.l.

□ No. of detectors  $0.5 \text{ m}^2 \times 789$  (7.5m spacing)

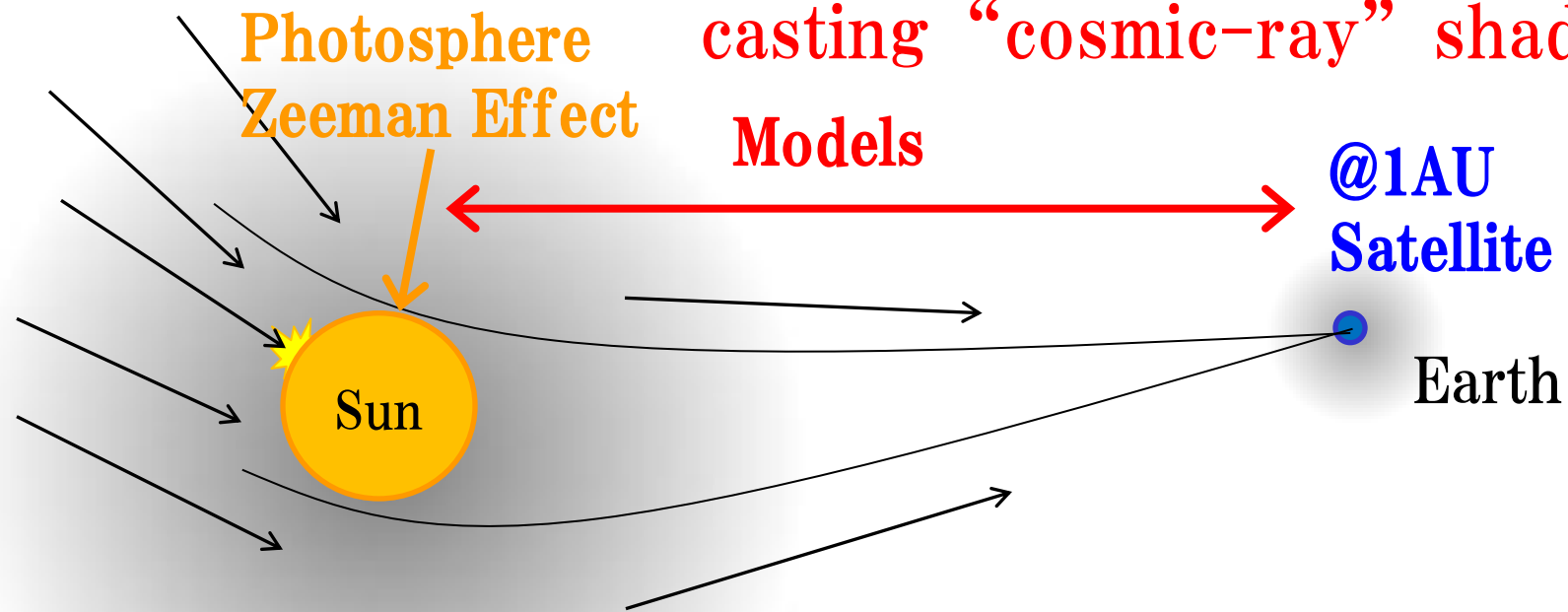
→To keep the AS data consistency from 1996,  
we use the Tibet-II array configuration  
(221 detectors, 15m spacing)

□ Modal Energy 10 TeV  
□ Angular Resolution  $0.9^{\circ}$



# Sun's Shadow

Sun's shadow



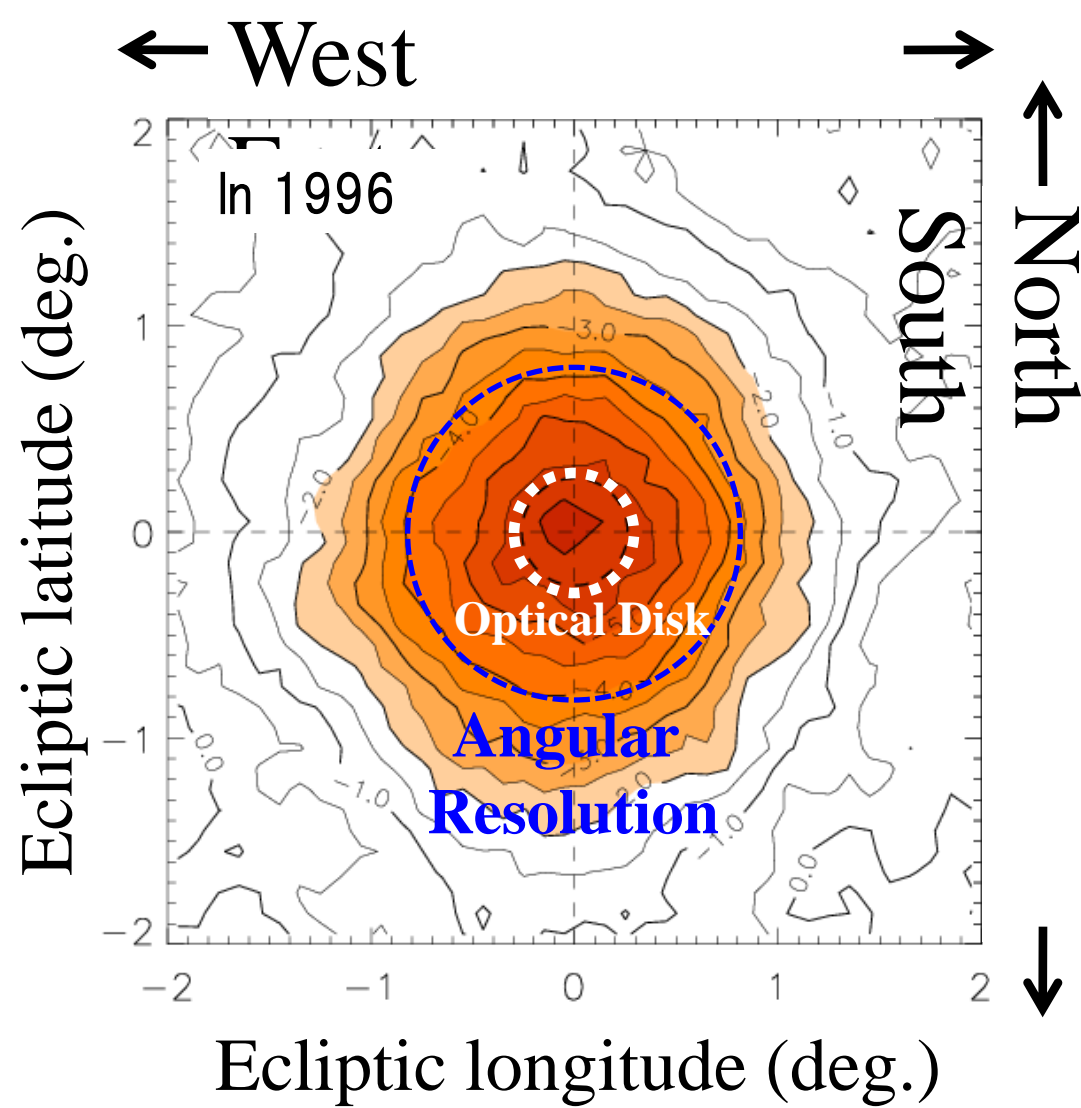
TeV Charged Particles  
Larmor Radius

$\sim 7.4 \text{ AU}$  ( $B = 30 \mu\text{G}$  near Earth)

$\sim 0.16 R_\odot$  ( $B = 300 \text{ mG}$  near Sun)

Probe of solar magnetic fields!

# Analysis of the Sun's Shadow

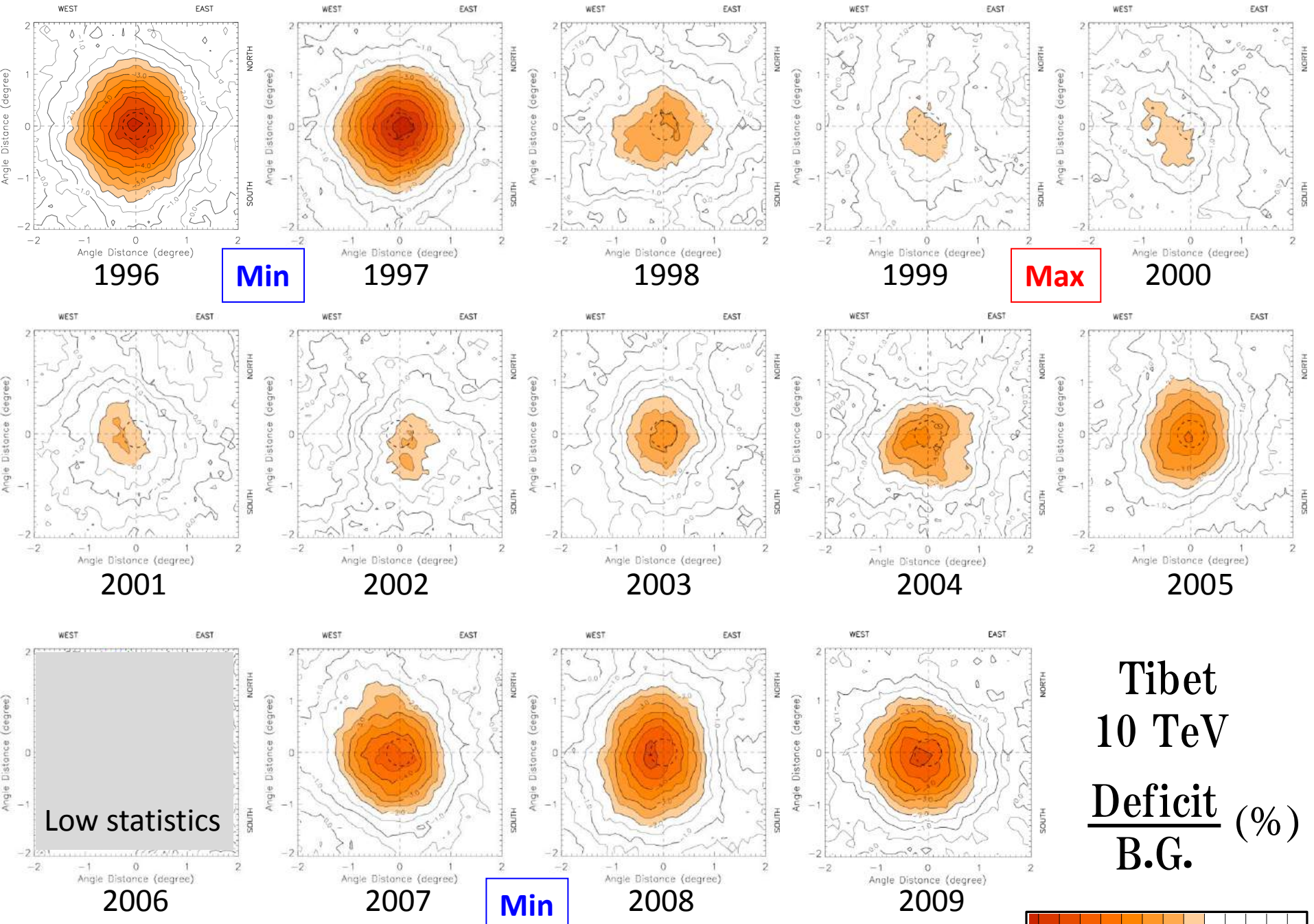


$4^{\circ} \times 4^{\circ}$  Cosmic ray density  
Map centered at the Sun  
(Ecliptic coordinate)

Deficit ratio to CR flux  
Maximum -6% to CR flux

Angular resolution( $0.9^{\circ}$ )  
Optical disk size( $0.26^{\circ}$ )

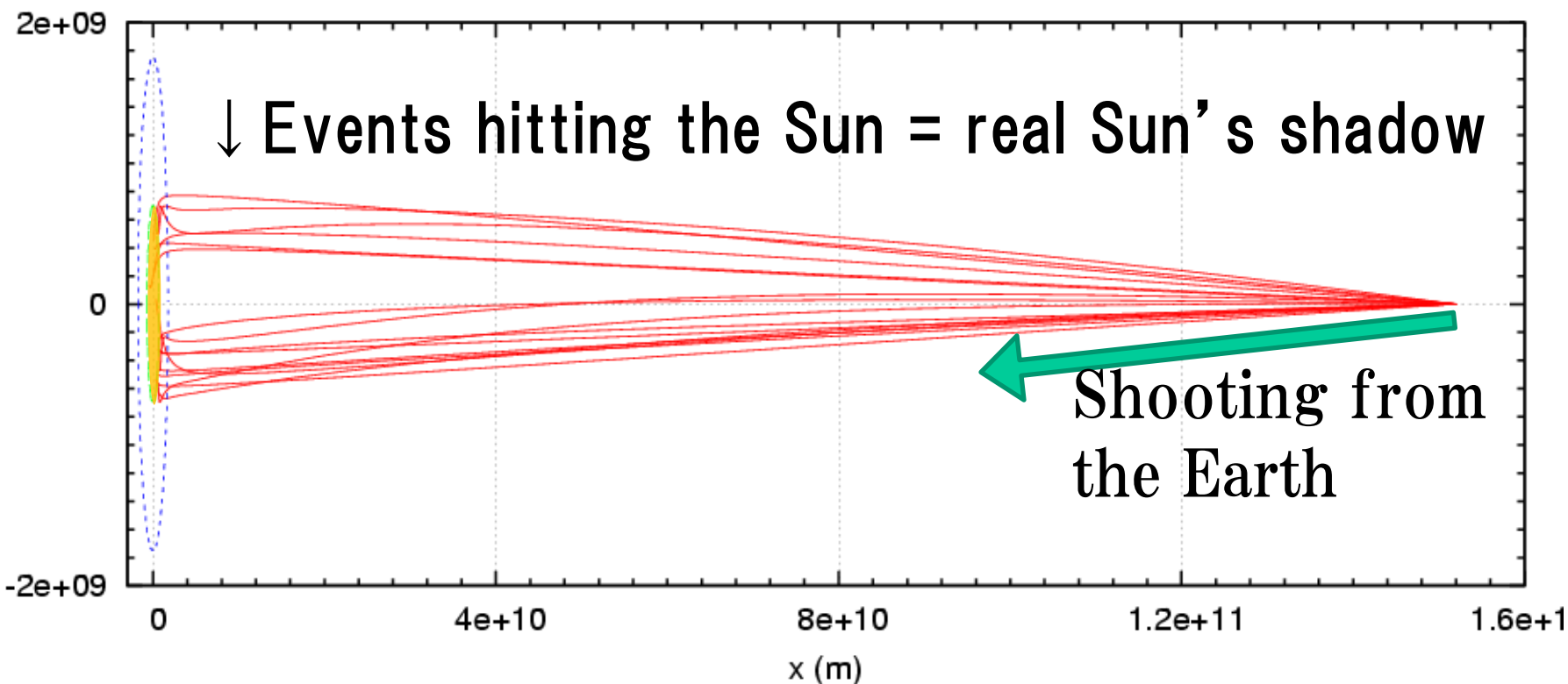
In this map, we analyze  
**deficits** and **positions**  
depending on properties  
of the solar magnetic field<sup>62</sup>



Tibet  
10 TeV  
Deficit (%)  
B.G.

# MC Simulation

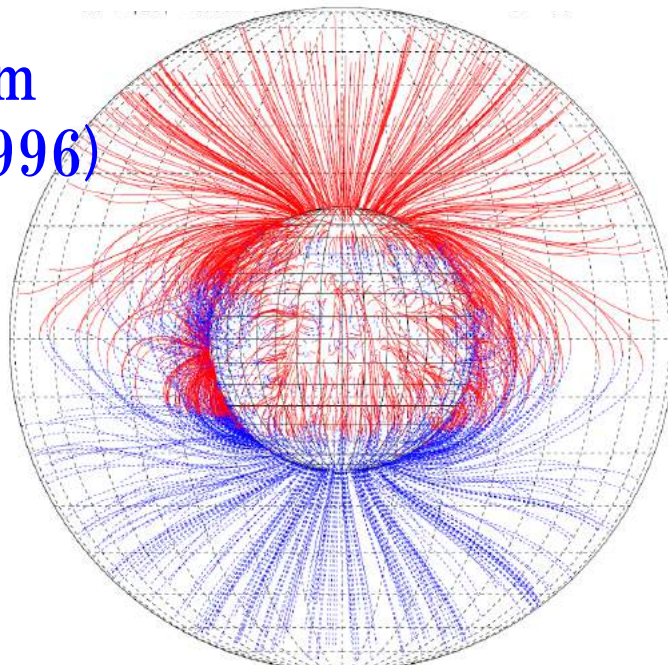
Antiparticles are traced back to the Sun from the Earth assuming the detailed magnetic fields



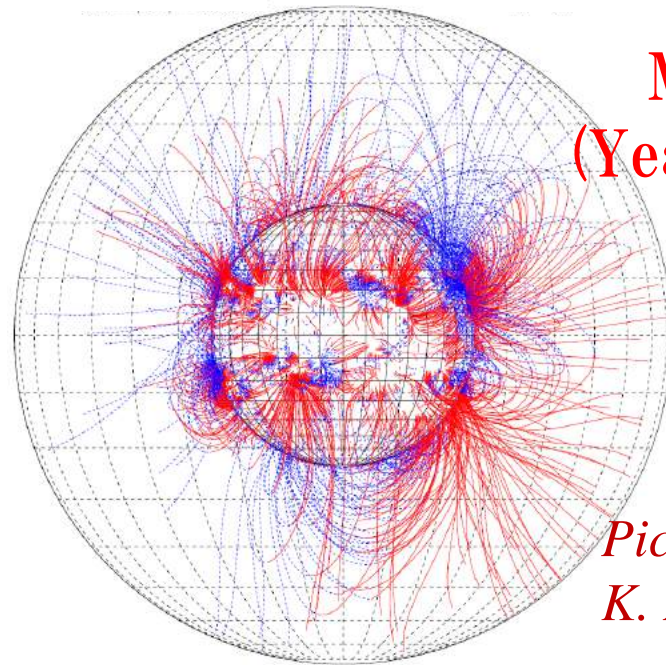
# Magnetic fields

- Coronal → Source Surface models (PFSS / CSSS)  
derived from photospheric MF observation  
for each Sun rotation ( $\sim 27$  days)
- IMF → Parker Spiral Model  
including latitudinal dependence of solar wind
- Geomag. → Dipole model

Minimum  
(year 1996)  
PFSS



Maxmum  
(Year 2000)  
PFSS



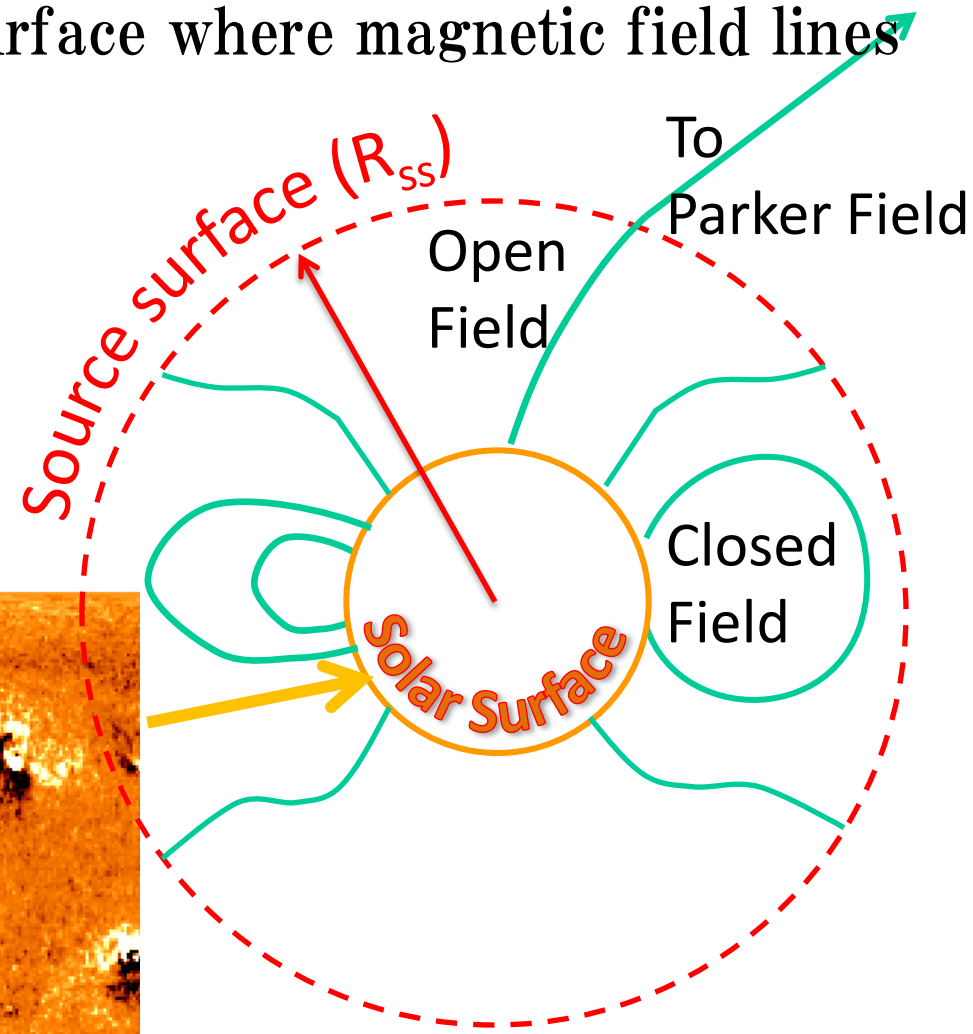
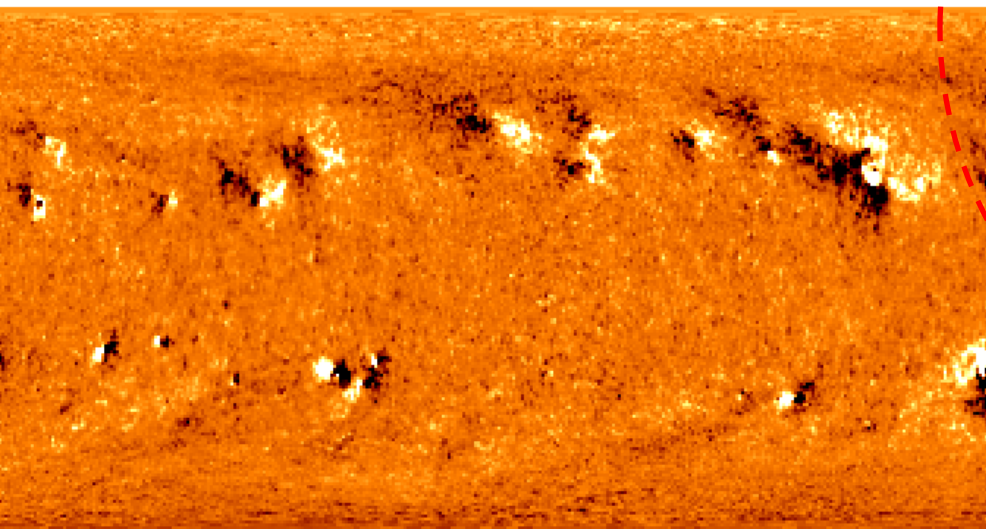
*Pictures from  
K. Hakamada*

# Source Surface Model

B is calculated from observed photospheric magnetic fields based on the Maxwell equation. The source surface is defined as a boundary spherical surface where magnetic field lines become purely radial.

Standard  $R_{ss} = \sim 2.5R_\odot$

Magnetograph (Zeeman Effect)  
The Kitt Peak Vacuum Telescope  
(FeI 868.8, 630.1 and 630.2nm)



# Source Surface Models

1. PFSS (Potential Field Source Surface) [widely used]  
assumes electric currents are negligible in the corona

$$\nabla \times \mathbf{B} = 0 \rightarrow \mathbf{B} = -\nabla \Psi$$

$$\nabla \cdot \mathbf{B} = 0$$



Laplace Equation

$$\nabla^2 \Psi = 0$$

*Hakamada, Solar Physics (1995)*

2. CSSS (Current Sheet Source Surface)

includes large-scale horizontal currents

$$\frac{1}{4\pi} (\nabla \times \mathbf{B}) \times \mathbf{B} - \nabla p - \rho \frac{GM}{r^2} \hat{\mathbf{r}} = 0$$

Magnetostatic force  
balance equation

$$\mathbf{J} = \frac{1}{\mu_0 r} [1 - \eta(r)] \left[ \frac{1}{\sin \theta} \frac{\partial^2 \Psi}{\partial \phi \partial r} \hat{\theta} - \frac{\partial^2 \Psi}{\partial \phi \partial r} \hat{\phi} \right]$$

$$\mathbf{B} = -\eta(r) \frac{\partial \Psi}{\partial r} \hat{r} - \frac{1}{r} \frac{\partial \Psi}{\partial \theta} \hat{\theta} - \frac{1}{r \sin \theta} \frac{\partial \Psi}{\partial \phi} \hat{\phi}$$



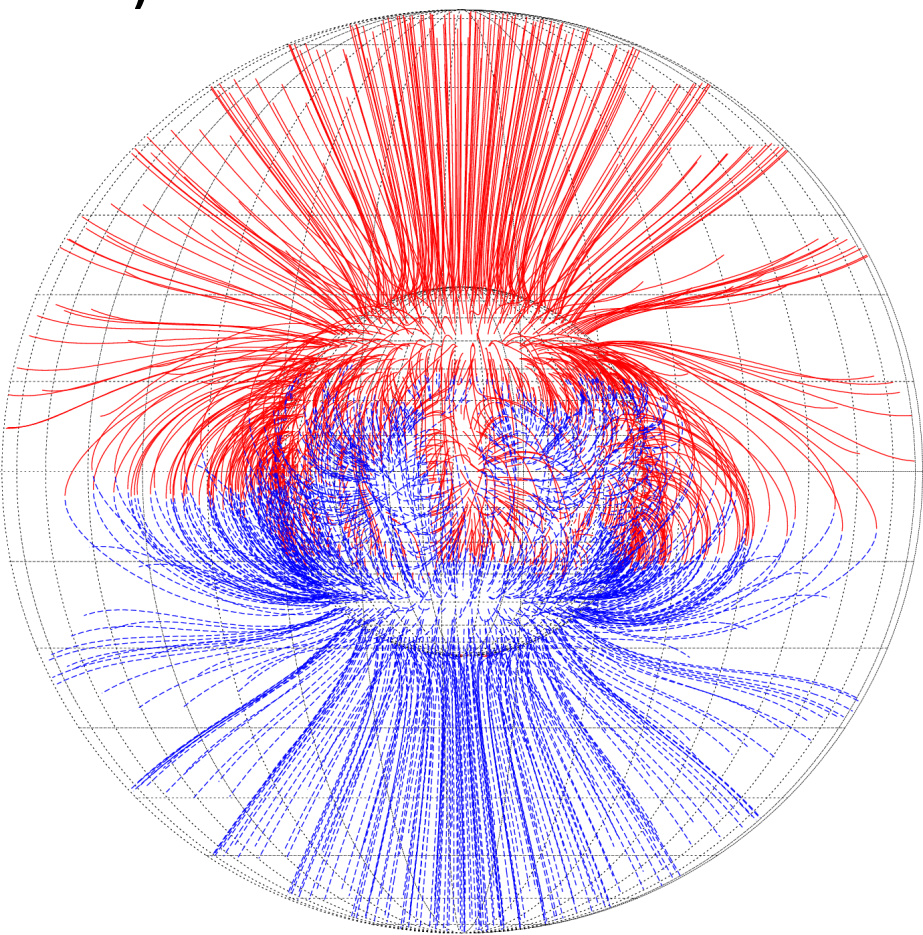
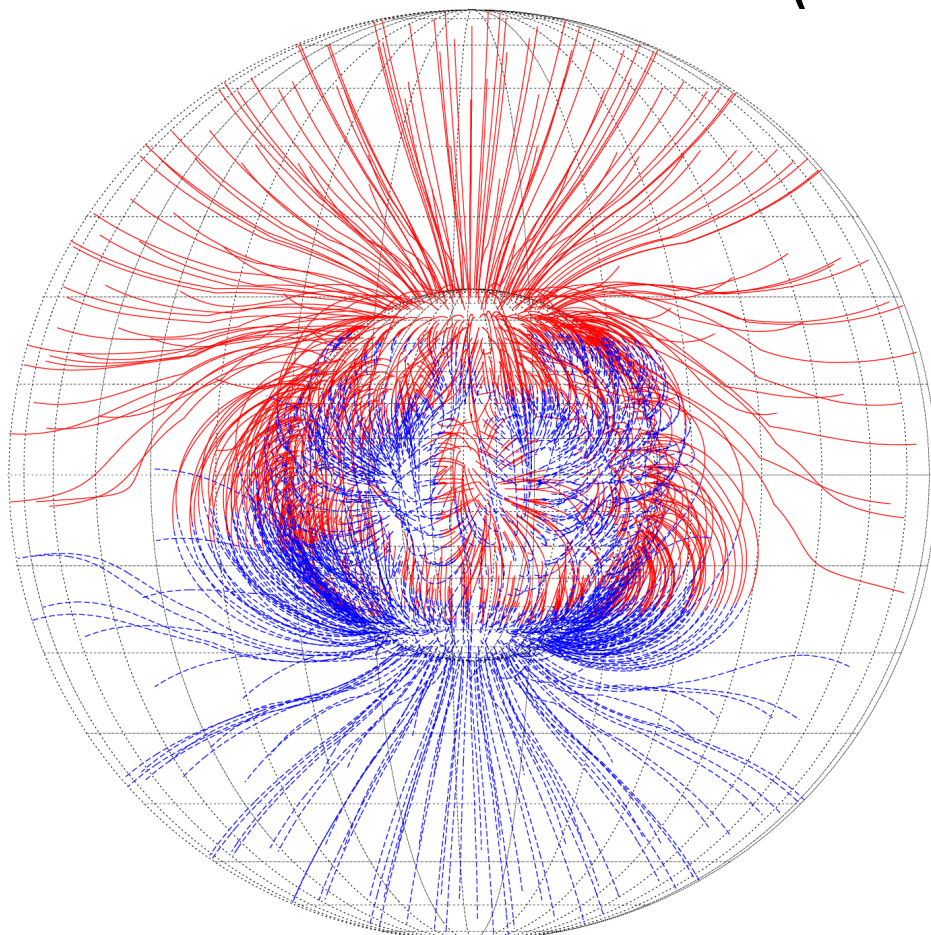
*Zhao & Hoeksema, JGR (1995)*

# Coronal Field Models

CSSS

CR1910  
(Year1996)

PFSS

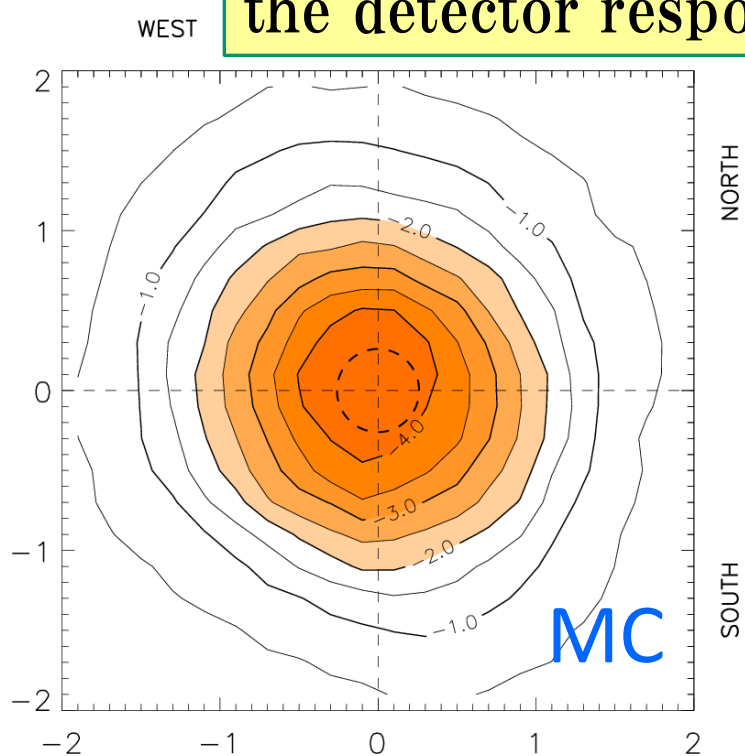


Magnetograph: Kitt Peak  
Harmonic order N=10

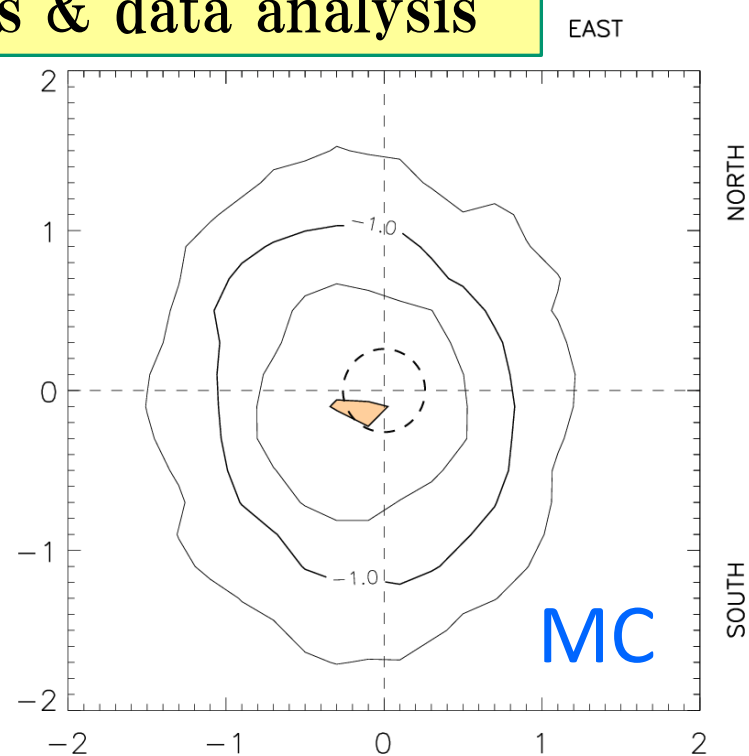
# Examples of MC Result (PFSS)

Density map of events hitting the Sun

MC takes into account of  
Cosmic-ray compositions & spectra  
the detector responses & data analysis

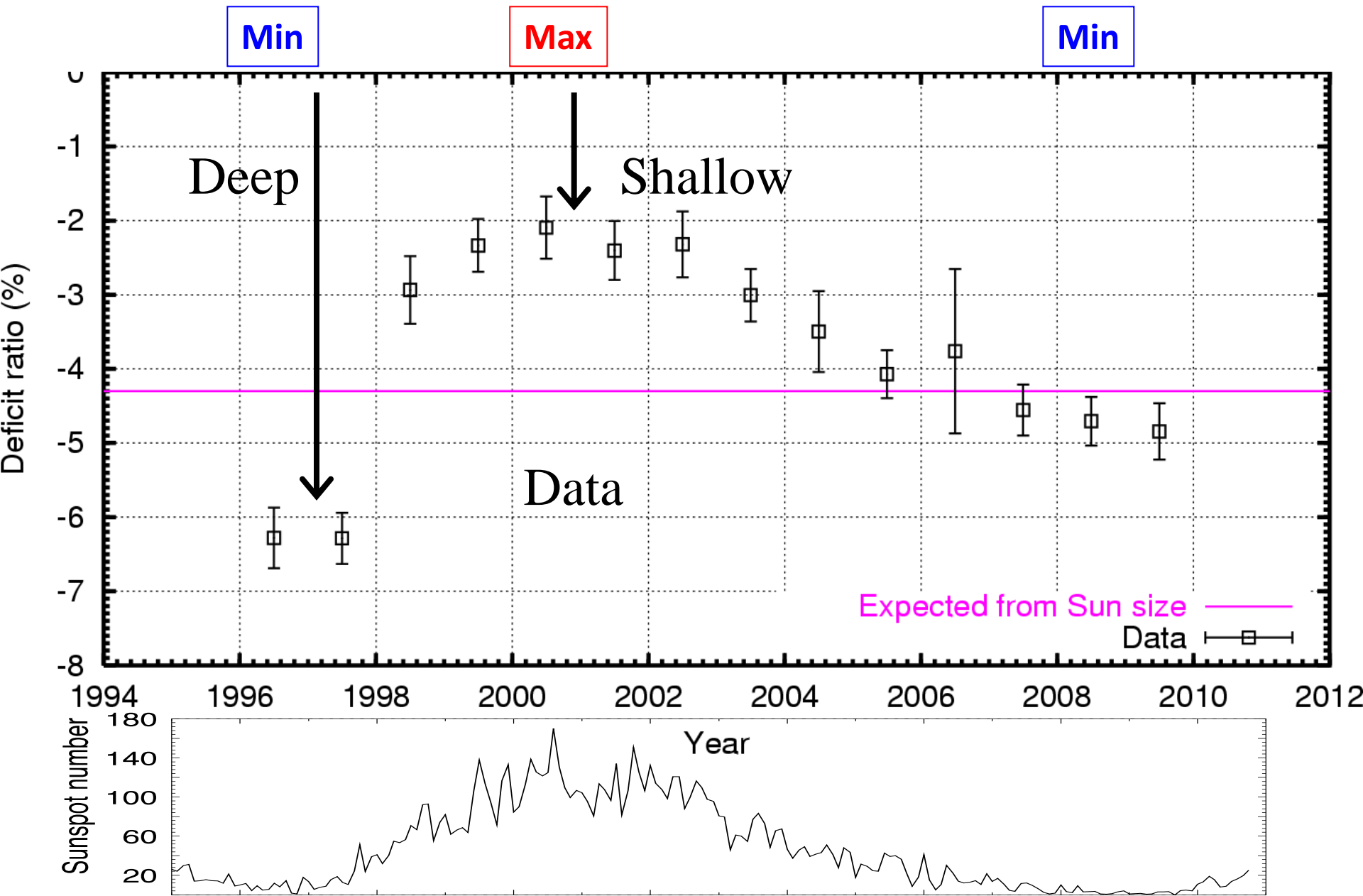


Minimum  
in 1996 (CR1910)

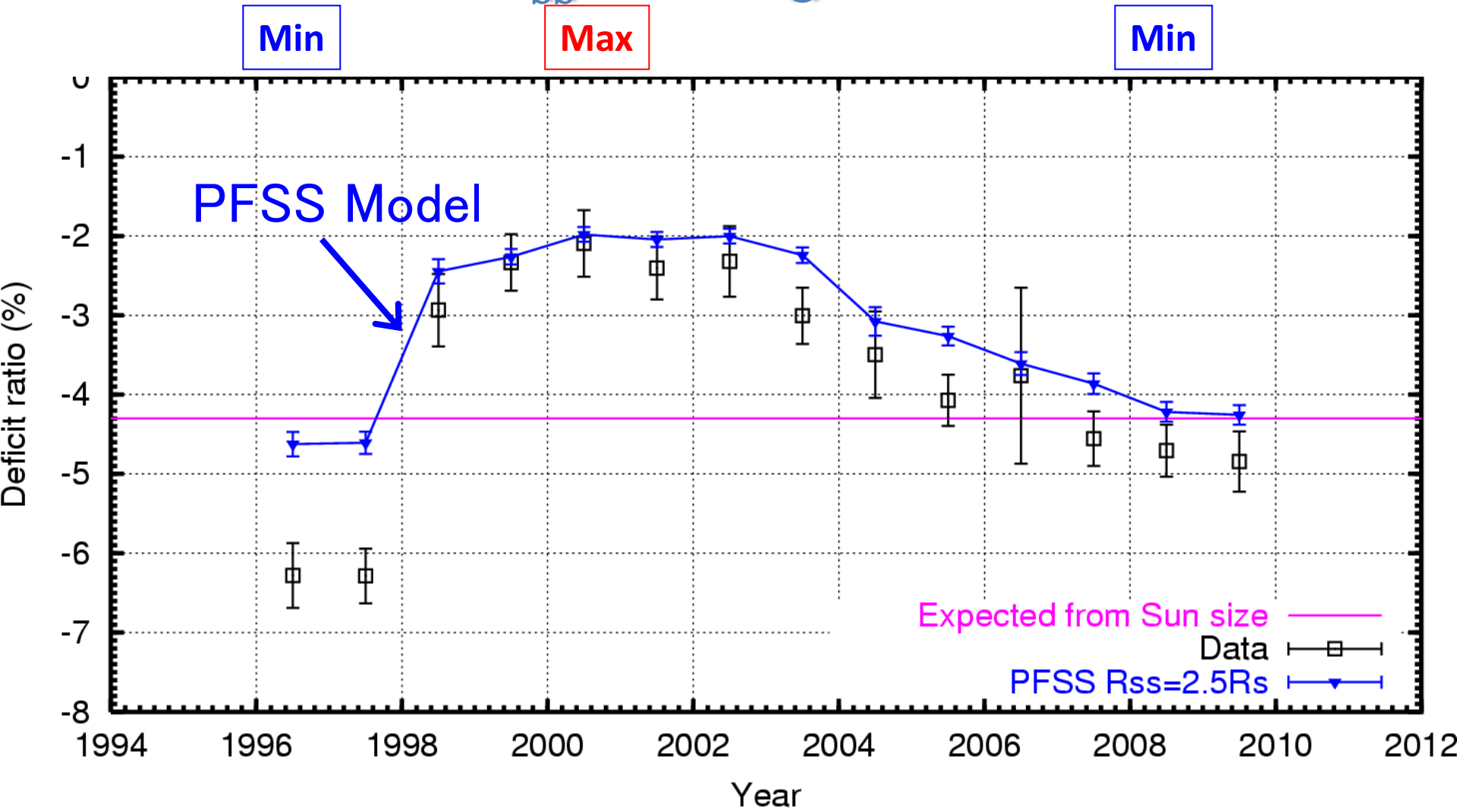


Maximum  
In 2001 (CR1978)

# Observational Data (10TeV)

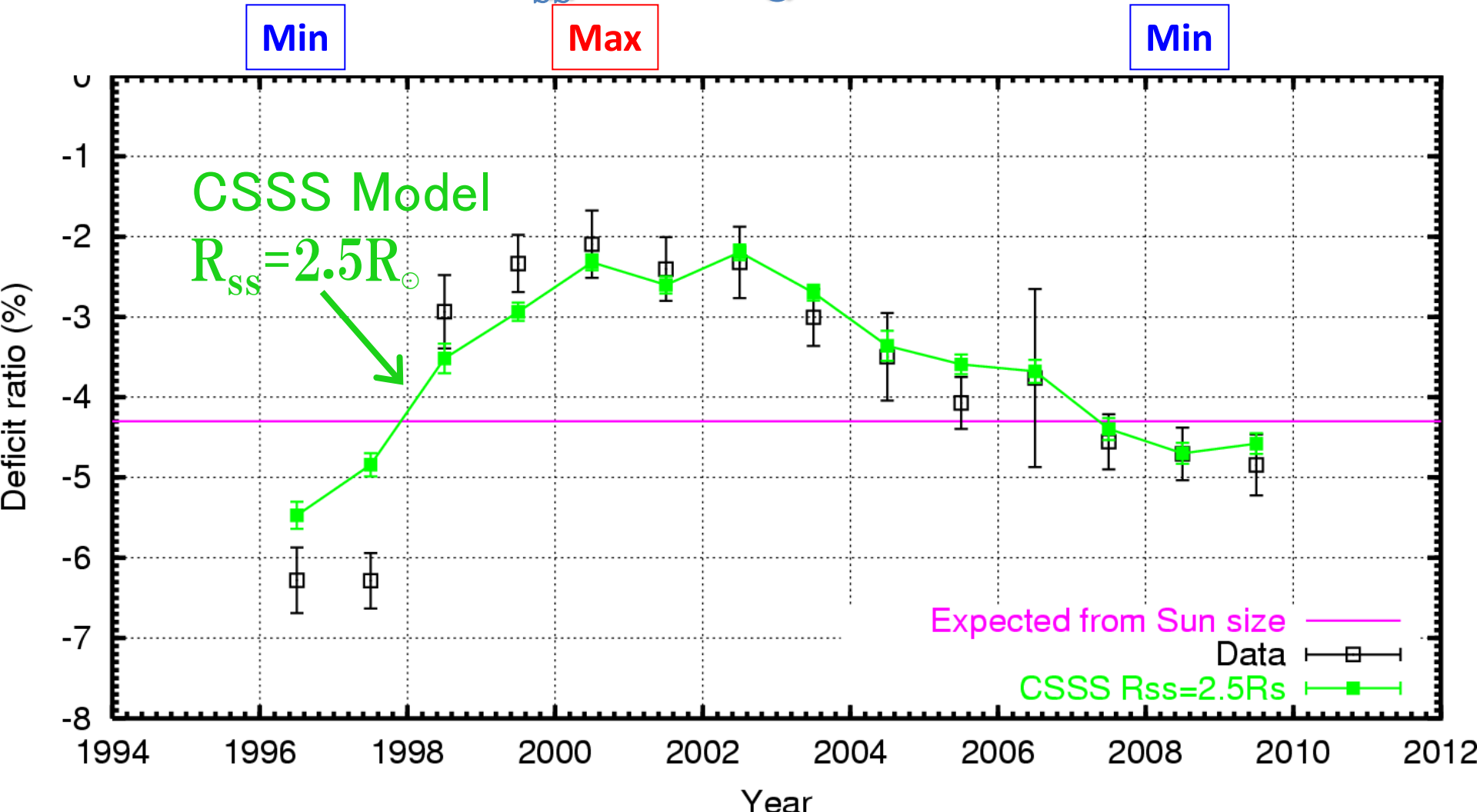


# PFSS Model $R_{ss} = 2.5R_\odot$ (10TeV)



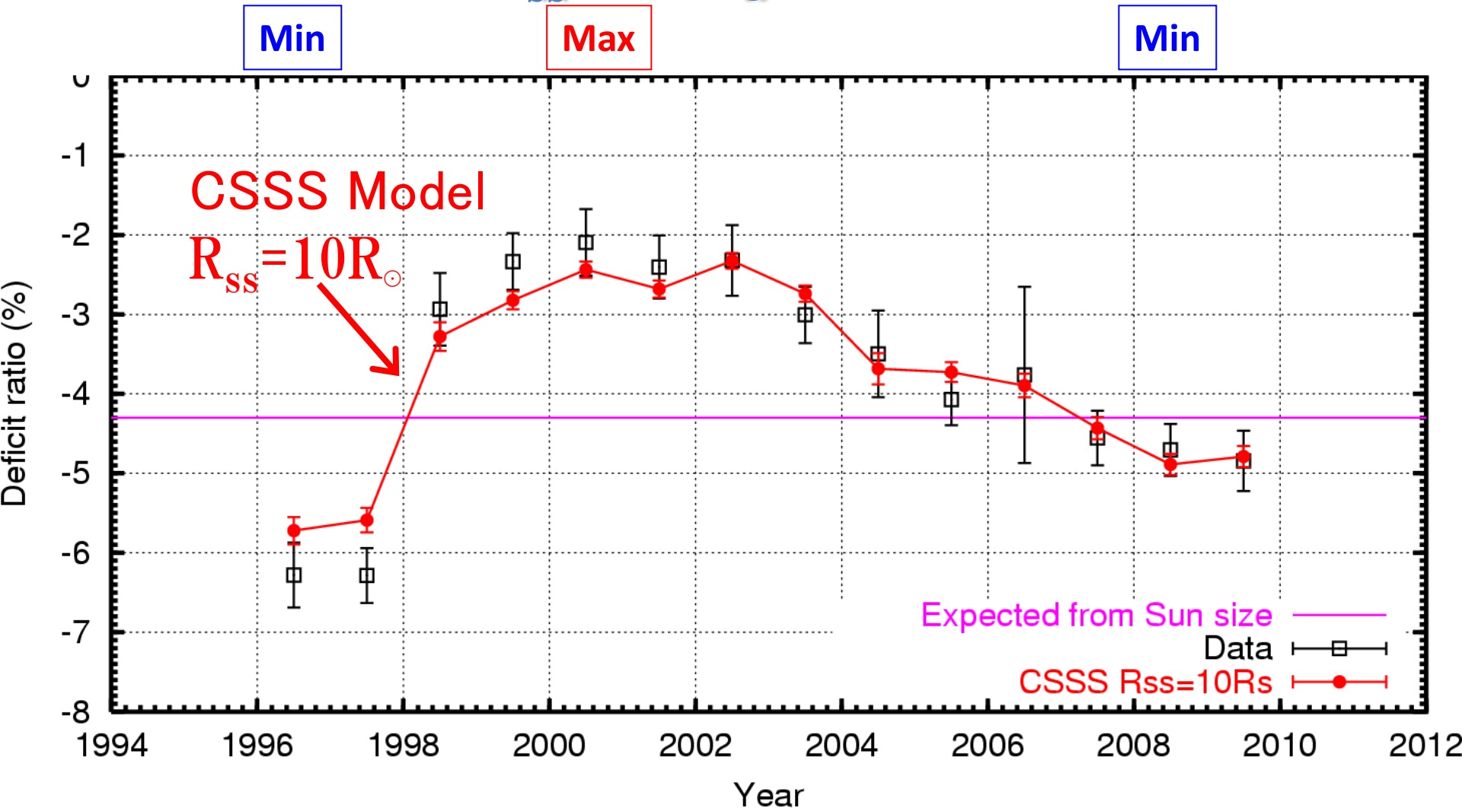
Data - MC  $\chi^2/\text{dof} = 55.2/14 (7.9 \times 10^{-7})$   
Tendency Ok

# CSSS Model $R_{ss} = 2.5R_{\odot}$ Result (10TeV)



Data - MC  $\chi^2/\text{dof} = 26.2/14$  (0.024)  
Consistent

# CSSS Model $R_{ss} = 10R_\odot$ Result (10TeV)

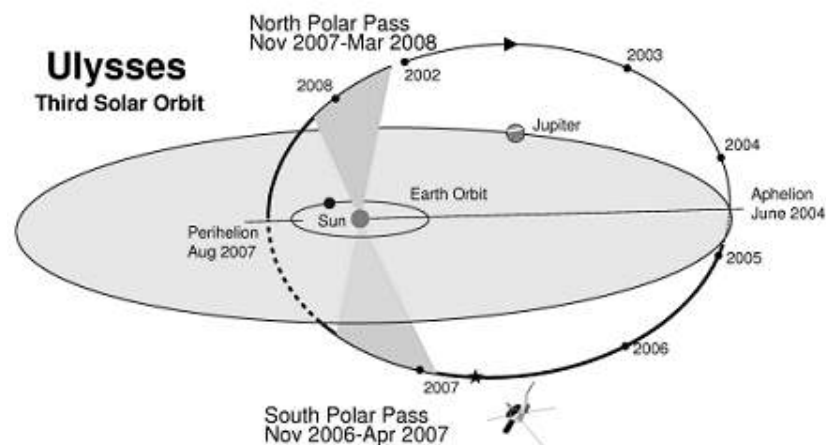
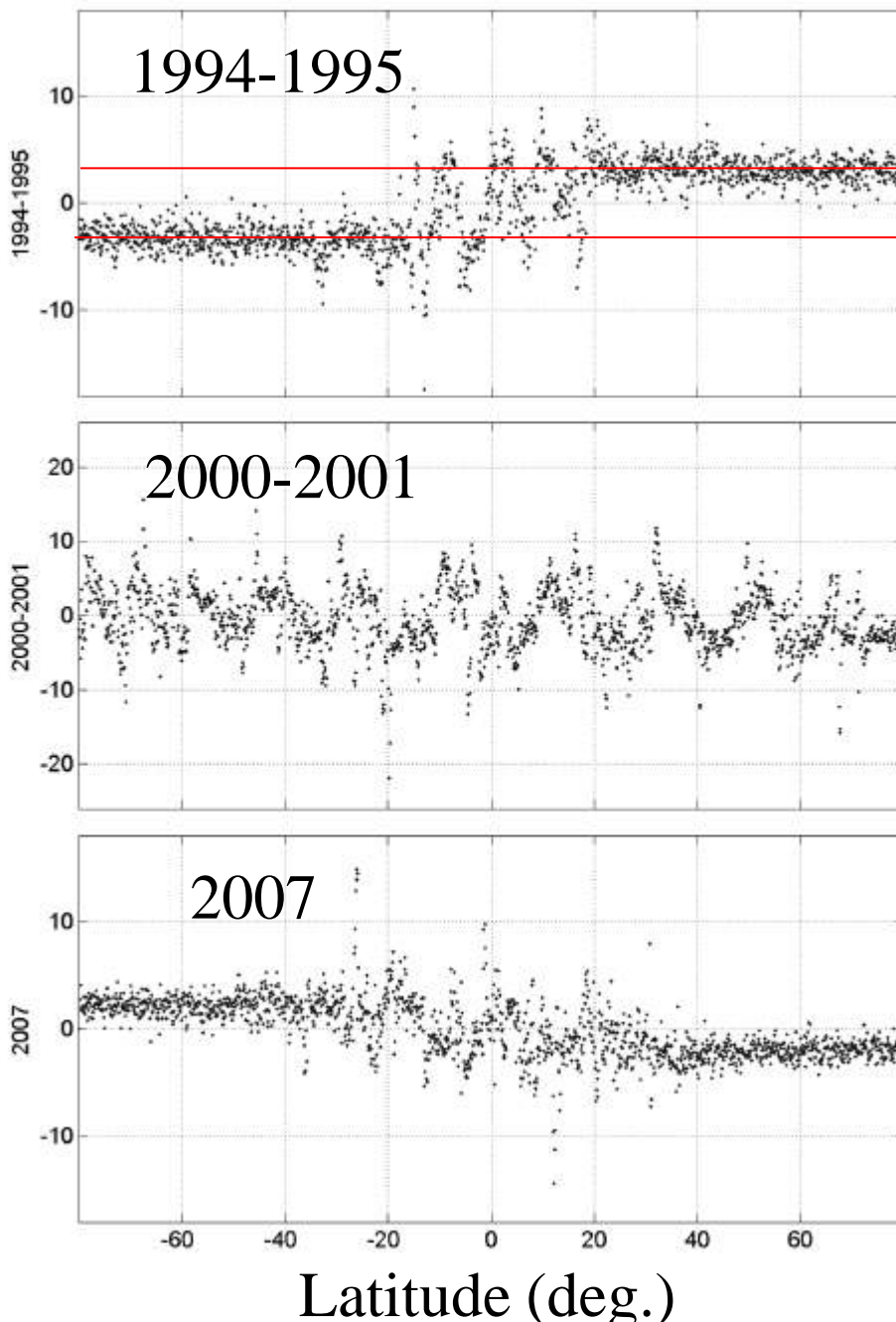


$\text{Data} - \text{MC} \quad \chi^2/\text{dof} = 10.3/14 \quad (0.74)$   
 MC well reproduces data

# Ulysses Observation

“Split monopole”  
Structure

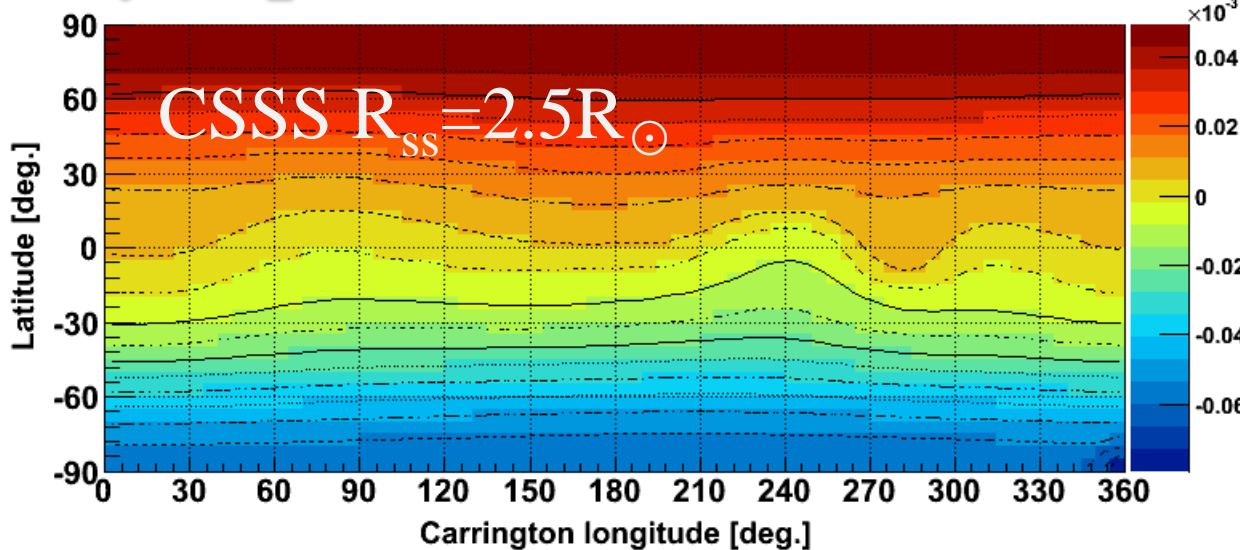
$B_r r^2$  (nT) normalized to 1 AU



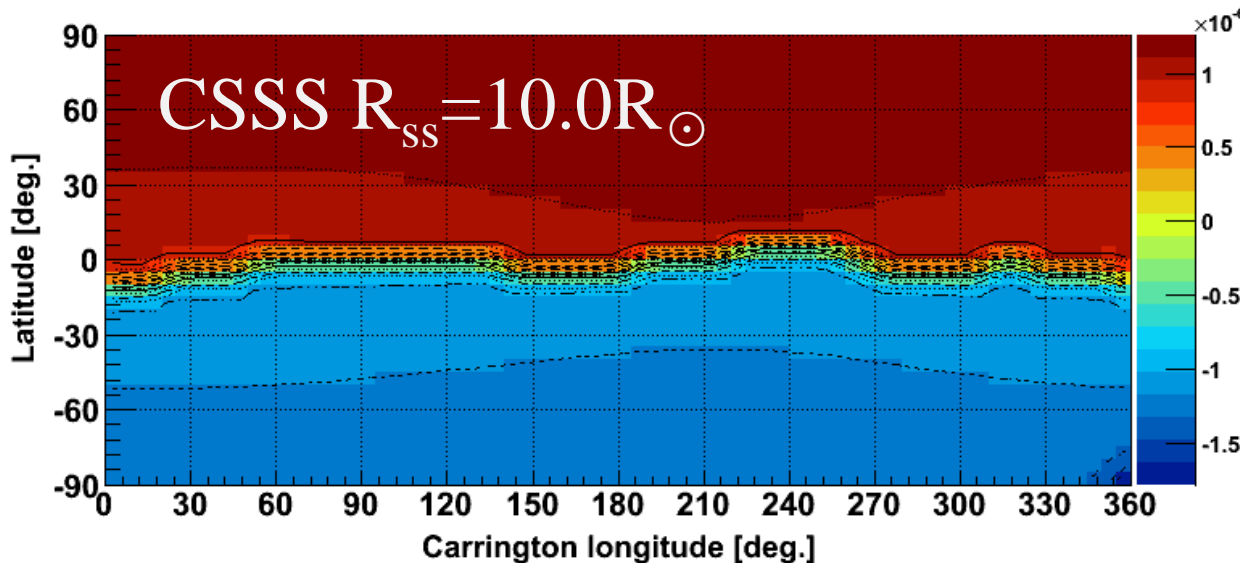
Ulysses data  
Perihelion 1.3AU  
Aphelion 5.4AU

*Virtanen and Mursula,  
JGR, 115, A09110 (2010)*

# Synoptic Chart in CR1910 by the CSSS



Changing  
gradually



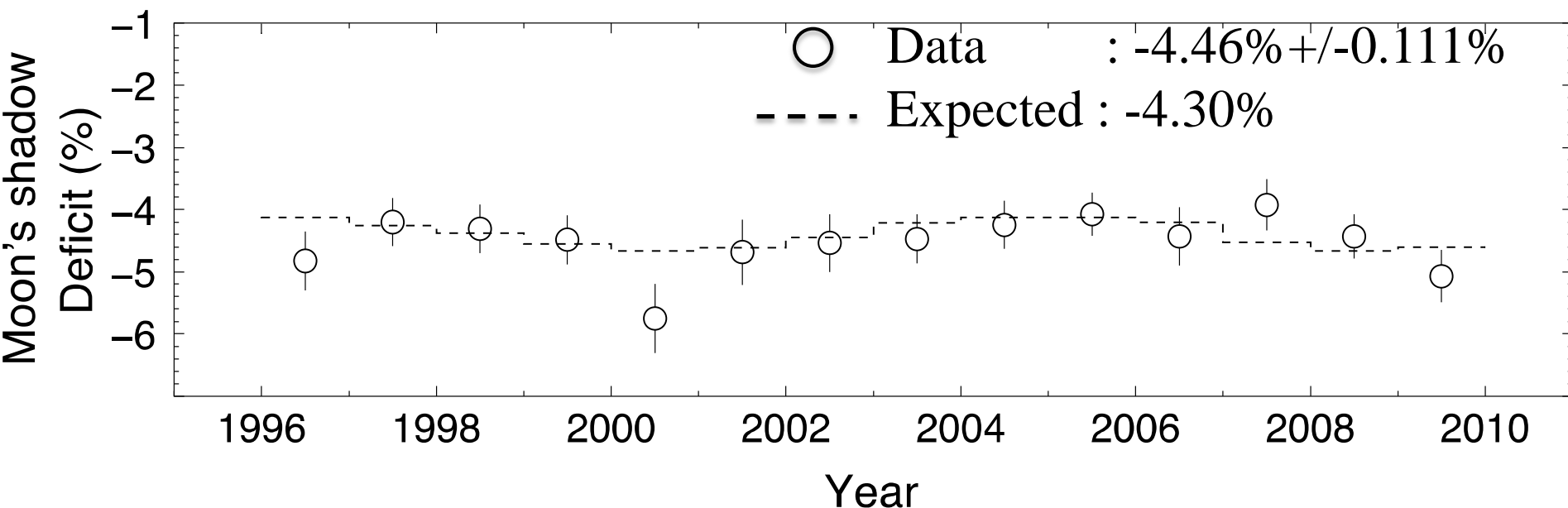
Step at  
the equator  
  
Reproduce  
Ulysses obs.

# Systematic Error

From Deficit Intensity Variation of the Moon's Shadow

Variation is consistent with flat.

Average deficits is **consistent** with the expected -4.3%.



Quadratic sum:

$$S_{\text{sys}} = \sqrt{(D_{\text{data}} - D_{\text{expected}})^2 + S_{\text{data}}^2} = \sqrt{(4.46 - 4.30)^2 + (0.111)^2} = 0.19\%$$

# Summary of $\chi^2$ Test (Data-MC)

$$\chi^2 = \sum_{i=1}^{14} \frac{(D_{\text{obs}}^i - D_{\text{MC}}^i)^2}{(\sigma_{\text{obs}}^i)^2 + (\sigma_{\text{MC}}^i)^2 + \langle \sigma_{\text{sys}} \rangle^2}$$

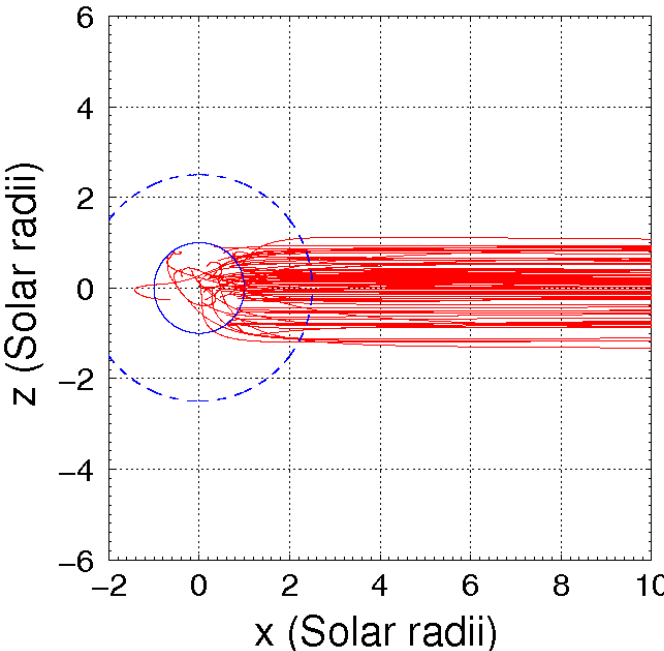
Models	Data - MC $\chi^2/\text{d.o.f.}$	Probability
PFSS $R_{\text{ss}} = 2.5R_\odot$	44.5(55.2)/14	$4.9 \times 10^{-5}$ ( $7.9 \times 10^{-7}$ )
CSSS $R_{\text{ss}} = 2.5R_\odot$	21.1(26.2)/14	0.099(0.024)
CSSS $R_{\text{ss}} = 10R_\odot$	8.3(10.3)/14	0.87(0.74)

- \* PFSS  $R_{\text{ss}} \gg 2.5$  omitted  $\rightarrow$  unrealistic structure
- \* ( ) only statistical error

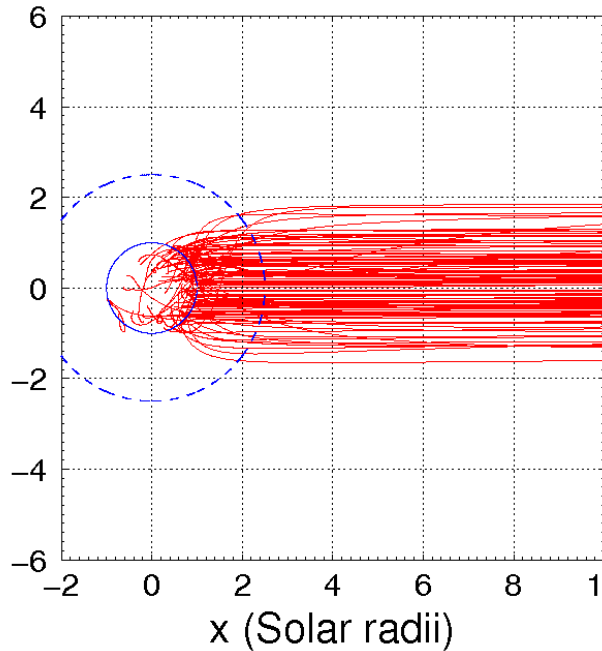
# Cosmic Ray Trajectory ~10TeV in 1996 (CR1910)

Focusing effect

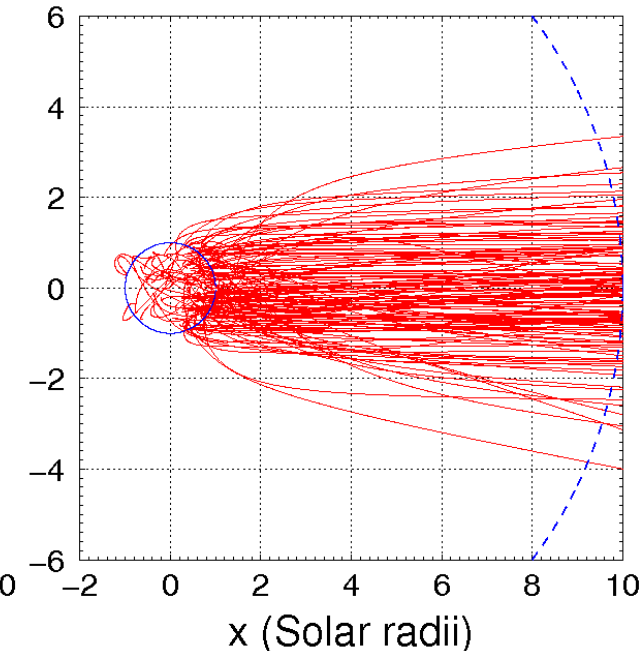
a PFSS  $R_{ss}=2.5 R_\odot$



b CSSS  $R_{ss}=2.5 R_\odot$



c CSSS  $R_{ss}=10 R_\odot$



In the CSSS model case,  
antiparticles can easily move along the open field lines of  
the ordered coronal magnetic field through the source surface  
at high latitude.

# Sun's shadow summary

- Observation of the Sun's shadow (1996~2009) covering Solar Cycle 23
  - anti-correlation to 11-yr period solar activities
- Sensitivity to Sun-Earth magnetic field
  - Sun's shadow sensitive to coronal magnetic field
  - CSSS magnetic field model adopting currents in the coronal atmosphere reproducing DATA better than PFSS model

Reference: M. Amenomori et al., Phys. Rev. Lett., 111, 011101 (5pp) (2013)

# 6. Future Prospects

## What we have found out:

Crab, Mrk501 , Mrk421, Fermi-source Correlation observed,  
Possible diffuse  $\gamma$ -ray signal from Cygnus region?

P, He, all-particle E-spectrum (Galactic cosmic rays  
accelerated to the knee region  $\sim 10^{15}$  eV)

Sharp Knee!?

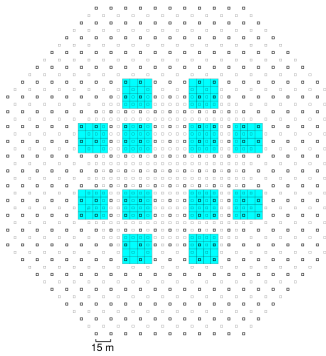
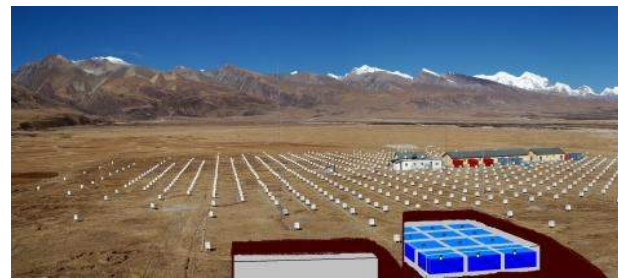
## What we should do next:

1. 100 TeV (10 – 1000 TeV) region  $\gamma$ -ray astronomy  
*Where do galactic cosmic rays under knee come from?*
2. E-spectrum of heavy component around ‘knee’  
*All-particle knee = CNO? Fe knee?*

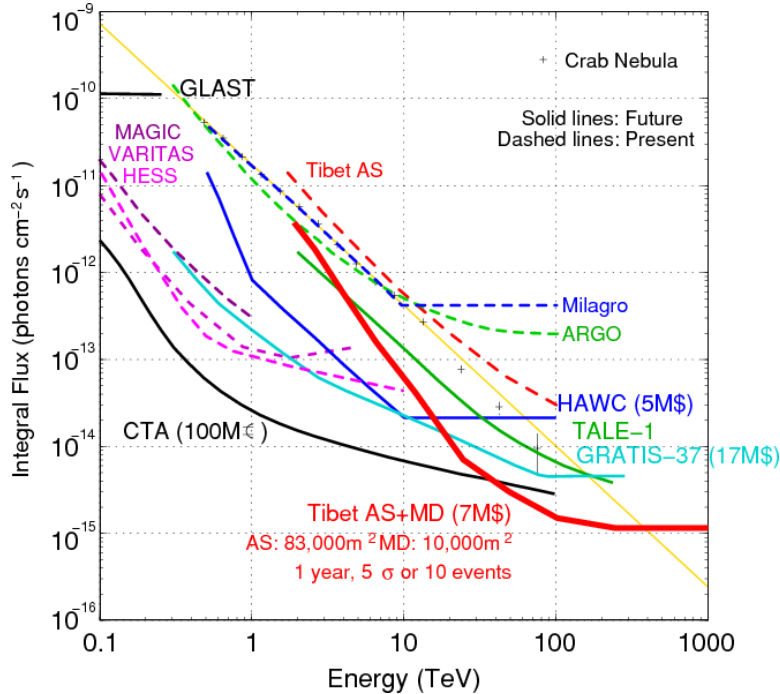
## □ Next Plans

Gamma ray: Tibet Muon Detector (**MD**) Project  
&  
Cosmic Rays: Tibet Yangbajing Airshower Core (**YAC**)  
Detector Project

# Tibet Muon Detector (MD) Project

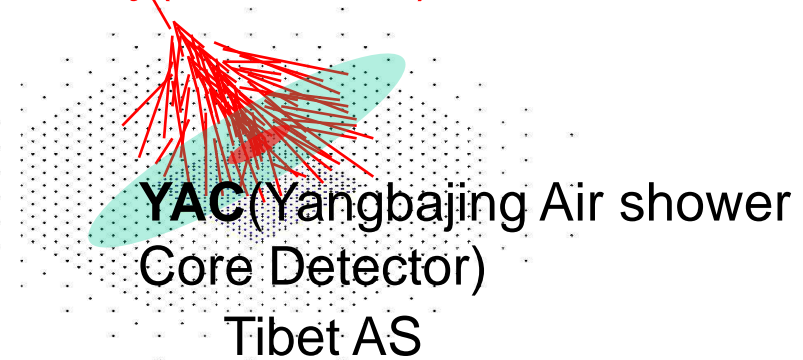


10-1000TeV Gamma

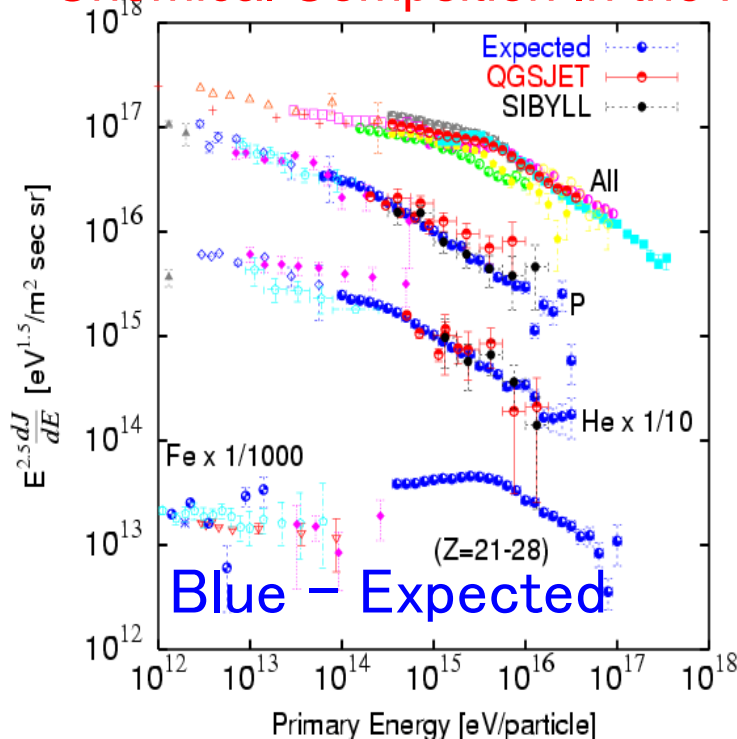


# Tibet Air Shower Core Detector (YAC) Project

Cosmic ray(P,He,Fe...)



Chemical Composition In the Knee



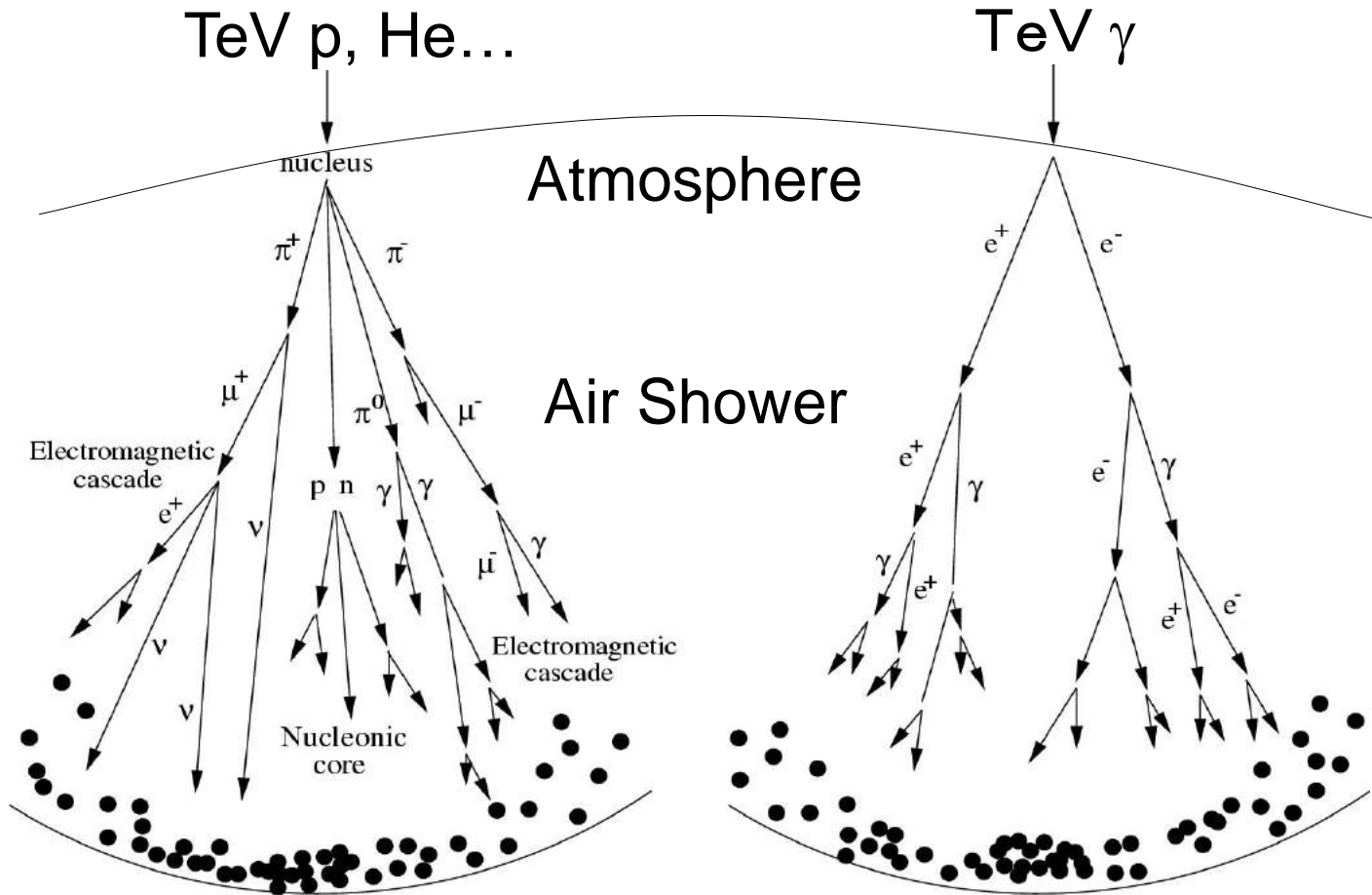
## 1. 100 TeV $\gamma$ -ray astronomy

Let's see 100 TeV-region (10-1000TeV)  
gamma rays by

Tibet-III (AS) + a large underground  
muon detector array (MD)  
(~10000m<sup>2</sup> in total)!

- >Origin of cosmic rays and acceleration mechanism and limit at SNRs.
- >Diffuse gamma rays

# p/ $\gamma$ discrimination by muons



Number of muons (<100 m from core, 4300m a.s.l.)

100TeV Proton  
~50

100TeV Gamma  
~1

# Tibet Muon Detector (MD) Array

7.2m x 7.2m x 1.5m depth Water pool

20"ΦPMT x 2 (HAMAMATSU R3600)

Underground 2.5m (~515g/cm<sup>2</sup>~19X<sub>0</sub>)

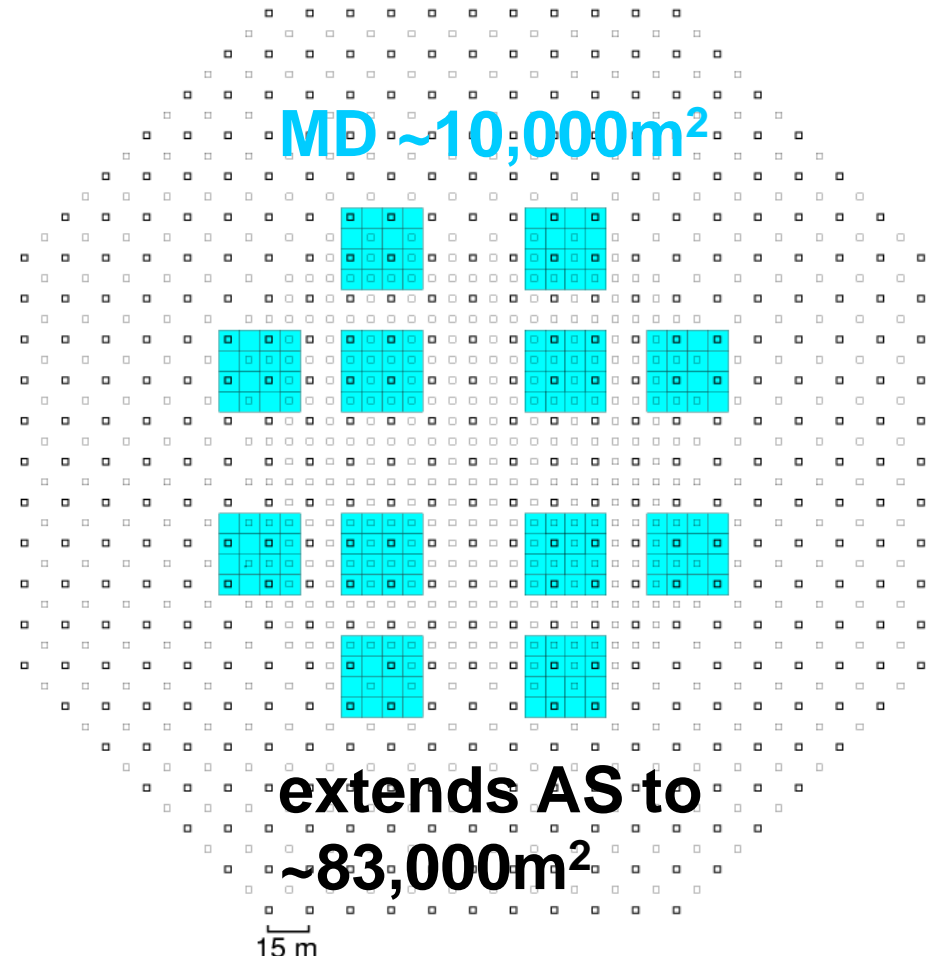
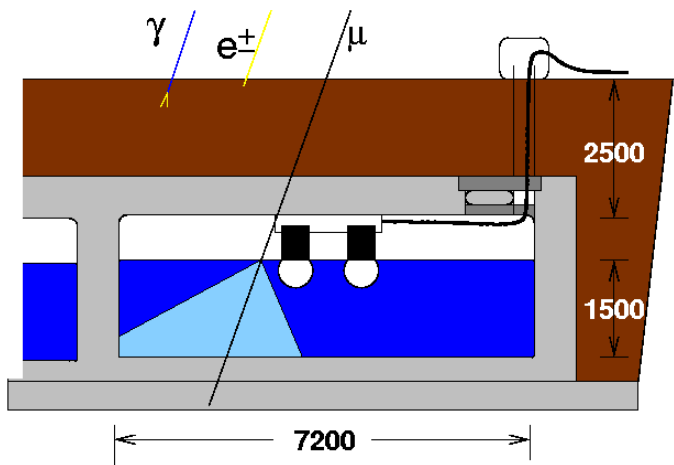
Material:

Concrete pool

White paint

192 detectors

Total ~10,000 m<sup>2</sup>



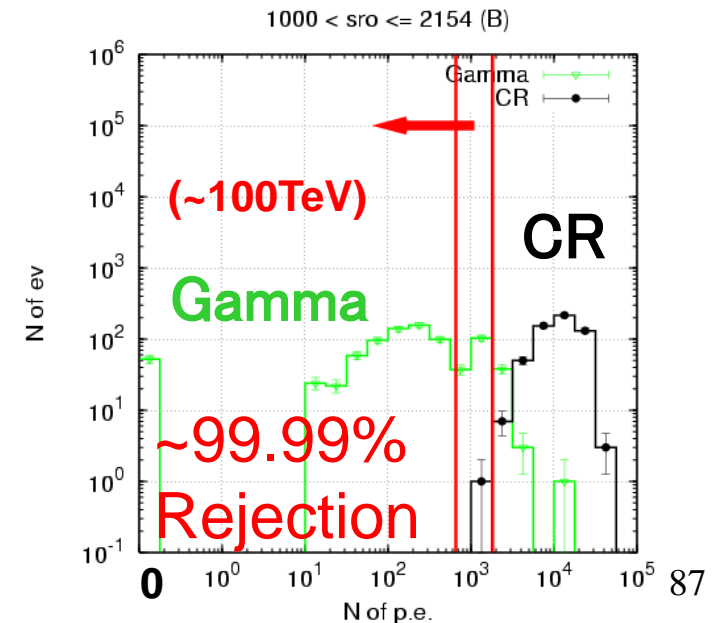
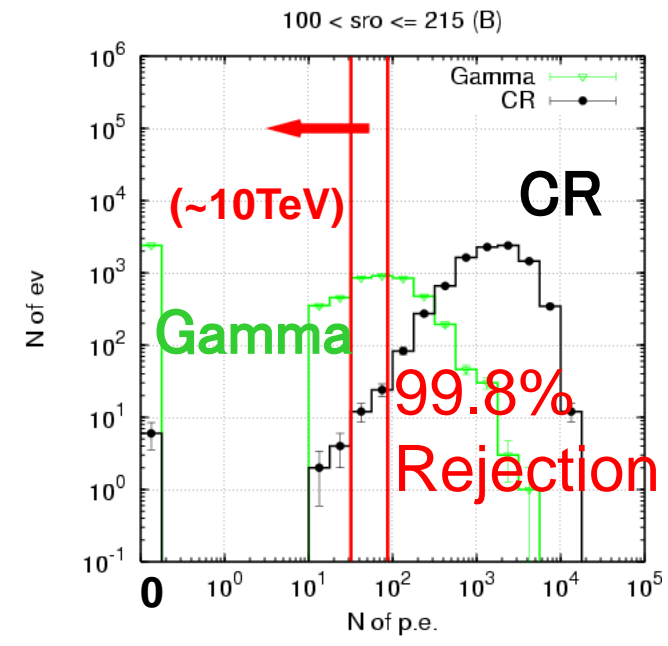
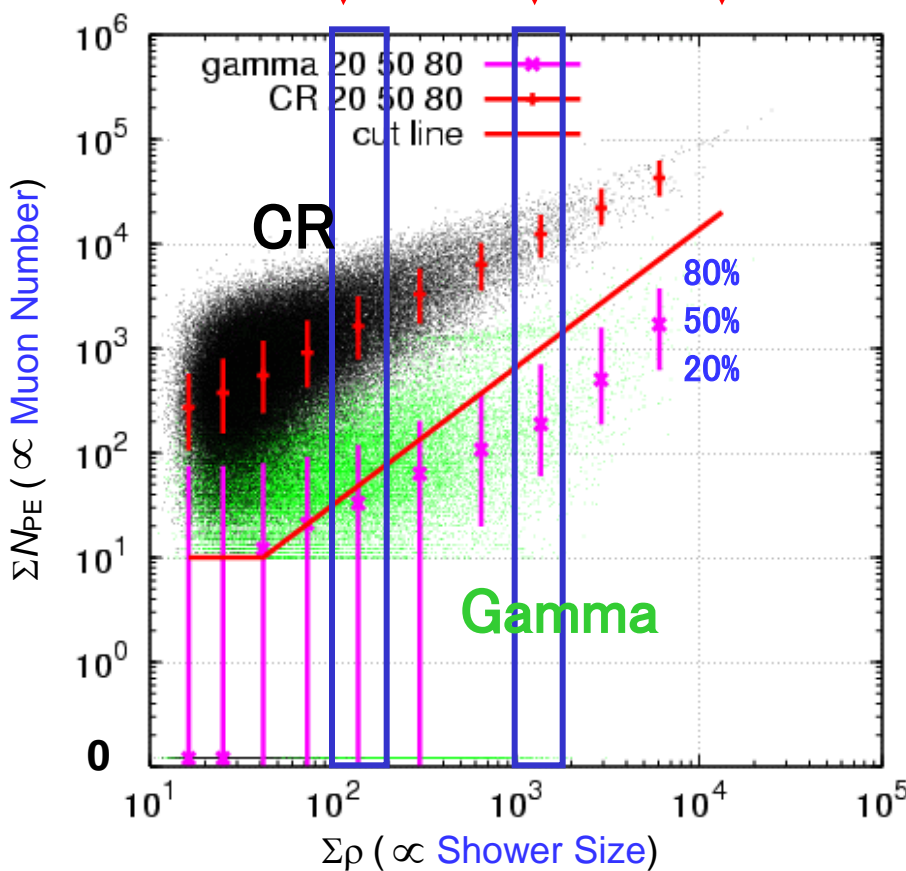
Counting the number of muons accompanying an air shower  
→ p/γ discrimination

# Muon Number vs. Shower Size (Simulation)

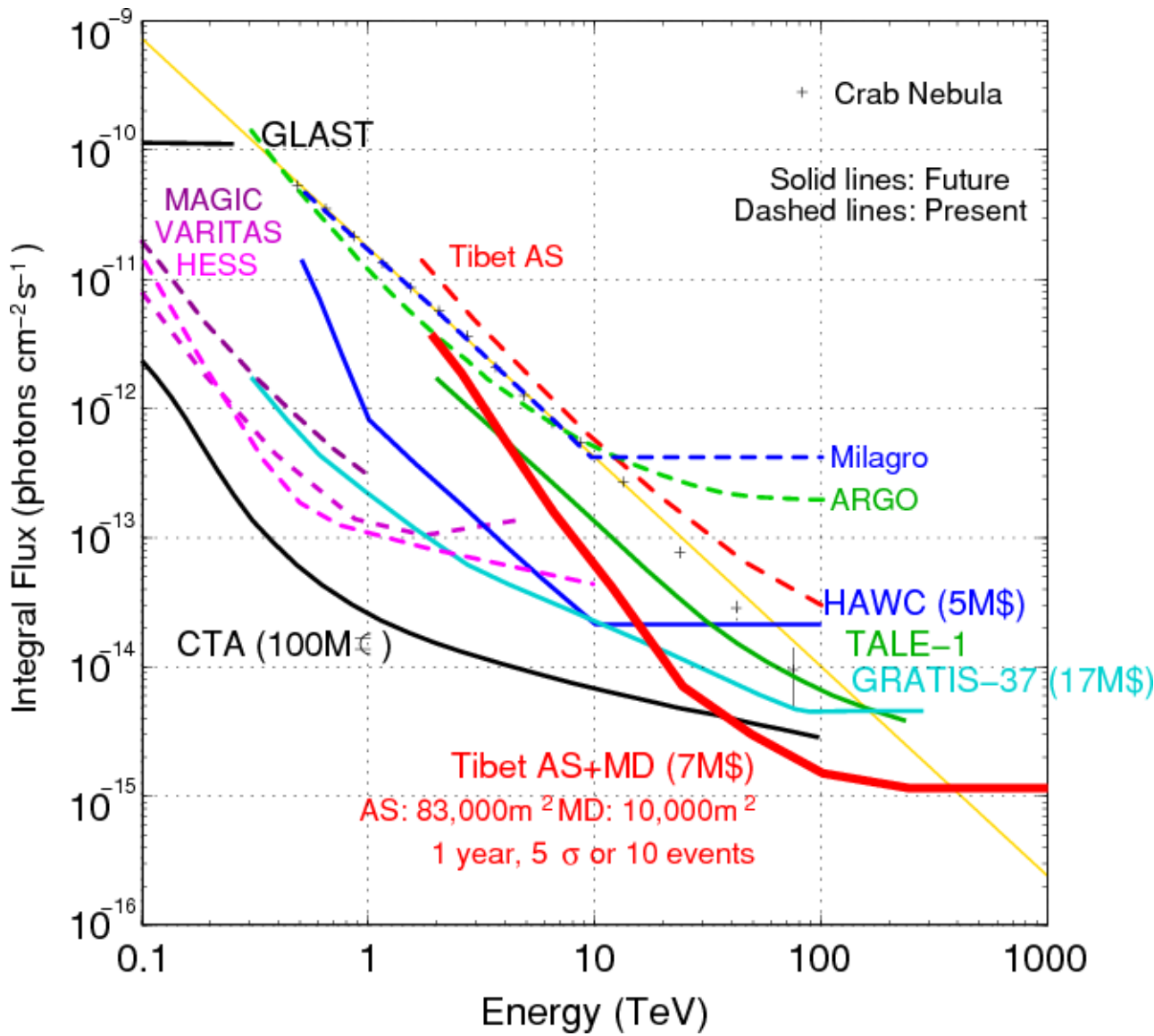
$\Sigma\rho$ : Sum of particle density by all scintillation det.  
 >> Shower Size

$\Sigma N_{PE}$ : Sum of photoelectrons by all muon det.  
 >> Muon number  
 (Threshold of MD  $N_{PE} > 10$  p.e.)

(gamma) 10TeV 100TeV 1000TeV



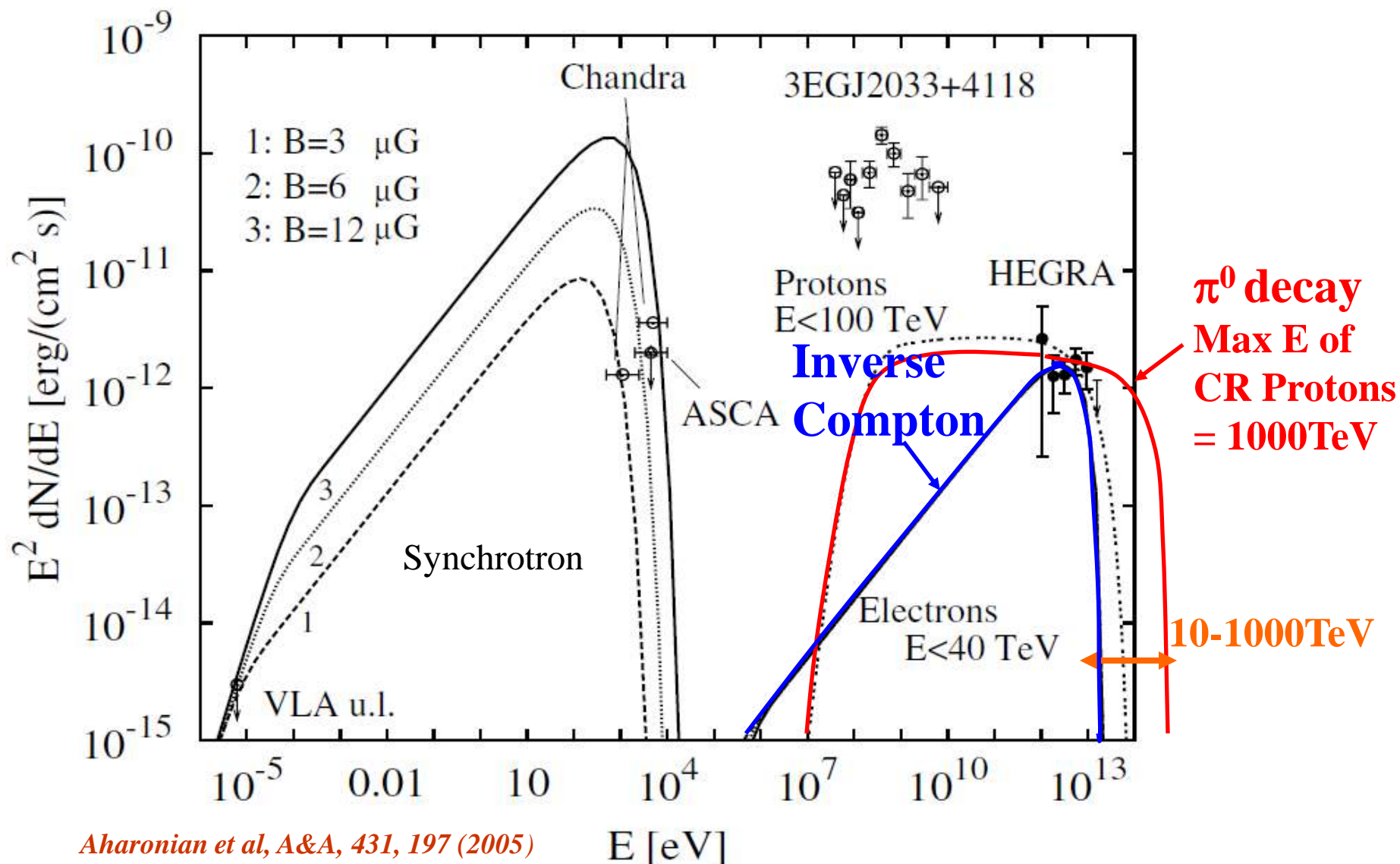
# Other Future Plans (5 $\sigma$ or 10 events)



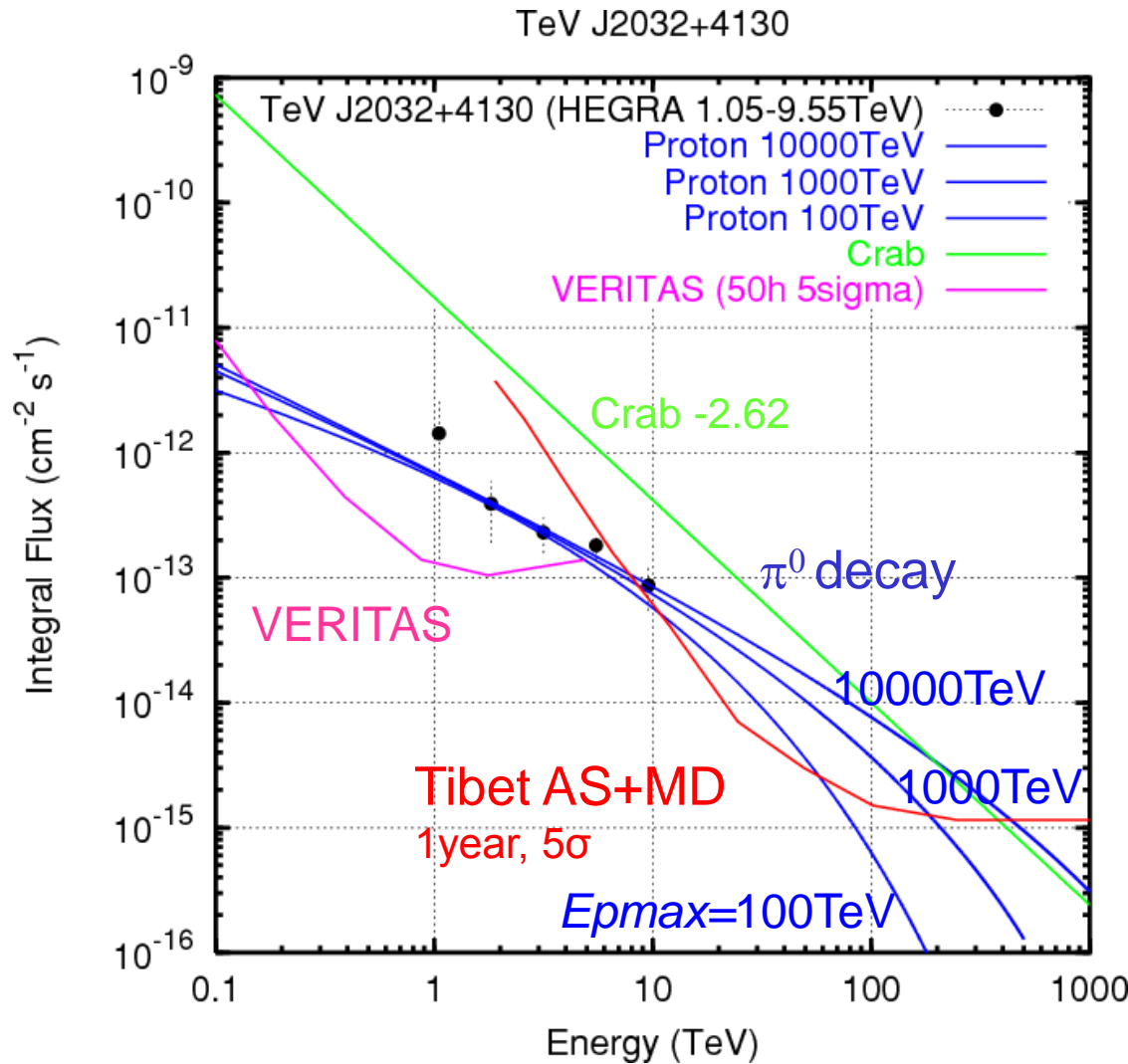
# Gamma Ray Observation in the 100 TeV region

TeV J2032+4130 (~5% Crab)

1. Hard spectral index at TeV energies
2. Faint in other wavelengths



# TeV J2032+4130 and $\pi^0$ decay model



Aharonian et al, A&A, 431, 197 (2005)

## TeV J2032+4130

Unidentified source

Cyg X-3 in Cyg OB2

HEGRA obs.~158 hours

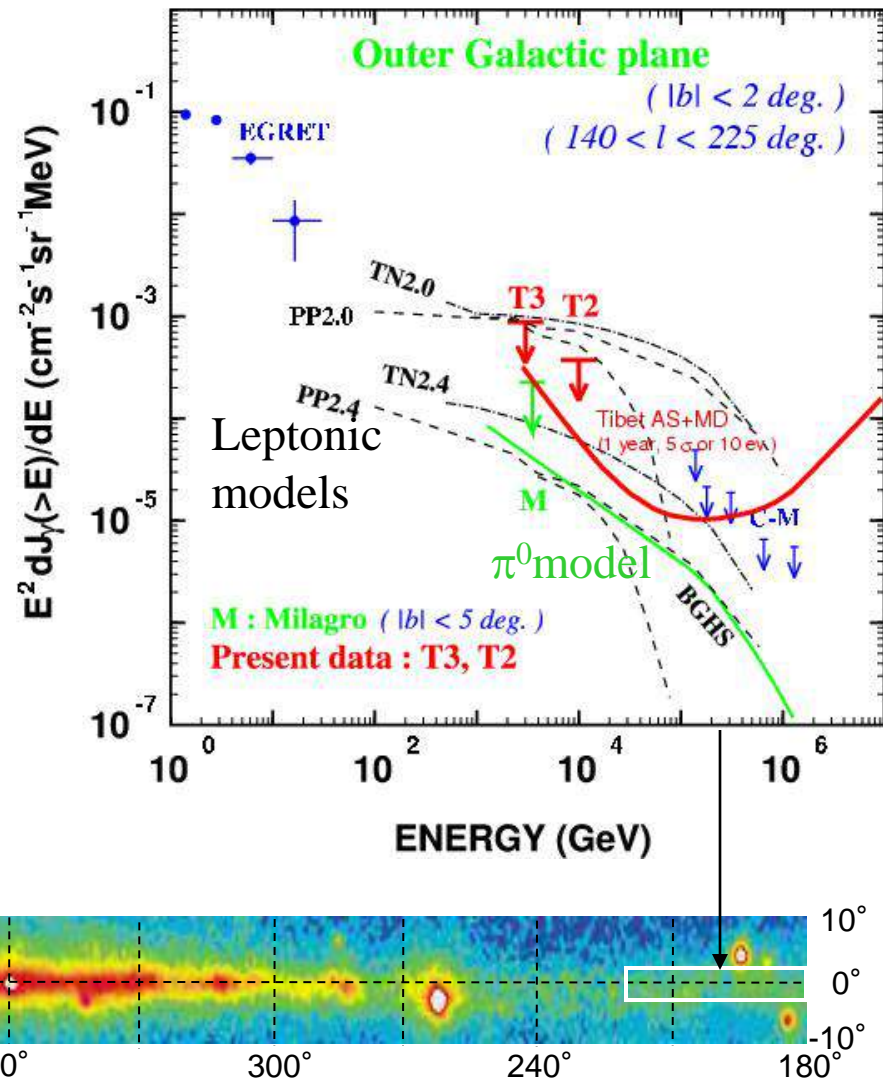
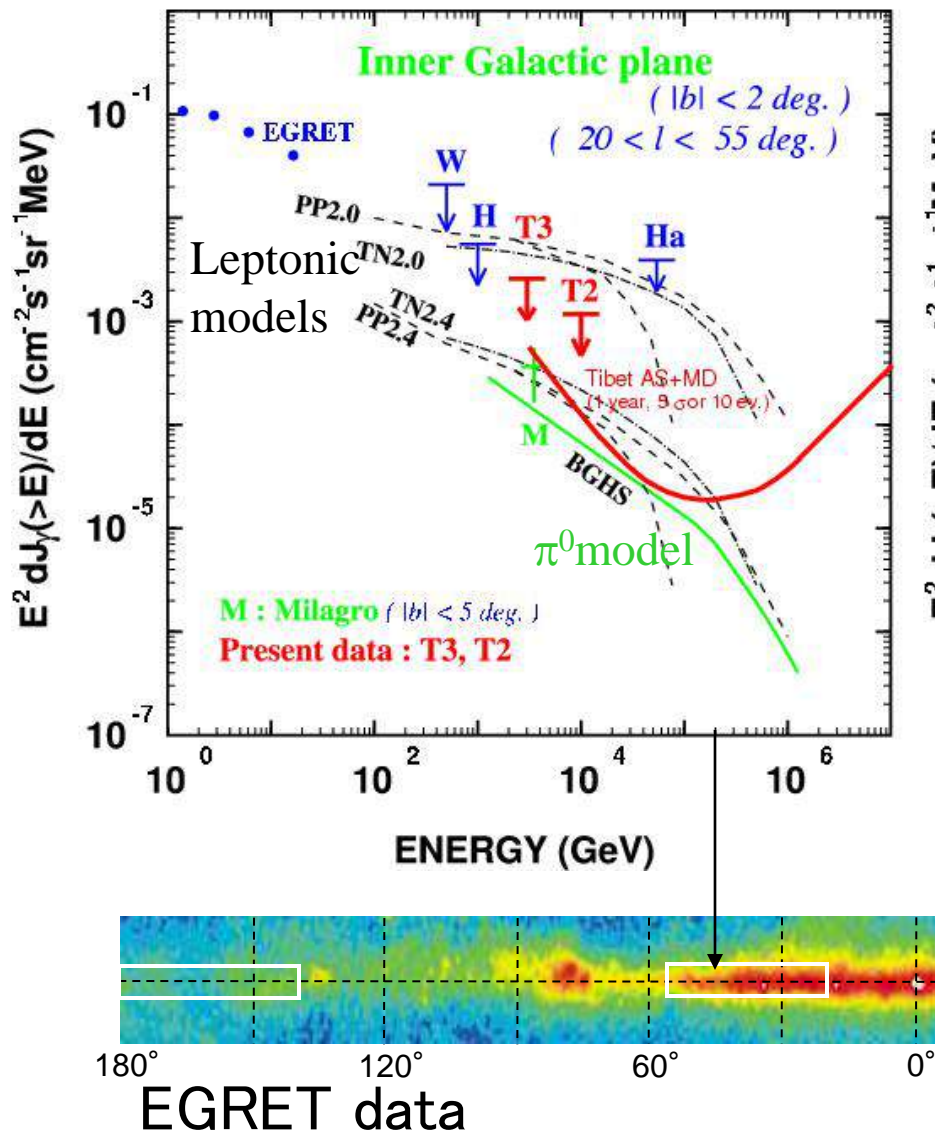
Extended ~6.2'

## $\pi^0$ decay model

Aharonian et al. A&A, 464, 235(2007)

Kelner et al., PRD 74, 034018 (2006)

# Diffuse gamma rays from Galactic Plane



# MD summary

## Tibet MD

~83000 m<sup>2</sup> Airshower Array (AS) +

~10000 m<sup>2</sup> Water Cherenkov Muon Detectors (MD)

→ 100 TeV(10–1000TeV)  $\gamma$ -ray observation (CR acceleration limit & Diffuse  $\gamma$ )

## Expected Sensitivity

$F(>100(20)\text{TeV}) \sim 10^{-15} \text{ cm}^{-2} \text{ s}^{-1} \sim 10(5) \% \text{ Crabs}$

→ More than 10 times better sensitivity

>HESS (>10–20TeV), >CTA (>30–40TeV)

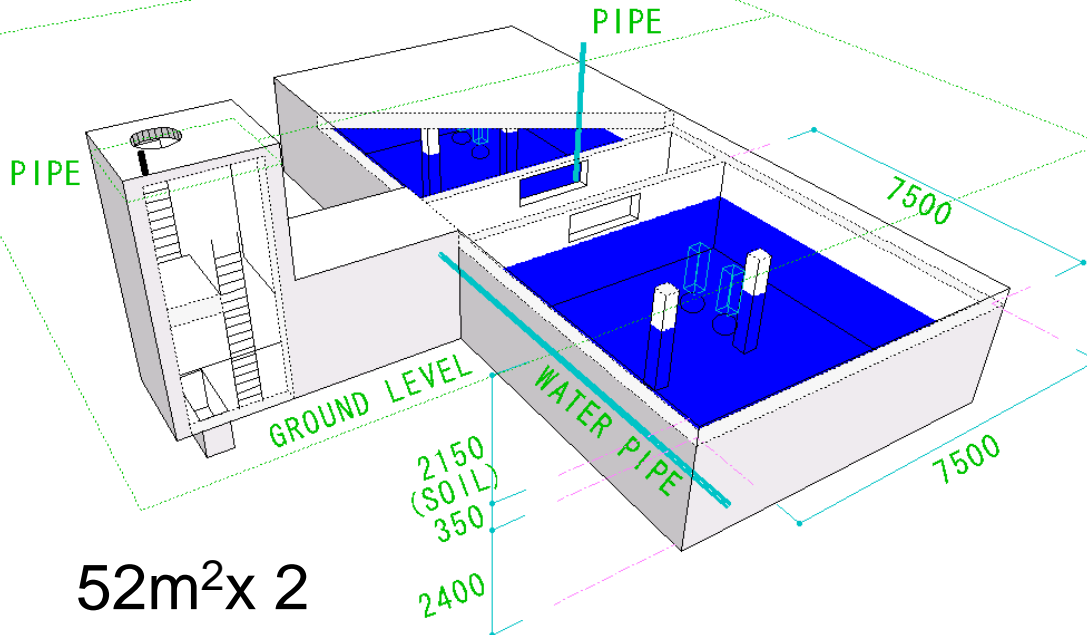
## Source Candidates for 100 TeV g-ray emission in our field of view.:

Possible : Diffuse  $\gamma$  from Milky way,  
(1 year) Crab, TeV J2032+4130,  
MGRO J2019+37, MGRO J1908+06, MGRO J2031+41  
HESS J1837–069, Mrk 421

Interesting : Cas A, M87, HESS J1834–089, HESS J0632+058  
(Several years) Mrk 501, LS I +61 303, IC443, Extragalactic Diffuse  $\gamma$ ???

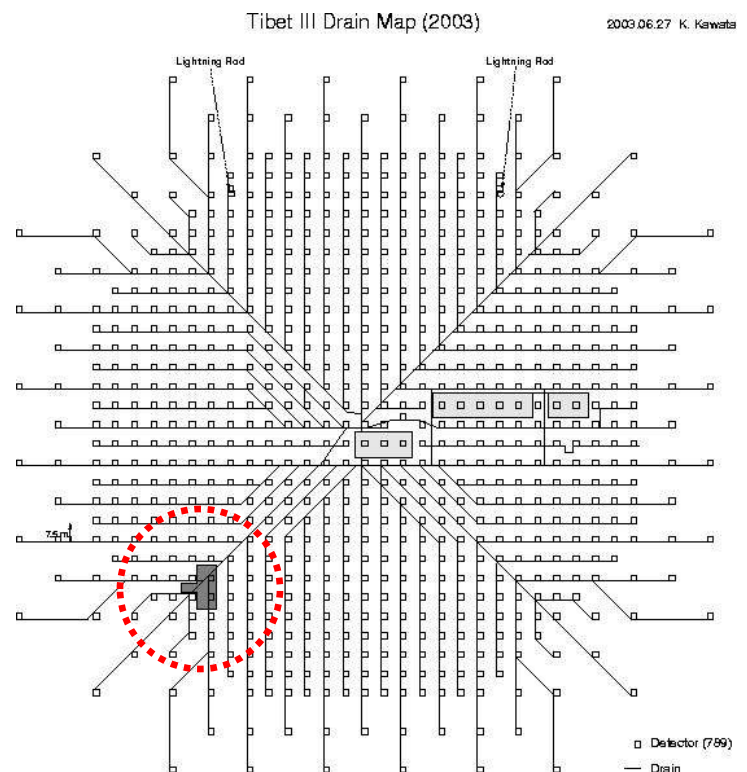
Unknown : several –10 !?

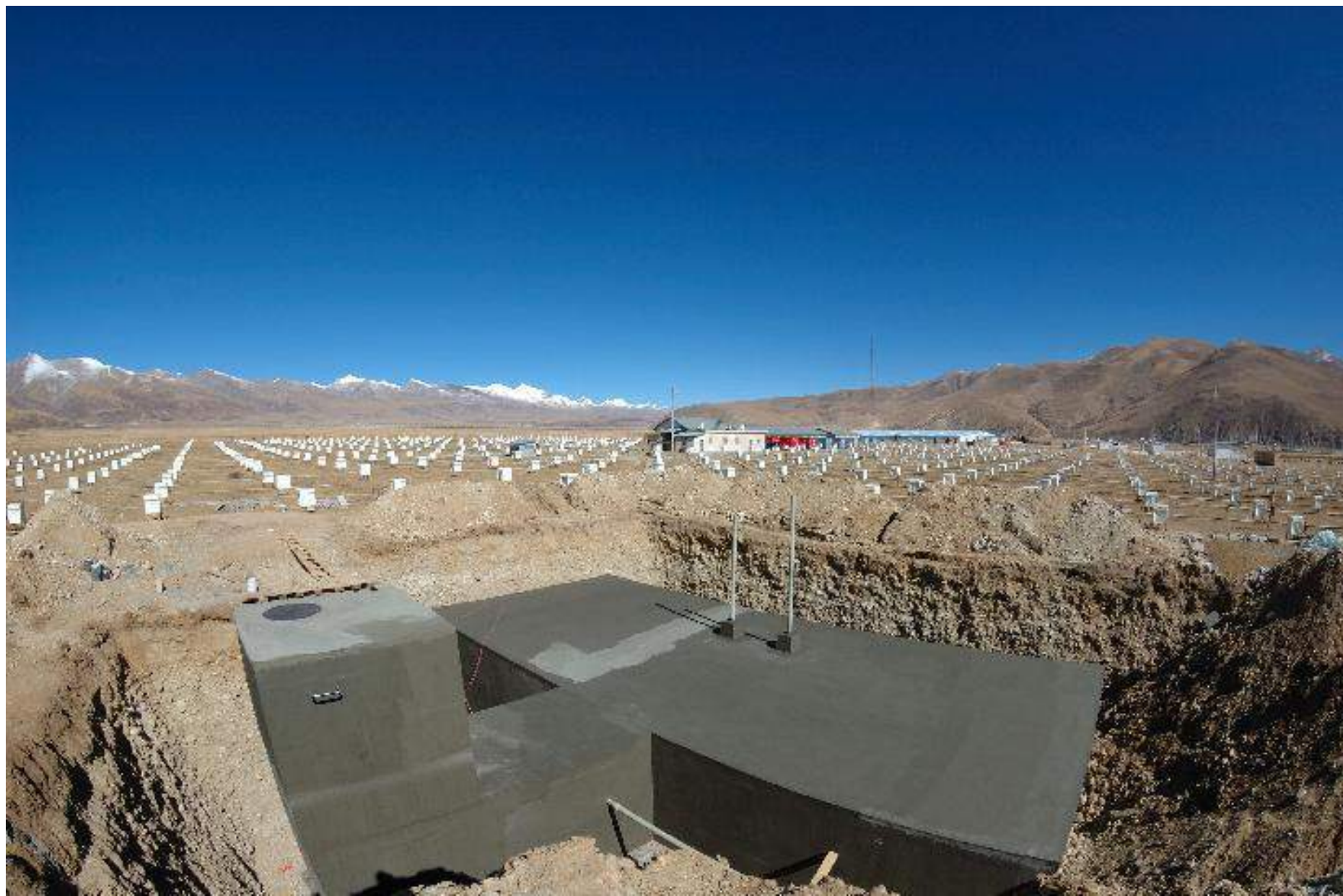
# Prototype Muon Detector in Tibet



Construction from  
Sep. 2007  
Data taking from  
Dec. 2007

- Construction feasibility in Tibet ?
- MC simulation OK?
- $\gamma$  observation above multi 100 TeV





16 November, 2007

Prototype Muon Detector



Prototype Muon Detector after backfilling

## Inside of the Prototype MD

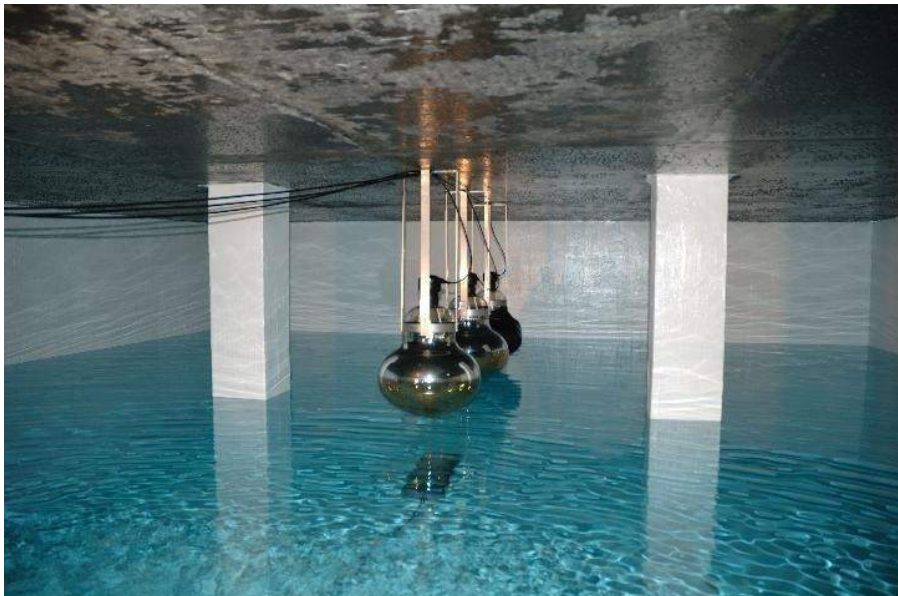
Clear underground water  
from a nearby well

20"φ PMT x 3:  
(Normal gain x 2, 1/100 gain x 1 for test)

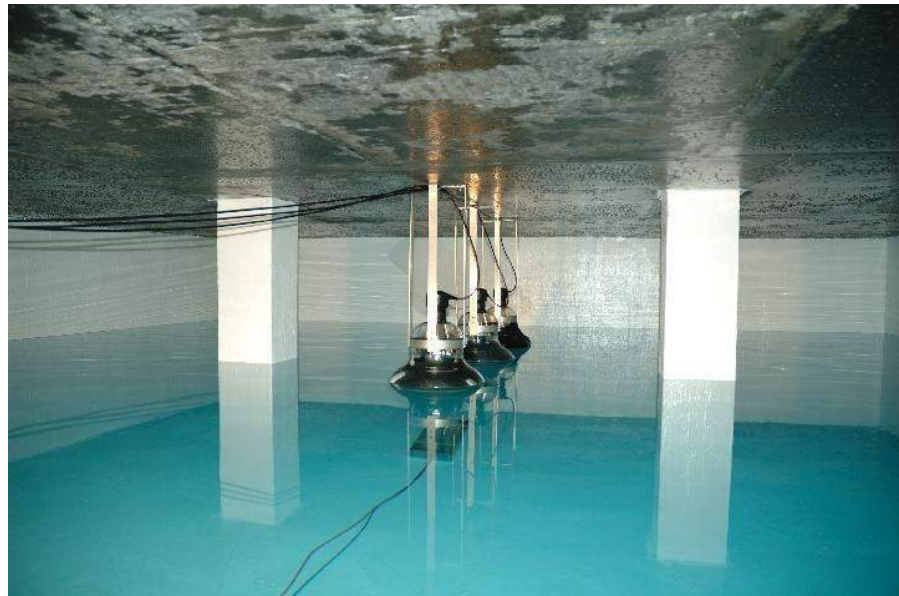
Water depth : 1.5 m



White paint



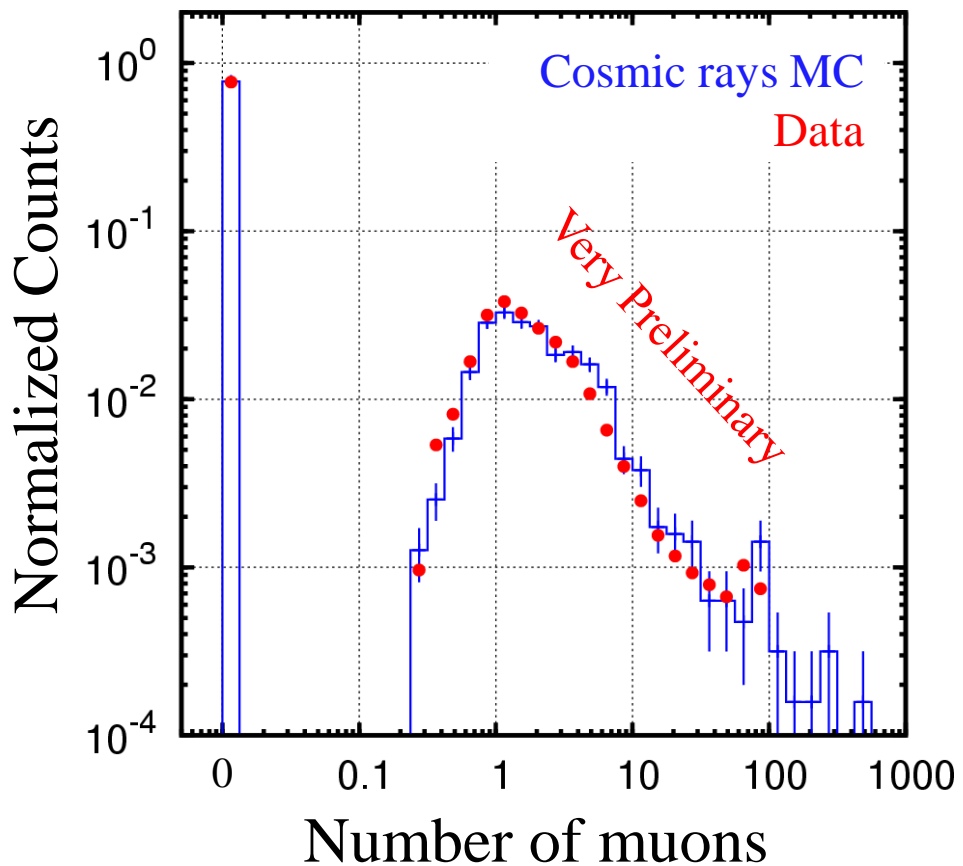
Pouring very clear well-water



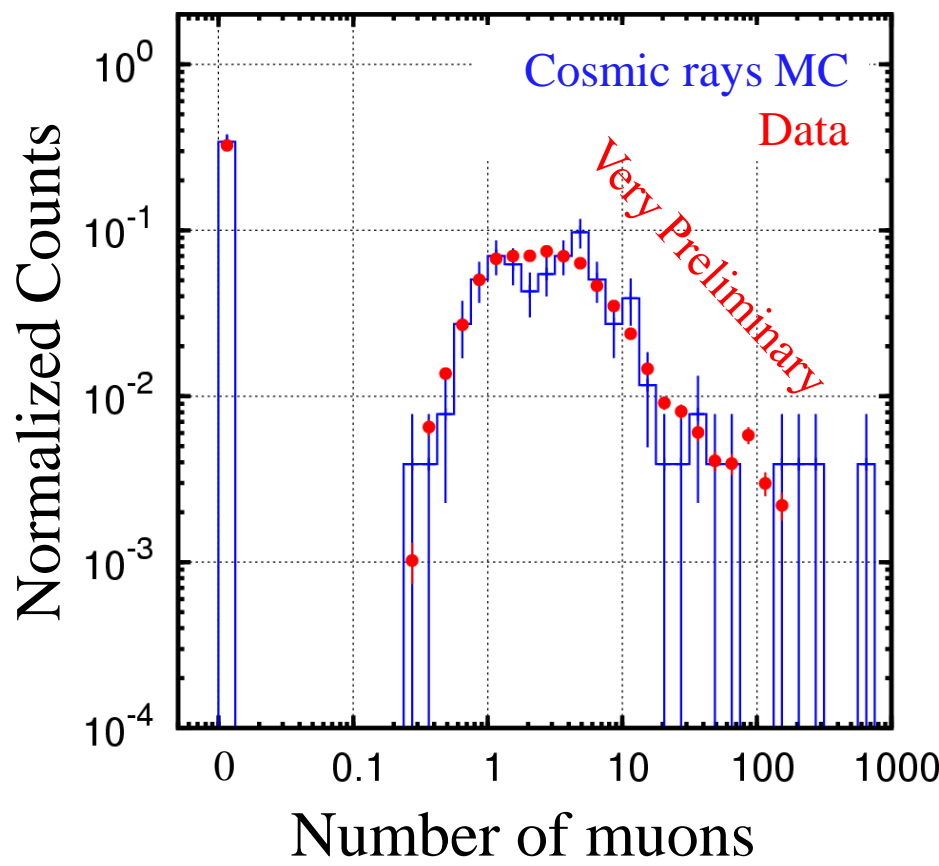
Filled up water 1.5 m in depth

# Number of muons

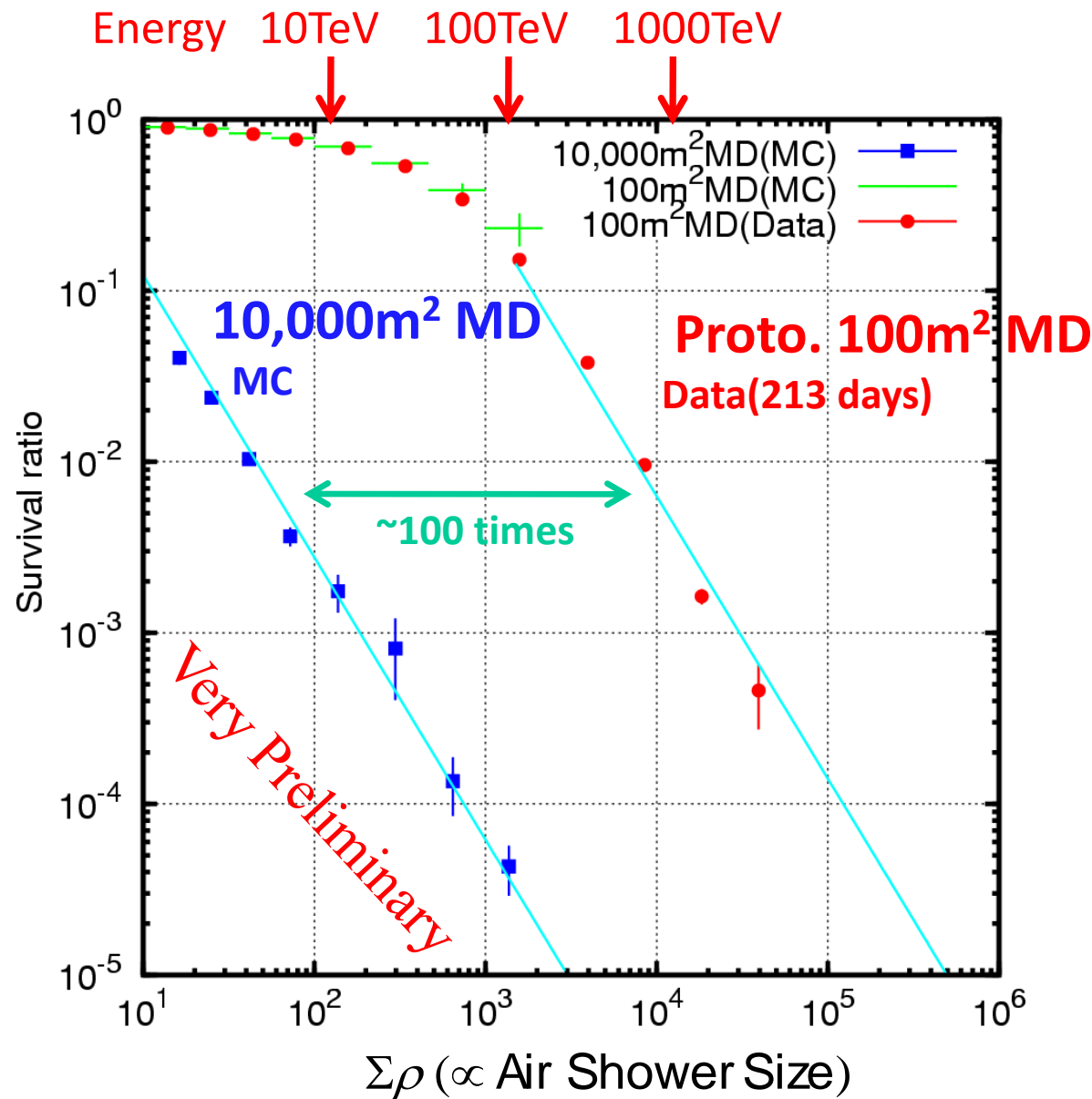
~10 TeV Air Showers



~100 TeV Air Showers



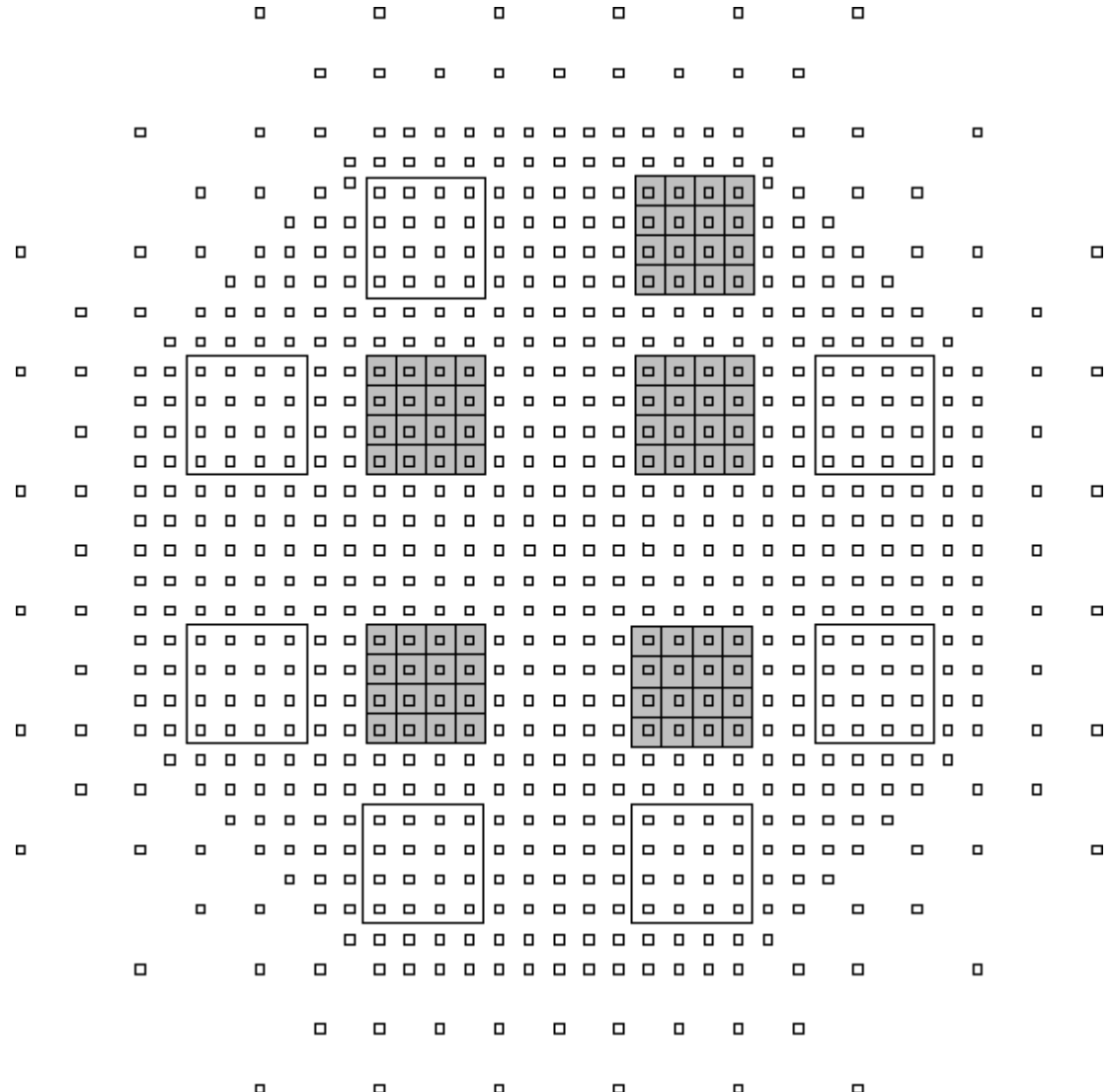
# Cosmic Ray (Nucleus) Survival Ratio



# Status of MD Construction

**5/12 Full MD**

**Construction  
Completed and  
Started Data-taking  
In 2014**





MD construction scene



Installing a 20 inch PMT in a MD cell.



Tyvek sheet walls and two 20 inch PMTs

# MD Summary

## **Prototype MD (52 m<sup>2</sup> x 2 cells)**

- Successfully completed (2007)**

**Data vs MC in reasonable agreement**

**CR survival ratio: ~0.2 %@~1 PeV**

**-> Full (10<sup>4</sup>m<sup>2</sup>) MD @~10 TeV**

**-> Full (10<sup>4</sup>m<sup>2</sup>) MD MC: OK up to ~10TeV**

**5/12 Full MD Data-taking Started in 2014**

# YAC II

(Dense version)

(under construction)

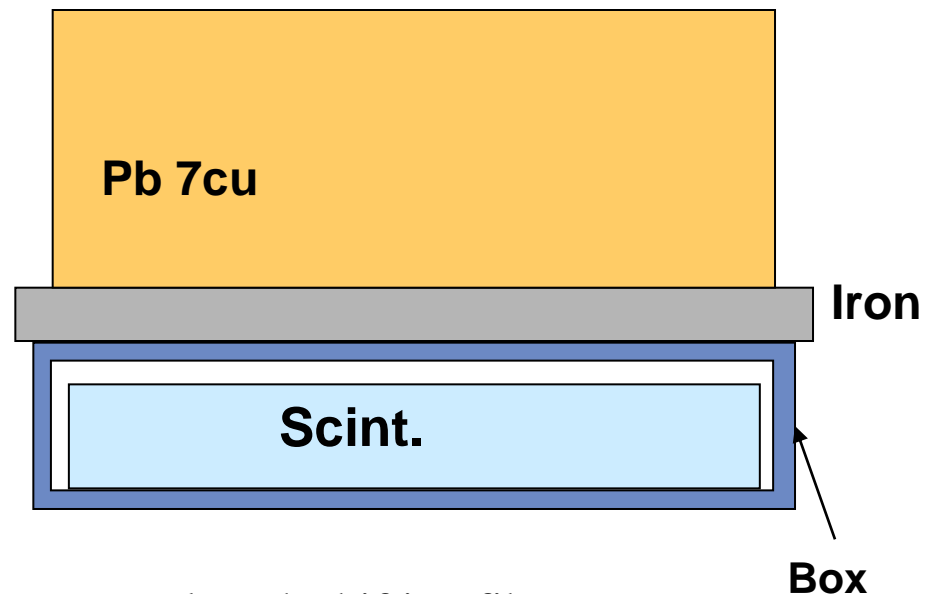
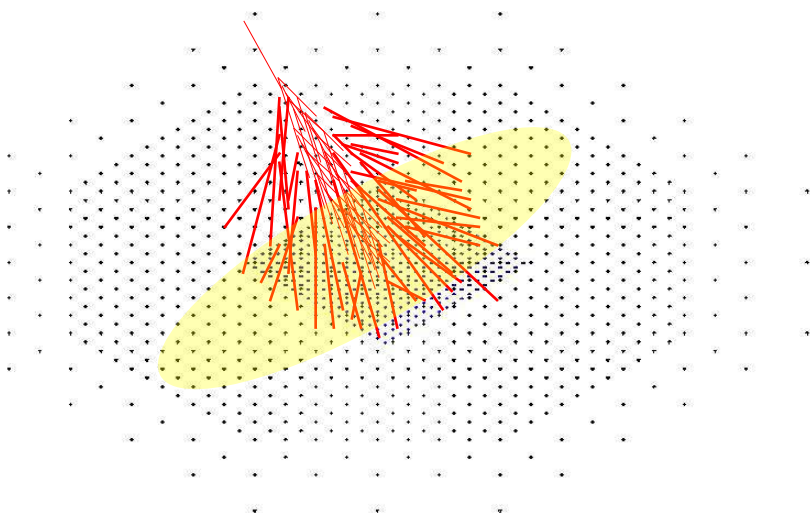
YAC II detector consists of 100 burst detectors with 1.5m spacing between detectors.

Total area of the array is 160 m<sup>2</sup> located near the center of Tibet III AS array.

It is designed to measure proton and helium spectra in the knee region. Expected number of protons (>100TeV) and helium (>200TeV) using HD model are 2300 and 800 per one year, respectively.

# Design of YAC-II

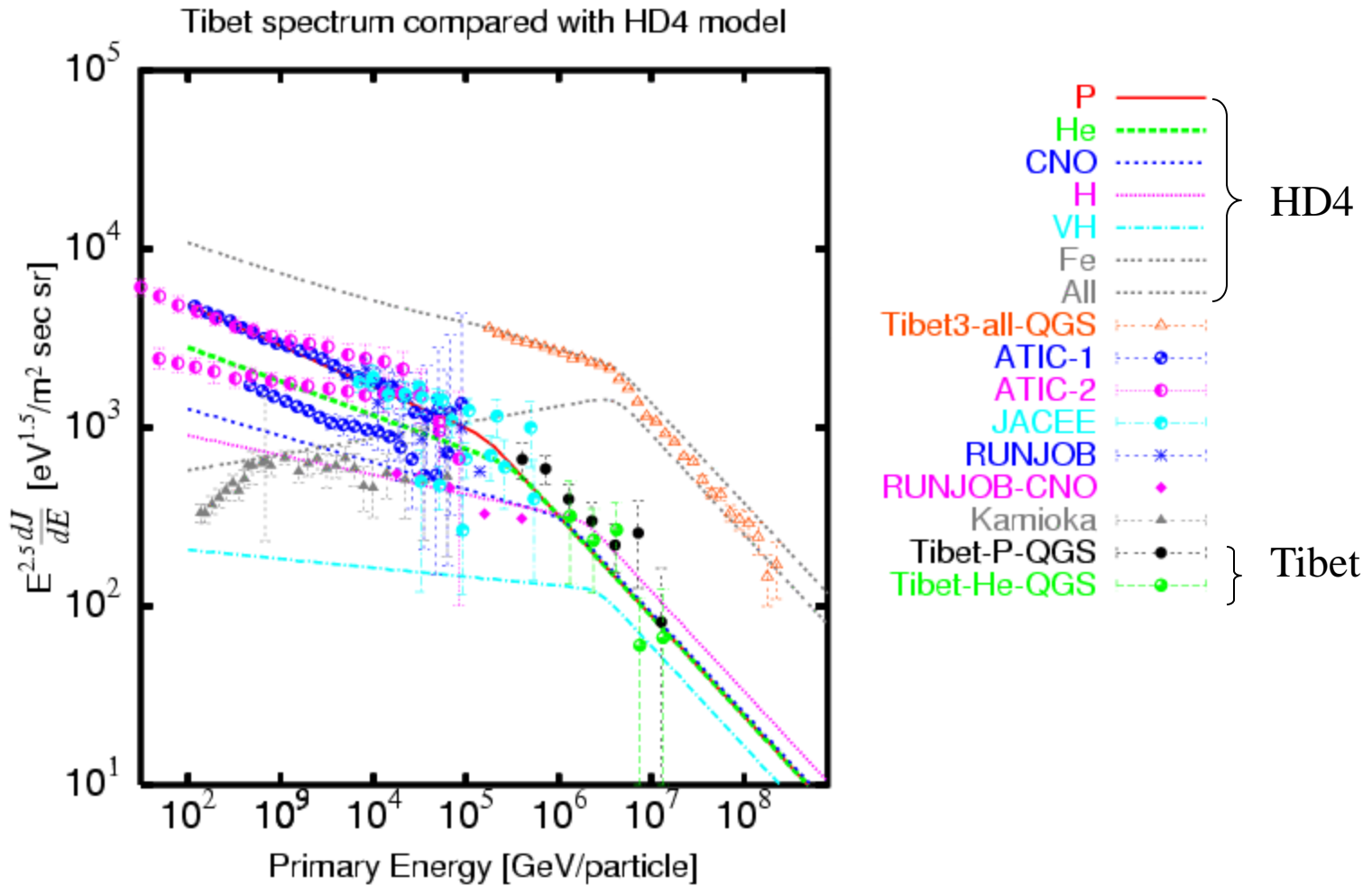
40cm x 50cm, 100 channels  $S=160\text{m}^2$



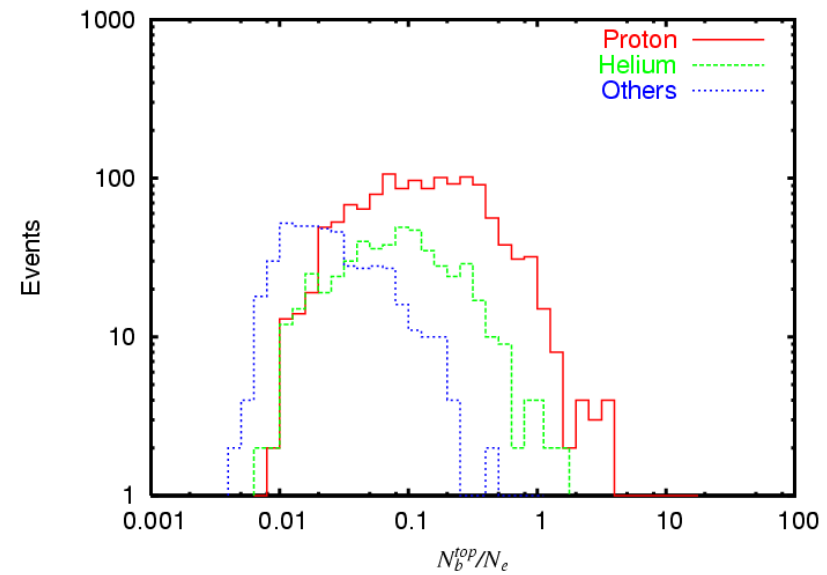
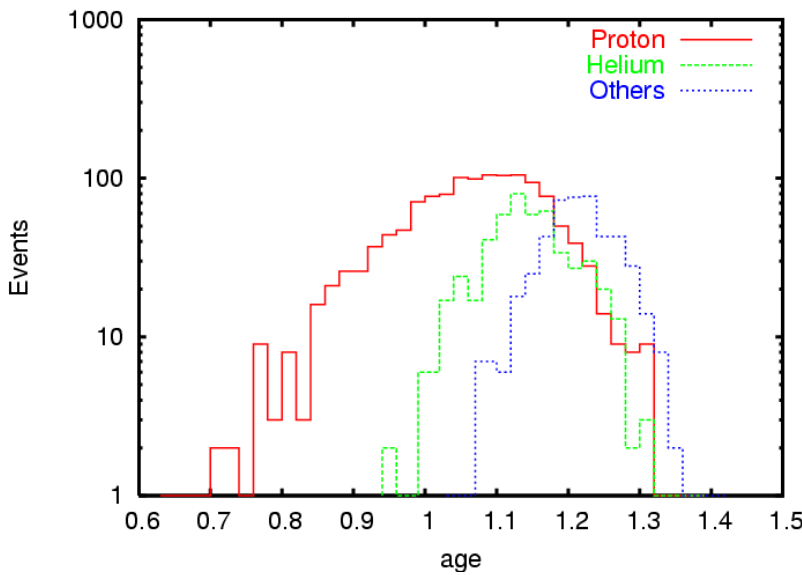
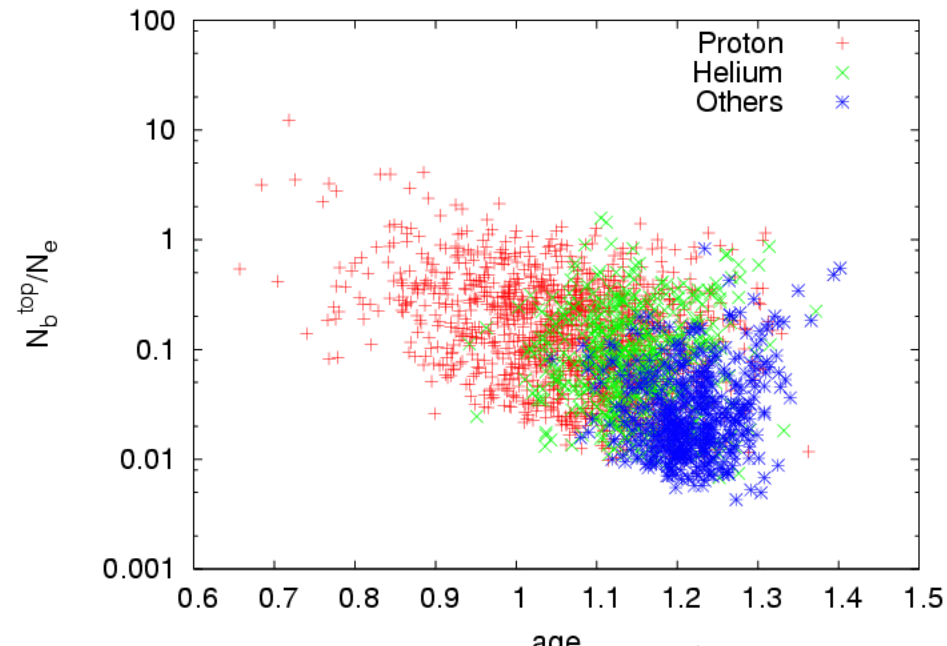
1.5m spacing 100ch  
 $N_b > 100$  electrons,  
any 1 ( $> 30\text{GeV}$ )

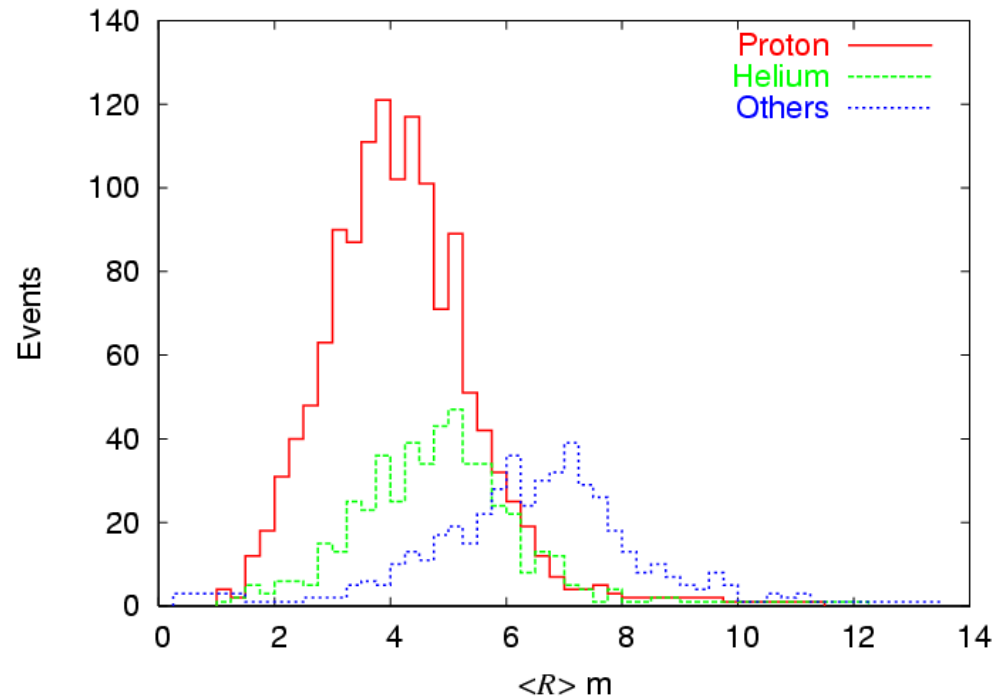
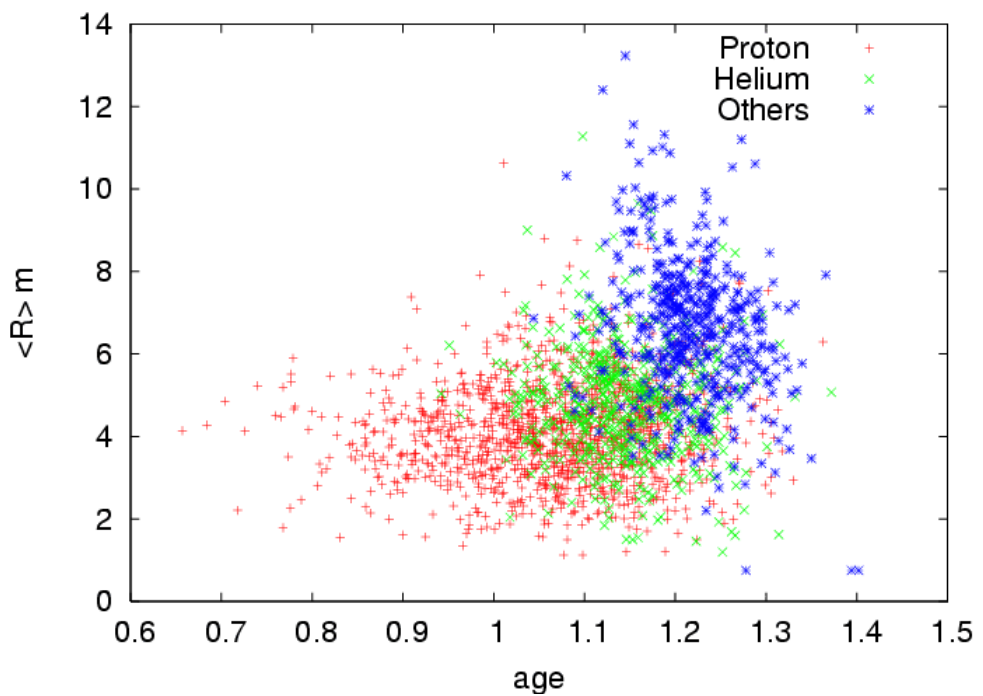
Wave length shifting fiber  
+ 2 PMTs  
(Low gain & High gain)  
 $10^2 < N_b < 10^6$

# Tibet All, P, He spectrum



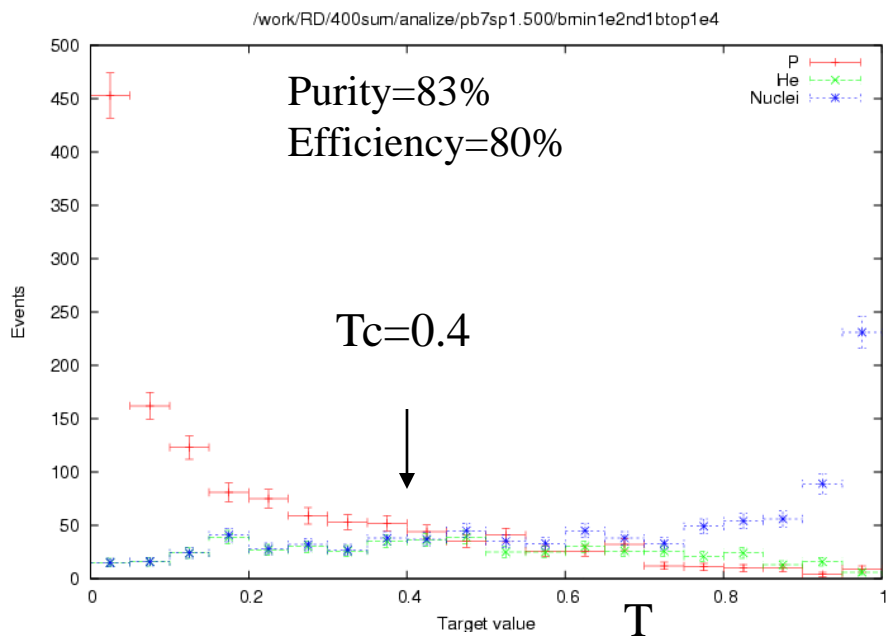
# Features of YAC-II observables





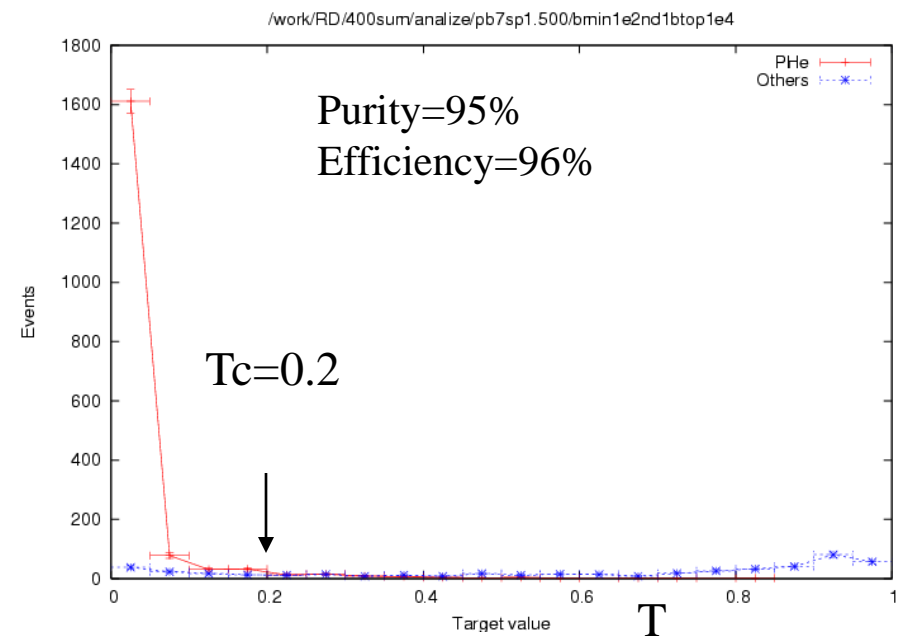
# ANN output

## Proton separation



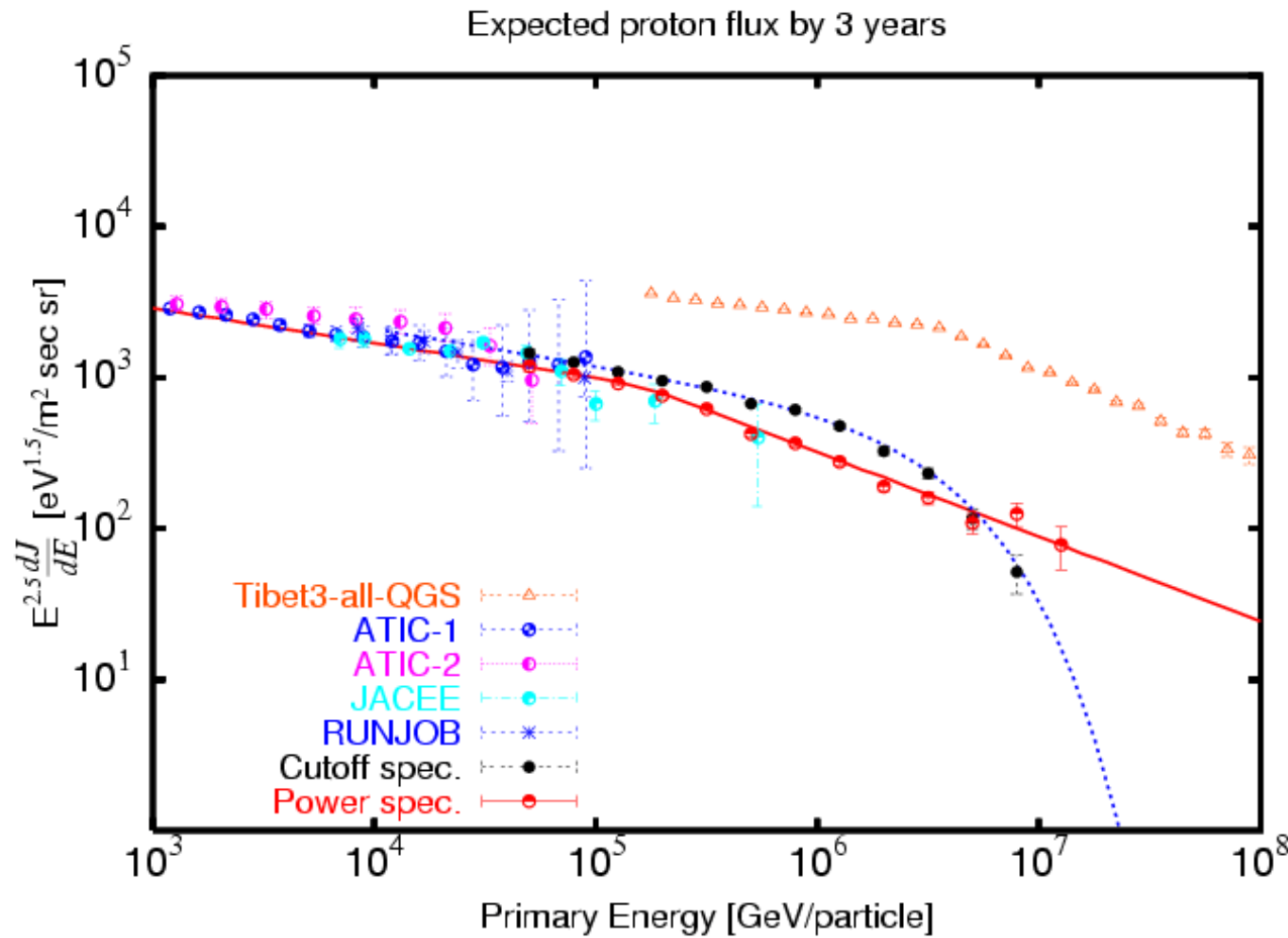
Contamination is exclusively by helium nuclei.  
The fraction of helium events missidentified as protons is about 40% of helium events by  $T_c=0.4$ .

## P+He separation

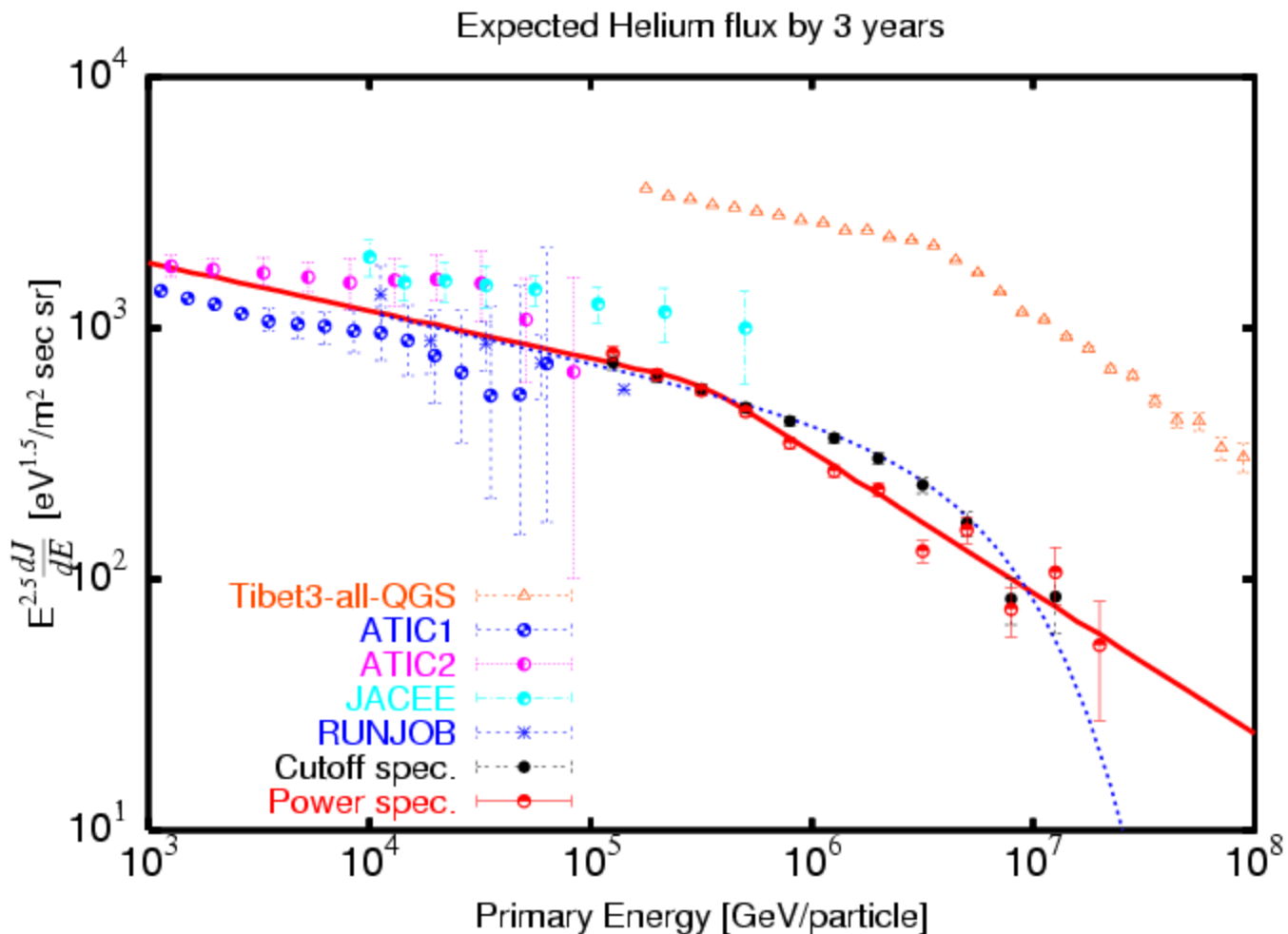


20% of heavier nuclei than helium contaminates to P+He region.

# Expected proton spectrum (YAC-II)



# Expected He Spectrum (YAC-II)



# **YAC III**

## **(Wide version) 2.5 M USD**

**YAC III** detector consists of 400 burst detectors with 3.75m spacing between detectors.

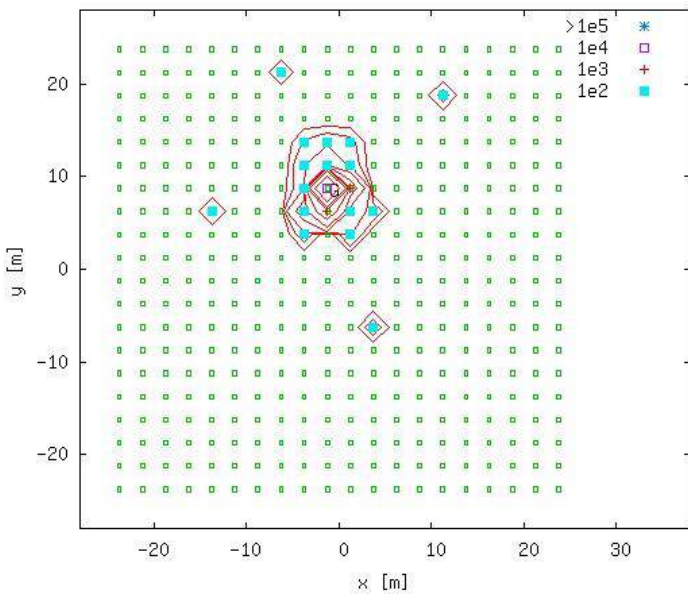
Total area of the array is  $5000 \text{ m}^2$  located near the center of Tibet III AS array.

It is designed to measure iron group spectra in the knee region. Expected number of irons ( $>1000\text{TeV}$ ) using HD model is 4400 per one year.

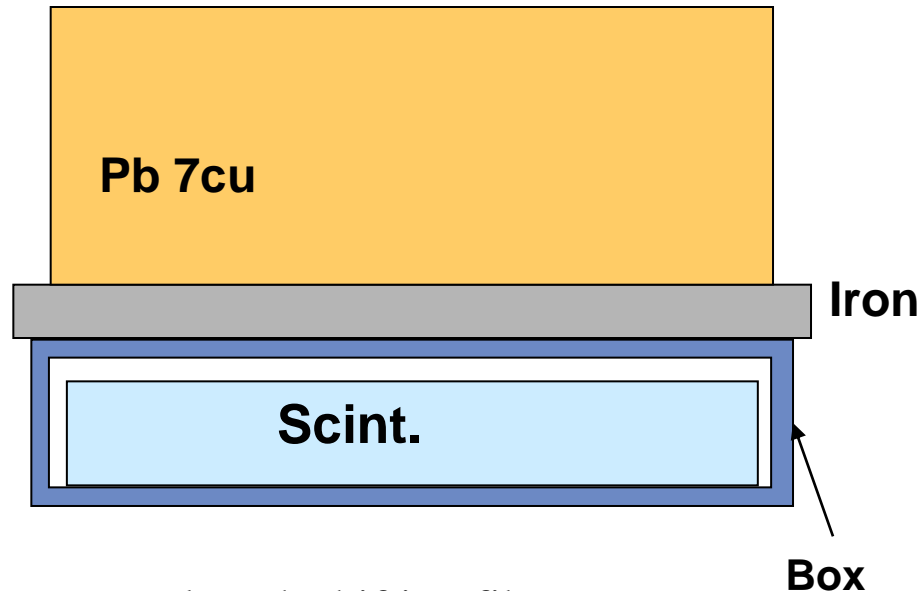
# Design of YAC-III

40cm x 50cm, 20x20 channels  
 $S=5000\text{m}^2$

$Q=2 E_0=1.5\text{E}+06 N_e=9.6\text{E}+05 s=1.18 Z=0.91 N_b=5.0\text{E}+04 T_{\text{op}}=4.2\text{E}+04$

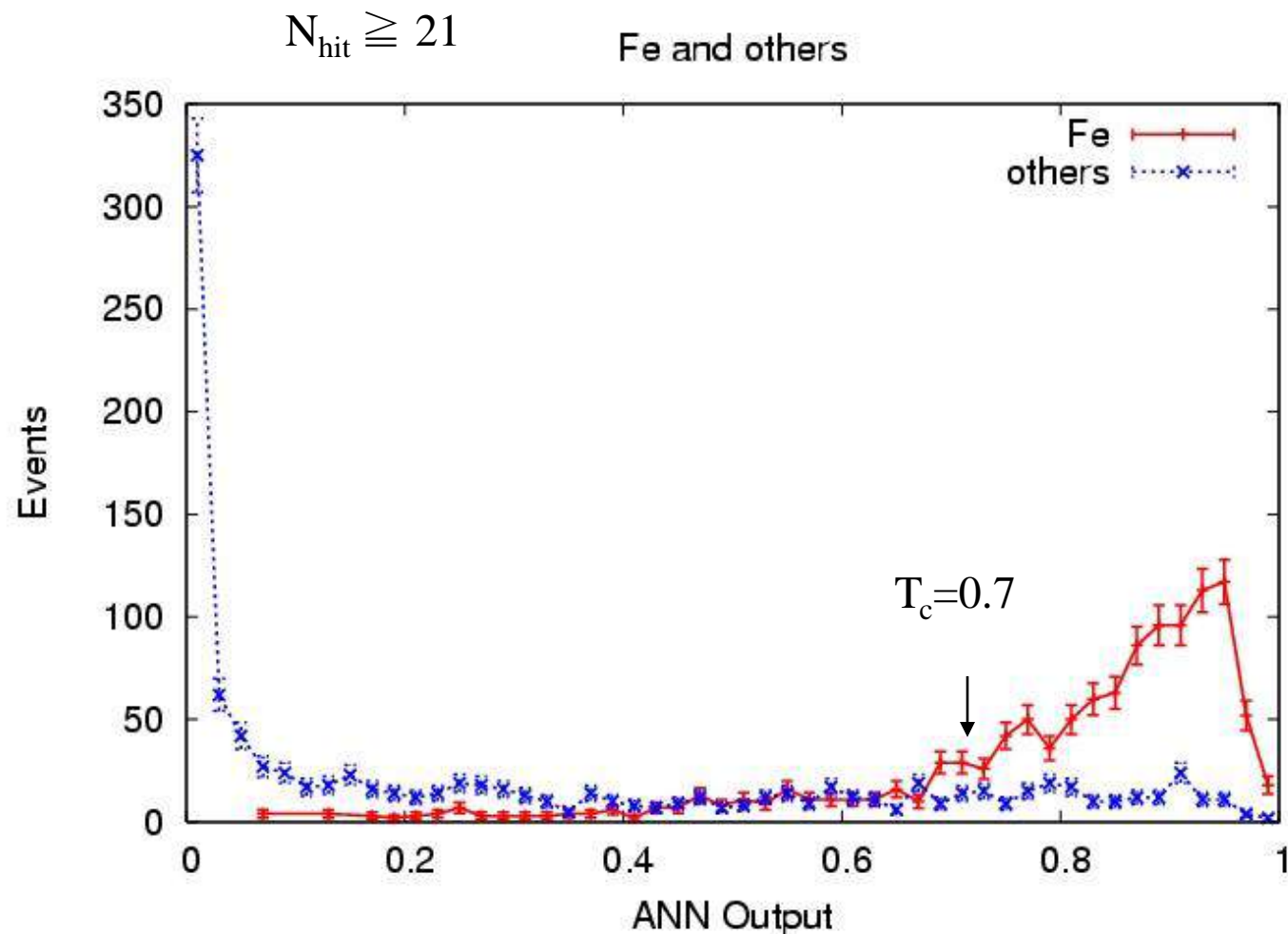


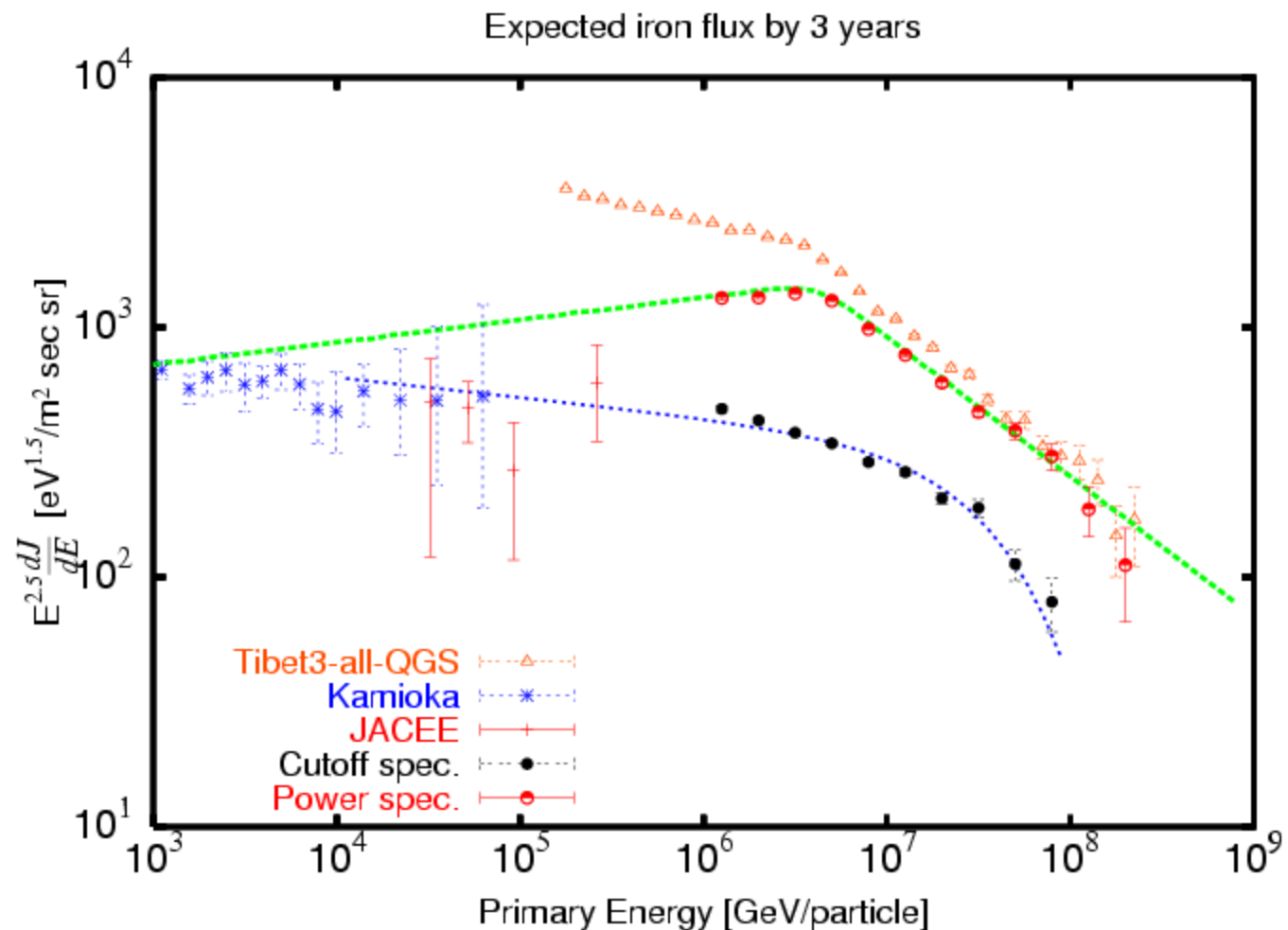
3.75m spacing 400ch  
 $N_b > 100$ , any 5  
( $>30\text{GeV}$ )

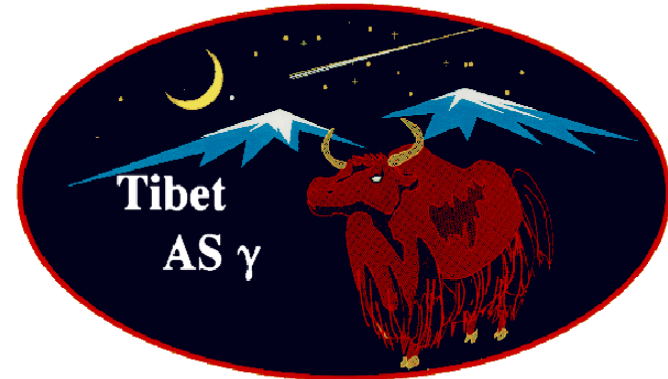
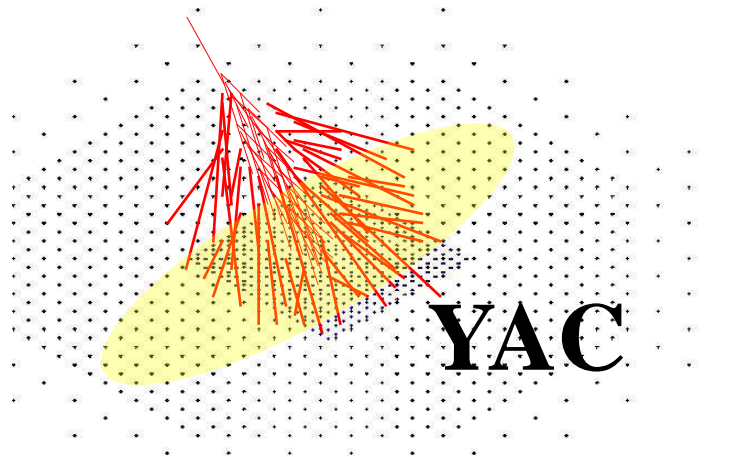


Wave length shifting fiber  
+ 2 PMTs  
(Low gain & High gain)  
 $10^2 < N_b < 10^6$

# Separation of Fe by YAC III

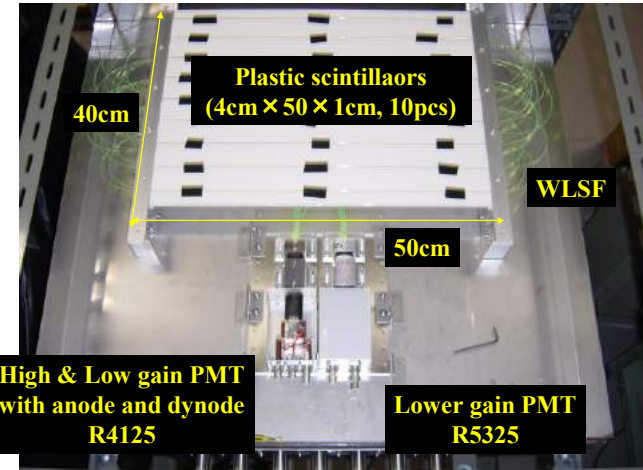






# *Proto-type YAC Detector*

Prototype of YAC  
(Yangbajing Air shower Core detector)



# YAC-II Data-taking Started in 2014



# Summary of MD & YAC status

- R&D DONE for MD&YAC
- 5/12 MD Data-taking started in 2014  
YAC-II Data-taking started in 2014
- Good timing for you:
  - 100 TeV  $\gamma$  astronomy
  - CR chemical composition

End